

Regulation of Adhesion Mechanosignaling by Fibronectin Matrix Structure

A Dissertation

Presented to
the faculty of the School of Engineering and Applied Science
University of Virginia

in partial fulfillment
of the requirements for the degree

Doctor of Philosophy

by

Rachel Elizabeth Evans

August

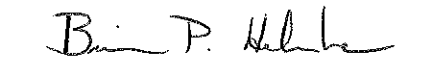
2012

APPROVAL SHEET

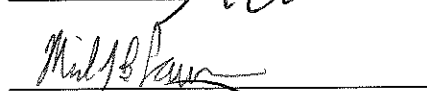
The dissertation
is submitted in partial fulfillment of the requirements
for the degree of
Doctor of Philosophy


AUTHOR

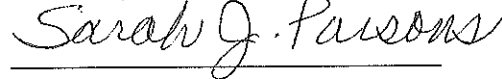
The dissertation has been read and approved by the examining committee:


Advisor

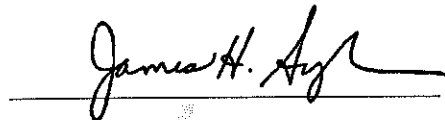








Accepted for the School of Engineering and Applied Science:



Dean, School of Engineering and Applied Science

August
2012

Acknowledgements

I would like to first and foremost thank my advisor, Dr. Brian Helmke, for his excellent mentorship and training. I'd also like to thank my committee members Dr. Richard Price, Dr. William Guilford, Dr. Michael Lawrence and Dr. Sally Parsons for their helpful guidance, valuable scientific perspective and input in our discussions.

Thank you to all the members of the Helmke Lab I've worked with, including Deb, Jenn, Jessie, Christina, Liz, Xiefan, Lawrence and especially Rosie. I learned a lot from working with all of you. All the other grad students in the department were also invaluable in gladly providing technical help and graciously sharing equipment. I'd especially like to thank the Schwartz lab for generously providing reagents.

Finally, I'd like thank my husband, Kerry, and my parents. I couldn't have done this without your support.

Table of Contents

Abstract	iv
List of Figures	vi
List of Tables	xii
List of Abbreviations	xiii
Chapter 1: Background and Significance	1
1.1 Significance	1
1.2 Endothelial structural adaptation to shear stress	2
1.3 Fibronectin Assembly	10
1.4 Fibronectin and shear stress	13
Chapter 2: Experimental Methods	15
2.1 Preparing Endothelial Cells	15
2.1.1 General Endothelial Cell Culture	15
2.1.2 Transfection	15
2.1.3 Rhodamine Labeling of Fibronectin	16
2.1.4 Preparing sparse BAEC interacting with unassembled fibronectin	16
2.1.5 Preparing sparse BAEC interacting with assembled fibronectin	17
2.1.6 Preparing confluent BAEC interacting with unassembled fibronectin	18
2.1.7 Preparing confluent BAEC interacting with assembled fibronectin	20
2.1.8 Function Blocking Antibodies	20
2.2 Shear Stress Application	20
2.2.1 Flow Loop and Shear Stress	20
2.2.2 Fluorescence Imaging Studies	22
2.2.3 Cell Migration Studies	23
2.3 Data Collection	23
2.3.1 Microscopy	23
2.3.3 Integrin Crosslinking	25
2.4 Data Analysis	26
2.4.1 Image Analysis and Tracking	26
2.4.2 Statistics	28
Chapter 3: Results	29
3.1 Sparse Cells	29

3.1.1 Migration.....	29
3.1.2 F-actin Remodeling.....	32
3.1.3 Focal Adhesion Displacement	34
3.1.4 Fibronectin Fibril Displacement	37
3.1.5 Integrin Distribution.....	40
3.1.6 Integrin Blocking and Migration	46
3.2 Confluent Monolayers	51
3.2.1 Migration and Alignment.....	51
3.2.2 F-actin Remodeling.....	54
3.2.3 Focal Adhesion Displacement	56
3.2.4 Fibronectin Fibril Displacement	59
3.2.5 Integrin Distribution.....	60
Chapter 4: Discussion	67
4.1 Modulation of shear stress responses in single cells by fibronectin assembly	72
4.2 Modulation of shear stress responses in monolayers by fibronectin assembly	74
Chapter 5: Conclusions	78
5.1 Achievements of this study	78
5.2 Future work.....	79
REFERENCES	83

Abstract

Fibronectin is an extracellular matrix (ECM) component found in atherosclerotic lesions, which form in regions of disturbed shear stress and are associated with endothelial dysfunction. When shear stress is applied to the endothelium, forces are transmitted through the cytoskeleton of endothelial cells to focal adhesions, which are sites of integrin-dependent mechanotransduction that link the cytoskeleton and the ECM and are required for structural remodeling in response to shear stress. Integrin-mediated signaling is also required for fibronectin assembly, but how fibronectin assembly might in turn modulate integrin-mediated signaling under shear stress had not been addressed. We hypothesized that fibronectin assembly regulates shear stress-induced structural remodeling through regulation of integrin binding.

To test this hypothesis we developed methods to control fibronectin assembly independent of cell density. Bovine aortic endothelial cells interacting with assembled or unassembled fibronectin were then subjected to a step increase from 0 to 15 dyn/cm² unidirectional shear stress in a parallel plate flowchamber. We then measured how fibronectin assembly modulated shear stress-induced changes in motility, cytoskeletal organization, and focal adhesion displacement in both single endothelial cells and confluent endothelial monolayers. We also evaluated the effects of fibronectin assembly and shear stress on the distribution and binding of $\alpha_5\beta_1$ and $\alpha_v\beta_3$ integrins.

In single endothelial cells, fibronectin assembly inhibited shear stress-induced downstream mechanotaxis and spreading. Fibronectin assembly also inhibited baseline stress fiber assembly, shear stress-induced ruffling, and shear stress-induced focal adhesion arrest. We also observed that fibronectin assembly promoted $\alpha_5\beta_1$ binding over

$\alpha_v\beta_3$, and by using blocking antibodies we showed that $\alpha_v\beta_3$ is important for shear stress-induced mechanotaxis.

In confluent endothelial monolayers, fibronectin assembly slowed shear stress-induced monolayer alignment. Fibronectin assembly also promoted shear stress-induced stress fiber disassembly and inhibited shear stress-induced focal adhesion arrest. Finally, we observed an assembly dependent switch in integrin binding. Monolayers interacted with unassembled fibronectin through $\alpha_v\beta_3$, but interacted with assembled fibronectin through $\alpha_5\beta_1$.

These results demonstrate for the first time that fibronectin assembly inhibits endothelial mechanosensing under shear stress and alters the specificity of $\alpha_5\beta_1$ versus $\alpha_v\beta_3$ binding. Inhibition of $\alpha_v\beta_3$ suggests that this integrin plays an important role in guiding mechanotaxis. Overall, our data suggest that fibronectin assembly-dependent regulation of $\alpha_5\beta_1$ and $\alpha_v\beta_3$ binding results in activation of different downstream signaling pathways to control shear stress-induced structural remodeling.

List of Figures

Figure 1. Fibronectin immunostaining of (A) assembled fibronectin matrix underneath a confluent monolayer. (B) assembled fibronectin matrix isolated from a confluent monolayer, before plating sparse BAEC.

Figure 2 Dose response to assembly blocking peptide. Fibronectin staining in BAEC treated with (A) 0, (B) 0.1, (C) 0.25, or (D) 0.5 $\mu\text{g/mL}$ assembly blocking peptide. Fibrous structures are extracellular fibronectin fibrils, while punctate, perinuclear structures are intracellular fibronectin not yet secreted by the cell.

Figure 3. Gravity-driven recirculating flow loop. Media in the lower reservoir (A), is drawn through tubing connected to a peristaltic pump (B) to maintain a constant fluid level in the upper reservoir (C). Media flows from the upper reservoir through the flow chamber (D) and back to the lower reservoir. Fluid flow through the chamber is controlled by stopcocks (E). Temperature and pH are maintained by a humidified supply of CO₂ (F) and a water bath (G) and heat block (H) to maintain the lower and upper reservoirs at 37°C. The CO₂ line and upper reservoir outlet to the atmosphere contain sterile gas filters (I) to maintain the sterility of the system.

Figure 4. Migration speed of sparse BAEC interacting with assembled (closed circles) or unassembled (open circles) fibronectin under shear stress. Migration speed is not significantly different between the two fibronectin assembly conditions for any time point. ($p > 0.05$, t test)

Figure 5. Migration paths of individual BAEC tracked for 6 hours after the onset of shear stress. BAEC interacting with unassembled fibronectin (A), display downstream mechanotaxis (flow is from left to right), while BAEC interacting with assembled fibronectin (B) migrate randomly under flow.

Figure 6. Migration in the direction of flow, as measured by cumulative x displacement, is significantly higher ($*p < 0.05$, t test) in cells interacting with unassembled fibronectin than in cells interacting with assembled fibronectin starting 1 hour after the onset of shear stress.

Figure 7. Area of sparse BAEC exposed to shear stress interacting with unassembled (closed circles) or assembled (open circles) fibronectin. Cell area at each time point was normalized to cell area at the onset of shear stress ($t=0$). At 15 minutes after the onset of shear stress, the transient increase in area caused by the onset of shear stress is significantly larger in BAEC interacting with unassembled fibronectin than in BAEC interacting with assembled fibronectin. ($*p < 0.05$, t test)

Figure 8. F-actin staining in sparse BAEC interacting with assembled or unassembled fibronectin. BAEC interacting with unassembled fibronectin under no-flow conditions (A) are well spread and display an organized stress fiber network. When shear stress is applied, these cells form peripheral actin ruffles (arrowheads, B). BAEC interacting with assembled fibronectin under no-flow conditions (C) are less spread and have fewer stress fibers, and when shear stress is applied (D), do not form an increased number of visually obvious actin ruffles.

Figure 9. Ruffling at edges of sparse BAEC interacting with assembled or unassembled fibronectin. Ruffling was quantified from images of F-actin staining as the fraction of the cell perimeter that displayed a ruffled morphology. BAEC interacting with unassembled fibronectin display a significantly increased fraction of edge ruffling when exposed to shear stress, (* $p < 0.05$, t test) while BAEC interacting with assembled fibronectin do not. (n.s.=not significant, $p = 0.35$, t test)

Figure 10. Focal adhesion displacement rate is assembly dependent. Box plots of the distribution of individual focal adhesion displacement rates for sparse BAEC on unassembled fibronectin (left pair of box plots) and assembled fibronectin (right pair of box plots). The red line represents the population median, the blue box represents the interquartile range, and the red crosses represent outliers. In each pair of box plots, the left box plot is displacement rates over 15 minutes before the onset of shear stress (No SS), and the right box plot is displacement rates over 15 minutes after the onset of shear stress (SS). Shear stress causes a significant decrease in median focal adhesion displacement in cells on unassembled fibronectin, (* $p < 0.01$, Mann Whitney U test) but not cells on assembled fibronectin (n.s.=not significant, $p = 0.16$, Mann Whitney U test). Focal adhesion displacement rate under no shear stress conditions was significantly higher in cells on assembled fibronectin than cells on unassembled fibronectin. (* $p < 0.01$, Mann Whitney U test)

Figure 11. Angular distribution of focal adhesion displacement in sparse BAEC interacting with assembled fibronectin. Under no-flow conditions (A), focal adhesions appeared to move randomly. After 1 minute of flow (B), focal adhesions displacement is directed downstream, but displacement returns to a distribution similar to the no-flow condition after 15 minutes of shear stress (C).

Figure 12. Rate and direction of displacement of fibronectin fibrils beneath sparse BAEC on assembled fibronectin. (A) box plots of fibronectin fibril displacement in 15 minutes before the onset of shear stress (No SS) and 15 minutes after the onset of shear stress (SS). (n.s.= not significant, $p = 0.08$, Mann Whitney U test) (B) angular distribution of fibronectin fibril displacement under no-flow conditions, after 1 minute of shear stress, and after 15 minutes of shear stress.

Figure 13. Correlation between displacement of focal adhesions and nearby fibronectin fibrils in sparse BAEC interacting with assembled fibronectin. Both angle (A) and magnitude (B) of focal adhesion displacement significantly correlate with fibronectin fibril displacement both under no flow conditions (red) and after 15 minutes of shear stress (blue) ($p < 0.05$, t test).

Figure 14. $\alpha_v\beta_3$ and $\alpha_5\beta_1$ immunostaining in sparse BAEC interacting with unassembled fibronectin under no shear stress and after 15 minutes of shear stress. $\alpha_v\beta_3$ was distributed (A and B) in adhesion-like spots towards the leading edge of the cell (arrowheads, A), while $\alpha_5\beta_1$ (C and D) was distributed into structures reminiscent of fibrillar adhesions towards the back of the cell (arrowheads, C and inset, D).

Figure 15. $\alpha_v\beta_3$ and $\alpha_5\beta_1$ immunostaining in sparse BAEC interacting with assembled fibronectin. Under no shear stress (A) and after 15 minutes of shear stress (B), $\alpha_v\beta_3$ staining is distributed across the basal surface and punctate. $\alpha_5\beta_1$ staining (C and D) is also punctate, but organized into larger fibrillar adhesion-like structures (arrowheads, C).

Figure 16. Crosslinked α_v , $\alpha_5\beta_1$, and rhodamine-fibronectin staining in sparse BAEC on unassembled fibronectin. α_v (A) was distributed into focal adhesions, and was recruited to adhesion spots after 15 minutes of shear stress (arrowheads and inset, B). $\alpha_5\beta_1$ distribution (C and D) was limited to small, punctate spots (inset, D). Rhodamine-fibronectin (E and F) demonstrates minimal fibronectin assembly.

Figure 17. Crosslinked α_v , $\alpha_5\beta_1$, and rhodamine-fibronectin staining in sparse BAEC on assembled fibronectin. Both under no shear stress and after 15 minutes of shear stress α_v staining is almost non-existent (A and B). $\alpha_5\beta_1$ is distributed in punctate spots throughout the cell, reminiscent of small adhesions (C and D, inset C). Rhodamine-fibronectin shows the organization of assembled fibronectin beneath the cell (E and F).

Figure 18. Example of crosslinked α_v staining on assembled fibronectin. (A) This cell displays a combination of $\alpha_5\beta_1$ (red) and α_v (green) staining. However, α_v -based adhesion spots are spatially segregated from $\alpha_5\beta_1$ -based adhesions. (B) α_v (green) is also spatially segregated from assembled fibronectin (red) and only visible in regions of the cell not interacting with assembled fibronectin (dark, non-fibrillar areas).

Figure 19. Example of variation in crosslinked $\alpha_5\beta_1$ staining on unassembled fibronectin. Depending on to what degree fibronectin assembly has been initiated, $\alpha_5\beta_1$ staining can vary from a very random, punctate distribution (A), to a more adhesion-associated distribution (B and C).

Figure 20. Migration tracks of sparse BAEC in the 6 hours after the onset of shear stress either (A) treated with LM609 or (B) untreated. Untreated cells migrated downstream, while BAEC treated with LM609 migrated more randomly.

Figure 21. Migration in the direction of flow, as measured by cumulative x displacement, is significantly smaller for LM609 treated cells than untreated cells during the first 40 minutes of shear stress. (* $p < 0.05$, t test)

Figure 22. Transient shear stress-induced spreading of sparse BAEC is inhibited by LM609 treatment. The shear stress-induced increase in area is significantly inhibited for the first 45 minutes after the onset of shear stress when BAEC are pretreated with LM609. (* $p < 0.05$, t test)

Figure 23. Migration tracks of sparse BAEC in the 6 hours after the onset of shear stress either (A) pretreated with anti- α_2 or (B) pretreated with anti- α_5 . In both cases, cells still display downstream migration.

Figure 24. (A) there is no significant difference in cumulative x displacement under shear stress between cells treated with anti- α_2 and untreated cells. ($p > 0.05$, t test) (B) Migration in the direction of flow, as measured by cumulative x displacement, is significantly greater for anti- α_5 treated cells after 2 hours of shear stress than untreated cells. (* $p < 0.05$, t test)

Figure 25. Example histogram of cell orientations within a monolayer. This example shows a fitted normal distribution in red, and when tested these data are normally distributed ($p < 0.05$, Jarque-Bera test)

Figure 26. Fibronectin assembly regulates speed of monolayer alignment. Average deviation of monolayer orientation under shear stress decreases more quickly for cells interacting with unassembled fibronectin (closed circles) than for cells interacting with assembled fibronectin (open circles) and is significantly different after 5 hours of shear stress. (* $p < 0.05$, t test)

Figure 27. Monolayer migration speed is not significantly affected by fibronectin assembly. The migration speed of cells interacting with unassembled fibronectin (closed circles) is not significantly different than that of cells interacting with assembled fibronectin (open circles) ($p > 0.05$, t test).

Figure 28. Representative images of F-actin staining in confluent monolayers interacting with assembled or unassembled fibronectin. Compared to the no shear stress condition (A), monolayers interacting with assembled fibronectin after 15 minutes of shear stress show regions devoid of stress fibers (arrowheads, B). In contrast, there is no visual decrease in stress fibers when comparing monolayers interacting with unassembled fibronectin under no shear stress (C) and 15 minutes of shear stress (D).

Figure 29. Quantification of F-actin content of monolayers from F-actin staining. Relative area of F-actin coverage is significantly decreased after 15 minutes of shear stress in monolayers interacting with assembled fibronectin (* $p < 0.05$, t test), but not significantly changes in monolayers interacting with unassembled fibronectin. (n.s.= not significant, $p = 0.10$, t test)

Figure 30. Focal adhesion displacement rate is increased at the onset of shear stress in confluent monolayers interacting with assembled fibronectin, but decreased in confluent monolayers interacting with unassembled fibronectin. . Box plots of the distribution of individual focal adhesion displacement rates for monolayers on assembled fibronectin (left pair of box plots) and unassembled fibronectin (right pair of box plots). In each pair of box plots, the left box plot is displacement rates over 15 minutes before the onset of shear stress (No SS), and the right box plot is displacement rates over 15 minutes after the onset of shear stress (SS). For monolayers on both assembled and unassembled fibronectin, the onset of shear stress caused a statistically significant change in focal adhesion displacement rate. (* $p < 0.01$, Mann Whitney U test)

Figure 31. Angular distribution of focal adhesion displacement (A) 15 minutes before the onset of shear stress, (B) one minute after the onset of shear stress and (C) 15 minutes after the onset of shear stress.

Figure 32. Angular distribution of fibronectin fibril displacement beneath confluent monolayers (A) 15 minutes before the onset of shear stress, (B) one minute after the onset of shear stress and (C) 15 minutes after the onset of shear stress.

Figure 33. Correlation of displacement direction (A) and magnitude (B) between focal adhesions and nearby fibronectin fibrils both under no-flow conditions (red) and after 15 minutes of shear stress (blue). All correlations shown are statistically significant ($p < 0.05$, t test).

Figure 34. Integrin $\alpha_v\beta_3$ and $\alpha_5\beta_1$ immunostaining in confluent monolayers on assembled fibronectin. Both under no shear stress (A) and after 15 minutes of shear stress (B), $\alpha_v\beta_3$ is visible in focal adhesion-like spots on the basal cell surface (arrowheads). In contrast, both under no shear stress (C) and after 15 minutes of shear stress (D), $\alpha_5\beta_1$ staining is punctate and relatively evenly distributed.

Figure 35. Integrin $\alpha_v\beta_3$ and $\alpha_5\beta_1$ immunostaining in confluent monolayers on assembled fibronectin. Both under no shear stress (A) and after 15 minutes of shear stress (B), $\alpha_v\beta_3$ staining is punctate and relatively evenly distributed. In contrast, both under no shear stress (C) and after 15 minutes of shear stress (D), $\alpha_5\beta_1$ is visible in large fibrillar adhesion-like structures on the basal surface (arrowheads).

Figure 36. Immunostaining of crosslinked α_v , $\alpha_5\beta_1$ and rhodamine-fibronectin in confluent monolayers interacting with unassembled fibronectin. α_v (A and B) was distributed into focal adhesions (arrowheads). $\alpha_5\beta_1$ (C and D) staining was minimal. Rhodamine-fibronectin (E and F) demonstrates minimal fibronectin assembly.

Figure 37. Immunostaining of crosslinked α_v , $\alpha_5\beta_1$ and rhodamine-fibronectin in confluent monolayers interacting with assembled fibronectin. A few α_v -based adhesion spots were visible. (A and B) $\alpha_5\beta_1$ (C and D) staining was distributed into fibrillar adhesion structures. Rhodamine-fibronectin (E and F) demonstrates fibronectin assembly beneath the monolayer.

Figure 38. Relative levels of crosslinked integrin staining in monolayers interacting with unassembled fibronectin quantified by total image intensity after background subtraction. After 15 minutes of shear stress, there is a significant increase in α_v intensity (* $p < 0.0$, t test), but no significant change in $\alpha_5\beta_1$ intensity (n.s.=not significant, $p = 0.54$, t test).

Figure 39. Overlay of isolated rhodamine-fibronectin exposed to 15 minute of shear stress. Image from immediately before the onset of shear stress (red) is overlaid with image after 15 minutes of shear stress (green).

Figure 40. Hypothesized model of how fibronectin assembly regulates shear stress-induced structural remodeling.

List of Tables

Table 1. Integrin blocking antibodies

Table 2. Antibodies used for immunofluorescence

Table 3. Readouts modulated in single cells by fibronectin assembly under no-flow conditions

Table 4. Readouts of shear stress responses in single cells significantly affected by fibronectin assembly.

Table 5. Readouts modulated in confluent monolayers by fibronectin assembly under no-flow conditions

Table 6. Readouts of shear stress responses in confluent monolayers significantly affected by fibronectin assembly.

List of Abbreviations

atomic force microscopy	AFM
bovine aortic endothelial cells	BAEC
bicinchoninic acid	BCA
bovine serum albumin	BSA
Chinese hamster ovary	CHO
Dulbecco's modified Eagle medium	DMEM
3,3'-Dithiobis[sulfosuccinimidylpropionate]	DTSSP
extracellular matrix	ECM
focal adhesion	FA
focal adhesion kinase	FAK
GTPase Activating Protein	GAP
green fluorescent protein	GFP
intercellular adhesion molecule-1	ICAM-1
normal calf serum	NCS
nuclear factor κ B	NF- κ B
normal goat serum	NGS
phosphate buffered saline	PBS
phosphatidylinositol-3-kinase	PI3K
protein kinase A	PKA
protein kinase C	PKC
vascular cell adhesion molecule-1	VCAM-1

Chapter 1: Background and Significance

1.1 Significance

The endothelium is a critical regulator of homeostasis, angiogenesis and thrombosis, and endothelial cell phenotype is regulated by local hemodynamics. Regions of the endothelium which are exposed to disturbed hemodynamic shear stress profiles, as found in branch points or regions of high curvature in the arterial tree, are more susceptible to the formation of atherosclerotic lesions. The endothelium in these regions exhibits inflammatory markers such as increased intercellular adhesion molecule-1 (ICAM-1) and vascular cell adhesion molecule-1 (VCAM-1) expression, activation of nuclear factor κ B (NF- κ B) signaling, and a cobblestone morphology. [1, 2, 3, 4] This is in contrast to the endothelium in regions exposed to laminar shear stress, which display lower levels of inflammatory signaling and align their cell shape and structure in the direction of blood flow. Since atherosclerosis is the leading cause of death in the United States, [5] understanding the links among hemodynamic shear stress profile, the endothelium, and atherosclerosis is important in improving prevention and treatment of this disease.

The endothelium is critical not only in its ability to promote or suppress the formation of atherosclerotic lesions but also in recovering normal function after lesion treatment. The most common treatment for arteries blocked by atherosclerotic lesions is angioplasty and stent insertion. While treatment of advanced lesions with stents or balloon angioplasty can alleviate symptoms and restore blocked blood flow, the underlying endothelial dysfunction remains unaddressed. Furthermore, restenosis or thrombosis can occur after the insertion of a stent, due to smooth muscle cell

overproliferation and a pro-thrombotic environment. These effects are thought to be caused by loss of the endothelium in the stented region or by alteration of the local hemodynamic shear stress profile by the presence of the stent. [6, 7]

Since the endothelium and its responsiveness to hemodynamic shear stress plays a critical role in the initiation of atherosclerotic lesion formation and recovery from treatment, it is important to understand the mechanisms behind endothelial mechanotransduction. Shear stress-induced structural adaptation is both associated with shear stress-regulated inflammatory signaling and important to controlling endothelial migration to promote reendothelialization. Understanding how shear stress controls endothelial phenotype will enable the design of interventions to suppress the pro-inflammatory, pro-atherogenic pathways stimulated by disturbed shear stress profiles, and to promote reendothelialization of stented regions. Progress has been made in identifying several mechanosensors and how they signal in response to shear stress. However, *in vitro* models of shear stress-induced structural remodeling have only begun to take into account the other microenvironmental factors that could regulate shear stress-induced mechanosignaling that we could use as tools to intervene in shear stress-regulated signaling pathways.

1.2 Endothelial structural adaptation to shear stress

Endothelial alignment to mechanical cues, including shear stress, stretch, and micropatterned lines, is associated with a decrease in inflammatory signaling. [8, 9, 10] Promoting an aligned phenotype is thought to promote anti-inflammatory signaling and

confer resistance to the development of atherosclerotic lesions, but the mechanism linking these two functions is unknown.

Structural adaptation of endothelial monolayers to laminar shear stress *in vitro* is a multiphasic process that progresses over hours to days and results in the alignment of both cell shape and subcellular structures with the direction of shear stress. Within minutes to several hours after the onset of shear stress, in confluent monolayers there is an initial response characterized by global F-actin depolymerization, local edge ruffling, and destabilization of cell-cell junctions. [11, 12, 13] In the reorientation phase, the cell establishes planar cell polarity in the flow direction, stress fiber assembly and migration speed increase, and the cell elongates in the flow direction. [14, 15] Once the cell has aligned, migration speed stabilizes and junctions are reestablished. [12, 14] There is some variation in reports of how long alignment takes to complete. There is some evidence that shear stress profile variables, such as magnitude and slew rate in pulsatile flow, can regulate speed of alignment. [16, 17] However, the mechanisms by which variations in shear stress regulate alignment have not been systematically studied.

Rather than alignment, exposure of single endothelial cells to unidirectional laminar shear stress *in vitro* results in an enhancement of migration in the downstream direction termed mechanotaxis. This response involves extension of new lamellipodial protrusions on the downstream side of the cell, followed by formation of new focal adhesions and reorientation of cell polarity. Like alignment, mechanotaxis requires activation of mechanosensitive signaling pathways controlling adhesion and cell shape.

At the subcellular level, focal adhesions and cytoskeletal structure adapt to shear stress to facilitate changes in cell shape and migration. Shear forces are transmitted from

the cell surface through the cytoskeleton to focal adhesions, which are sites of strain focusing and are individually mechanosensitive structures. Applying force to focal adhesions causes them to grow in the direction of force and promotes cytoskeletal reinforcement. [18, 19] At the level of individual focal adhesions in a cell exposed to shear stress, the direction of initial focal adhesion remodeling is associated with the orientation of an individual focal adhesion with respect to the attached stress fiber. [20] In confluent monolayers total focal adhesion area is unchanged by shear stress, but the area of individual focal adhesions increases due to merging of existing adhesions. As the cells align with the direction of flow, focal adhesions also align with the flow direction. [21] In single cells, the onset of shear stress stimulates not only the formation of new focal adhesions, but a transient increase in focal adhesion area followed by disassembly of existing adhesions as cells began to migrate in the direction of flow. [22] Force transmission to focal adhesions, which is critical for activating mechanotransduction, is regulated by the cytoskeleton. Depolymerization of the actin cytoskeleton using latrunculin results in decreased focal adhesion (FA) displacement, which is indicative of reduced force transmission. [13] Actin cytoskeleton depolymerization also inhibits Src activation that is induced throughout the cell by local magnetic bead pulling, suggesting that the actin cytoskeleton plays an important role in transmitting forces to distant sites of mechanotransduction. [23] The dynamic changes in cytoskeletal organization that occur under shear stress might then regulate force transmission to focal adhesions to modulate mechanosensing.

Cytoskeletal alignment of endothelial monolayers to the direction of shear stress is an active process that requires dynamic regulation of Rho and Rac activity. These two

small GTPases are central to regulating actin cytoskeletal organization. Rho is a major regulator of stress fiber assembly and cell contractility, while Rac regulates the formation of protrusive ruffles of polymerized actin. [24, 25] Shear stress-dependent regulation of Rho activity causes depolymerization of stress fibers, and then their reassembly in the flow direction, while regulation of Rac is required for establishing correct planar cell polarity. [26, 27] If cytoskeletal remodeling, Rac activity or Rho activity are blocked alignment does not occur, indicating that cell shape alignment is dependent on cytoskeletal remodeling. [28, 29, 30]

As in many other examples of directed cell migration, dynamic Rho and Rac activity are also required for proper regulation of shear stress-induced polarization and mechanotaxis of single cells. If single endothelial cells are transfected with dominant-negative Rho, migration speed under shear stress is unaffected. However, these cells migrate randomly rather than downstream. Similarly, cells transfected with dominant-negative Rac also migrate randomly under shear stress; however, their migration speed is reduced. Effects similar to Rho inhibition are also seen with myosin inhibitors, suggesting that disruption of cytoskeletal contractility is key in inhibiting mechanotaxis. [31]

The Rho and Rac signaling required for structural remodeling under shear stress is dynamic. In confluent endothelial monolayers, Rho activity is transiently downregulated 5 minutes after the onset of shear stress, in a manner similar to that previously observed to be due to new integrin ligation during the initial spreading and adhesion of cells. [26, 32] Rho activity then returns to baseline levels after 1 hour of shear stress. However, in subconfluent human umbilical vein endothelial cells, there is a quick burst of Rho activity

within 5 minutes, after which Rho activity is downregulated at 15 minutes and then is later reactivated after 2 hours. [31] This suggests that while dynamic Rho regulation is required for adaptation to shear stress, the exact pattern of Rho activity induced by shear stress depends on other factors in the microenvironment. Even though monolayer alignment takes hours, the initial downregulation of Rho activity that occurs within minutes of the onset of shear stress is hypothesized to be required for alignment since cells expressing a constitutively active mutant of Rho do not align. [26] Rac activation in monolayers under shear stress follows a pattern opposite of Rho. The onset of shear stress induces transient activation of Rac, which is required for monolayer alignment. [27] In single cells, Rac activity is also increased after the onset of shear stress, which promotes formation of downstream lamellipodia. [31] Consistent with its role in establishing polarity, in single cells Rac activation under shear stress is polarized and limited to the downstream edge of the cell. Rac also is an important link between structural remodeling and inflammatory signaling. Rac causes activation of NF- κ B, a transcription factor which upregulates the expression of ICAM-1 and VCAM-1 to promote leukocyte recruitment. [27]

Integrin signaling is required for the regulation of Rho and Rac activities that facilitate structural adaptation to shear stress. The onset of shear stress activates integrins in confluent monolayers through phosphatidylinositol-3-kinase (PI3K), which stimulates integrin conformational activation and subsequent binding to the extracellular matrix (ECM). [33] This integrin binding activates the downstream signaling that controls alignment and inflammatory signaling. Shear stress also induces integrin activation and

binding in single cells, which drives the formation of downstream protrusions that facilitate polarization and mechanotaxis. [34, 35]

When new integrin ligation is blocked, Rho is not regulated and structural adaptation does not occur. [26, 27] It has been recently shown that the GTPase activating protein (GAP) p190RhoGAP is required for Rho inactivation at the onset of shear stress in confluent monolayers. [36] Activation of p190RhoGAP, as measured by increased phosphorylation, is dependent on β_1 integrins and Src activation in a pathway consistent with previous reports of p190RhoGAP activation in the initial adhesion and spreading of cells. [37] If either β_1 integrins or Src activity is blocked, p190RhoGAP is not phosphorylated. This initial p190RhoGAP-dependent inactivation of Rho is required for cell alignment to the flow direction, as well as the formation of increased stress fibers during structural adaptation. Treating with siRNA against p190RhoGAP blocks both alignment and increased stress fibers, indicating that this pathway is critical for regulation of Rho activity and therefore structural remodeling under shear stress. [36] This pathway in confluent monolayers is clearly established, but the mechanism by which Rho is regulated in response to shear stress in single cells remains unknown.

In confluent monolayers Rac activation is dependent on integrin signaling, similar to what has been observed in shear stress-induced Rho inactivation. If integrin binding is blocked, Rac activation does not occur. [27] In the context of mechanotaxis and alignment which both require the cell to polarize in the direction of flow, Rac activation is limited to the downstream side of the cell. [27] It has been hypothesized that this polarized activation is due to a polarized distribution of integrin binding. Specifically, the integrin $\alpha_4\beta_1$ is phosphorylated at the downstream edge of endothelial cells exposed

to shear stress. This $\alpha_4\beta_1$ phosphorylation is dependent on protein kinase A (PKA), and is required for activation of Rac at the downstream edge of the cell. [38] Separate from Rac activation at the downstream edge, there is also a mechanism for suppressing Rac activity at the upstream side of single cells. This mechanism involves downregulation of paxillin phosphorylation, which in turn prevents phosphorylation and activation of p130Cas and the RacGEF DOCK180. [20]

Since the pathways controlling Rho and Rac activation are integrin-dependent, it is not surprising that extracellular matrix composition regulates integrin-dependent structural remodeling and inflammatory pathways by controlling which subsets of integrins are ligated. In cells interacting with fibronectin, the onset of shear stress activates NF- κ B signaling pathways that are not activated if the cells are interacting with collagen. [39] This differential regulation also controls structural remodeling, since cells interacting with fibronectin align to unidirectional laminar shear stress more quickly than cells interacting with collagen. [40] Furthermore, crosstalk between different integrins causes ECM-specific suppression of integrin activation. For example, cells interacting with collagen through $\alpha_2\beta_1$ integrins activate PKA, which suppresses the activation of $\alpha_v\beta_3$ through talin. Conversely, cells interacting with fibronectin through $\alpha_v\beta_3$ or $\alpha_5\beta_1$ activate protein kinase C (PKC), which suppresses $\alpha_2\beta_1$ activation. [41] This suggests integrin signaling under shear stress is matrix-specific and this specificity is maintained by active suppression of other sets of integrins that might be ligated such small amounts of other ECM proteins would not cause signaling and ECM composition would have to change significantly to overwhelm this crosstalk mechanism.

Other microenvironmental cues that guide integrin ligation and cytoskeletal organization can also regulate shear stress-induced responses. Endothelial cells have been plated on micropatterned lines of fibronectin of varying width and then subjected to laminar shear stress. Endothelial cells will align along the micropatterned lines, and this established organization inhibits mechanotaxis. Once the cells are released from this geometric constraint, they will proceed to migrate in the direction of flow. [14] Micropatterning can also control other cell behaviors, as evidenced by the combined effect of micropatterns and shear stress on endothelial apoptosis. Increased apoptosis is induced by limiting cell adhesion to narrow micropatterned lines; however, this effect can be countered by shear stress-dependent Rho activation and FAK phosphorylation. [42] Aside from flat micropatterns, studies using patterns of grooves or holes to establish substrate topology have shown that the dimensions of the topology can regulate how the cells respond to shear stress, suggesting that cells are integrating physical cues from both the substrate and shear stress. For anisotropic topographies, such as grooves, cells will align with the direction of the groove in the absence of flow. When shear stress is applied, depending on the direction of the grooves they will either compete with or add to shear stress induced mechanotaxis. [43] Varying the size of topographic cues shows that features perpendicular to flow that are larger than about 800 nm impede both cell alignment and mechanotaxis. [44] These studies suggest that not only ECM composition, but also the physical organization and structure of the extracellular matrix have the potential to regulate shear stress-induced structural remodeling.

1.3 Fibronectin Assembly

Fibronectin is an extracellular matrix protein important for guiding development and wound healing. The fibronectin monomer is made up of three types of domains (Type I, II, and III), and it is expressed as a dimer that contains a disulfide linkage at the C-terminus. The fibronectin monomer contains 12 Type I domains and 2 Type II domains which make up domains critical for fibronectin-fibronectin interactions, including an N-terminal region critical for formation of fibronectin fibrils, as well as interactions with other types of ECM proteins. Each monomer also contains 15-17 Type III domains, depending on alternative splicing of two domains named IIIA and IIIB. These two extra Type III domains are expressed in fibronectin secreted by most types of cells but not in plasma fibronectin, which is secreted into the blood by hepatocytes. Type III domains are especially important for cell interactions since the major binding site for integrins is in the 9th and 10th Type III domains of the fibronectin molecule.

The cell-mediated polymerization of fibronectin, called fibronectin fibrillogenesis or assembly, is required for formation of fibronectin-based ECM and as a provisional matrix for the assembly of other ECM components during development and wound healing. During development, fibrillogenesis is essential for guiding cell polarity and tissue morphogenesis. [45, 46] Fibronectin can also regulate assembly and turnover of other ECM components, as well as contribute to tissue mechanical strength. [47, 48, 49] Fibronectin assembly plays a vital role in vascular remodeling, since inhibiting fibronectin assembly blocks the intima-media thickening induced by a murine partial carotid ligation model not only by preventing ECM deposition but also by reducing cell proliferation, ICAM-1 and VCAM-1 expression, and infiltration of inflammatory cells.

[50] In the context of atherosclerosis, increased fibronectin expression and assembly stimulated by disturbed flow patterns results in deposition of fibronectin and activation of inflammatory signaling in lesion-prone regions. [51, 52] Cells assemble fibronectin dimers into supra-molecular assemblies of fibrils which are highly elastic and are maintained under tension. [53] Study of individual fibronectin fibrils has revealed that they can be stretched up to 8 times their relaxed length. [54] Fibronectin is gradually assembled into a complex fibrillar structure and is not maintained in the ECM unless this occurs. [55] Assembly is dependent on interactions with fibronectin binding integrins and other fibronectin monomers, as well as and the activation of Rho-dependent contractility. [56, 57] Blocking of either of these interactions will result in attenuation of fibril formation. Disassembly of fibrils due to treatment with a fragment of fibronectin from the first type III repeat results in inhibition of Rho-dependent cytoskeletal remodeling and phosphorylation of focal adhesion proteins, [588] indicating that fibrillar fibronectin and Rho may participate in a feedback loop in which Rho activity promotes fibrillogenesis and the presence of fibrils promotes continued Rho activation.

Endothelial cells predominantly express two major fibronectin binding integrins: $\alpha_v\beta_3$ and $\alpha_5\beta_1$. These two integrins have different binding sites within the fibronectin molecule. While both bind the RGD site in repeat 9, $\alpha_5\beta_1$ additionally binds a PHSRN synergy site in repeat 10, which appears to confer the ability to activate Rho and effectively promote fibrillogenesis. [59, 60, 61] There is also a second binding site for $\alpha_v\beta_3$ in the 5th type I repeat of the fibronectin dimer. [62] In bovine aortic endothelial cells (BAEC) treated with siRNA against the EDB variant of fibronectin, which includes an alternatively spliced exon between the 7th and 8th type III repeats, cells engage $\alpha_5\beta_1$

and $\alpha_v\beta_3$ equally. However, untreated BAEC engage $\alpha_5\beta_1$ almost exclusively. [63] In Chinese hamster ovary (CHO) cells interacting with fibronectin, cells normally used $\alpha_5\beta_1$ for migration, but if interacting with fibronectin that has had the synergy site deleted, they switch to $\alpha_v\beta_3$. [64] These studies indicate that changes in fibronectin structure or availability of binding sites can regulate whether cells engage $\alpha_5\beta_1$, $\alpha_v\beta_3$, or both. However, it is unknown whether fibrillogenesis regulates affinity of one integrin over the other or availability of particular binding sites.

Fibronectin fibrillogenesis may alter presentation of integrin binding sites, but the stiffness of the surface cells are interacting with *in vitro* is also changed during the process of fibronectin assembly. Initially, the fibronectin-coated glass surface is very stiff, since the modulus of glass is on the order of gigapascals. As assembly progresses, a layer of fibronectin is built up, the cells are less able to directly interact with the glass, and stiffness is reduced. The stiffness of individual fibronectin fibrils is a function of strain and varies from hundreds of kilopascals to several megapascals. [54] The stiffness of assembled fibronectin ECM *in vitro*, as measured by atomic force microscopy (AFM), is reported to be only 400 pascals, which is extremely soft. [65] Substrate stiffness is an important regulator of integrin-mediated signaling. Stiffer substrates promote integrin clustering, focal adhesion formation, and cytoskeletal organization. Since these structures are integral to shear stress-induced remodeling and alignment, substrate-dependent regulation of their organization could impact responses to shear stress. Therefore, fibronectin assembly could modulate integrin-dependent signaling through effectively lowering substrate stiffness.

1.4 Fibronectin and shear stress

The presence of fibronectin regulates endothelial responses to shear stress. Fibronectin deposition contributes to inflammatory signaling and is a marker of atherosclerotic lesions *in vivo*. [51] It has been shown that atheroprone shear stress profiles promote deposition and assembly of fibronectin into the extracellular matrix by activating both fibronectin expression and integrin activation, creating an inflammatory positive feedback loop in the endothelium. [52] However, whether structural remodeling of endothelial cells is also regulated by this fibronectin deposition mechanism remains unknown. Measurements of fibronectin fibril deformation under shear stress suggest that shear forces are not only transmitted into the cell, but through focal adhesions to the underlying ECM. After 48 hours of shear stress, ECM structures also align with the direction of flow in the same manner as endothelial cells. [66] Since applied forces can also cause fibronectin unfolding and increase assembly, [67] shear stress may not only alter the orientation of fibronectin fibrils, but their biochemical interactions with cells and other ECM components.

The two major fibronectin-binding integrins in endothelial cells, $\alpha_5\beta_1$ and $\alpha_v\beta_3$, are both implicated in mechanosensing. While both $\alpha_5\beta_1$ and $\alpha_v\beta_3$ integrins bind fibronectin, their downstream signaling is different. There is some evidence that Rho activity can be regulated differently during spreading by these two integrins. During spreading, adhesion through $\alpha_5\beta_1$ causes a larger increase in Rho activity than adhesion through $\alpha_v\beta_3$, but the mechanism is unknown. [59] In studies using magnetic beads bound to integrins, $\alpha_5\beta_1$ contributes to adhesion strength while $\alpha_v\beta_3$ is critical for recruitment of talin and reinforcement of the adhesive interface. [68] Since integrin-

mediated dynamic regulation of Rho activity is required for structural adaptation to shear stress, if $\alpha_5\beta_1$ and $\alpha_v\beta_3$ integrins regulate Rho differently they may regulate structural remodeling under shear stress differently by controlling the ability of the cell to remodel its cytoskeletal and focal adhesion structure.

Although current studies have linked fibronectin deposition and integrin binding to inflammatory signaling and structural remodeling that may promote atherosclerosis, it remains unknown whether fibronectin assembly can regulate the signaling pathways involved in structural adaptation to shear stress. Because feedback through Rho and integrin signaling are required for both fibronectin assembly and structural adaptation to shear stress, we hypothesized that fibronectin assembly regulates shear stress-induced structural remodeling through regulation of integrin binding. In this study, we show for the first time that fibronectin assembly regulates structural remodeling under shear stress. We also show that fibronectin assembly regulates the relative distribution and binding of $\alpha_v\beta_3$ and $\alpha_5\beta_1$ integrins. These data show that we can control sensitivity of mechanosignaling stimulated by shear stress by altering the organization of the extracellular microenvironment and provide insight into how the cell integrates mechanical signals.

Chapter 2: Experimental Methods

2.1 Preparing Endothelial Cells

2.1.1 General Endothelial Cell Culture

Bovine aortic endothelial cells (BAEC) were purchased from VEC Technologies (Rensselaer, NY). BAEC were maintained in complete growth media consisting of Dulbecco's Modified Eagle Medium (DMEM, Gibco, Carlsbad CA) supplemented with 10% heat inactivated newborn calf serum (NCS, HyClone, Logan UT), 2.92 mg/mL L-glutamine (Gibco, Carlsbad CA), 50 IU penicillin (Gibco, Carlsbad CA), and 50 µg/mL streptomycin (Gibco, Carlsbad CA). All BAEC used for experiments were between passages 11 and 17.

2.1.2 Transfection

To visualize focal adhesions, BAEC were transiently transfected to express an exogenous fluorescent protein using Lipofectin (Invitrogen, Carlsbad CA) according to the manufacturer's instructions. Briefly, plasmid DNA encoding a fusion protein of enhanced green fluorescent protein and vinculin (GFP-vinculin) was mixed with the Lipofectin reagent at a ratio of 1:14 in Opti-MEM media (Gibco, Carlsbad CA). The protein and Lipofectin were allowed to form complexes, and incubated on cells for 3 hours. Cells were rinsed with fresh complete growth media, and GFP-vinculin expressing cells were imaged 48 hours after transfection.

2.1.3 Rhodamine Labeling of Fibronectin

For experiments in which imaging of fibronectin ECM was required, BAEC were plated on rhodamine-labeled fibronectin. To randomly label fibronectin with rhodamine, bovine plasma fibronectin (Sigma-Aldrich, St. Louis MO) was reconstituted in 50 mM borate (pH 8.5) at 1 mg/mL, mixed with 5-(and 6)-carboxytetramethylrhodamine succinimidyl ester (NHS-rhodamine, Pierce, Rockford IL) at a molar ratio of 20:1, and incubated for 1 hour at room temperature in the dark. Labeled fibronectin was separated from remaining NHS-rhodamine by size by filtration through a cross-linked dextran column (Pierce, Rockford IL). Fractions were collected from the column with phosphate buffered saline (PBS, Invitrogen, Carlsbad CA) and protein concentration measured by a bicinchoninic acid (BCA) assay kit (Pierce, Rockford IL). Briefly, 200 μ L of BCA reagent was added to 10 μ L protein samples in duplicate and to a standard curve of samples of known concentration in triplicate in a 96-well plate, and incubated at 37°C for 30 minutes. Absorbance at 590 nm was then read in a plate reader, and total protein quantified from the standard curve. Rhodamine-fibronectin was aliquoted, flash frozen in LN₂, and stored at -80°C until use.

2.1.4 Preparing sparse BAEC interacting with unassembled fibronectin

A 15 μ g/mL solution of bovine plasma fibronectin (Sigma-Aldrich, St. Louis MO) in PBS was incubated on glass surfaces (1 μ g/cm²) for 1 hour at room temperature. Surfaces were then rinsed 3 times for 5-10 minutes each time with PBS, and finally rinsed with complete media before plating BAEC. To achieve sparse surface coverage, cells were plated at 5,000-10,000 cells/cm² and allowed to adhere overnight (14-18 hours) before application of shear stress. For experiments that required serum starvation,

sparse BAEC were plated in complete growth media for 4-6 hours and allowed to adhere, then starved in media containing 0.5% NCS for 12 hours before application of shear stress.

2.1.5 Preparing sparse BAEC interacting with assembled fibronectin

To create assembled fibronectin matrix, glass surfaces were coated with 15 $\mu\text{g/mL}$ bovine plasma fibronectin diluted in PBS for 1 hour at room temperature, rinsed 3 times for 5-10 minutes each time with PBS, and finally rinsed with complete growth media. BAEC were then plated at 50,000 cells/ cm^2 and allowed to grow for 48 hours, which allows time for the formation of a well-assembled layer of fibronectin ECM several microns thick. Fibronectin was then isolated by rinsing surfaces with 3% Triton X-100 in PBS followed by 1% sodium deoxycholate (Sigma-Aldrich, St. Louis MO) in Tris buffered saline (TBS, 50 mM Tris, 150 mM NaCl, pH8.0) to remove cellular material. Isolated fibronectin matrix was then rinsed twice with PBS and incubated in 1% bovine serum albumin (BSA, Sigma-Aldrich, St. Louis MO) in PBS for 1 hour at room temperature before cell plating. When immunostained for fibronectin, this isolated fibronectin was visually similar to assembled fibronectin underneath an intact endothelial monolayer, indicating that the isolation procedure did not disrupt the fibrillar structure of the fibronectin. (Figure 1) BAEC were plated at 5,000-10,000 cells/ cm^2 and allowed to adhere overnight (14-18 hours) before application of shear stress. For experiments that required serum starvation, sparse BAEC were plated in complete media for 4-6 hours and allowed to adhere, then starved in media containing 0.5% NCS for 12 hours before application of shear stress.

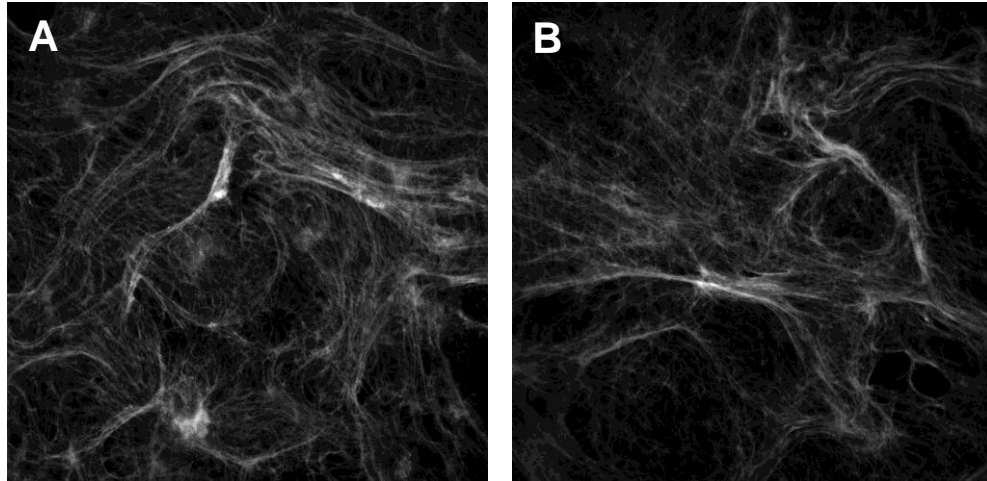


Figure 1. Fibronectin immunostaining of (A) assembled fibronectin matrix underneath a confluent monolayer. (B) assembled fibronectin matrix isolated from a confluent monolayer, before plating sparse BAEC.

2.1.6 Preparing confluent BAEC interacting with unassembled fibronectin

Glass surfaces were coated with 15 $\mu\text{g/mL}$ bovine plasma fibronectin in PBS for 1 hour at room temperature, rinsed 3 times for 5-10 minutes each time with PBS, and finally rinsed with complete growth media. BAEC were then plated at 50,000 cells/ cm^2 and allowed to grow for 60 hours. To create monolayers interacting with unassembled fibronectin, fibronectin assembly was prevented by adding a peptide derived from *S. pyogenes* that competitively binds the assembly domain of fibronectin at the time of plating. This peptide blocked the formation of assembled fibronectin matrix over the entire culture period. To determine the optimal dose of blocking peptide, BAEC were treated with 0, 0.25, 0.5, or 1 $\mu\text{g/mL}$ peptide and allowed to grow for 60 hours. These samples were immunostained for fibronectin to evaluate fibronectin assembly. (Figure 2) From this study, the dose of 0.5 $\mu\text{g/mL}$ peptide was found to be sufficient to block fibronectin assembly, and this concentration was used for all shear stress experiments.

For experiments that required serum starvation, BAEC were starved in media containing 0.5% NCS for 12 hours before application of shear stress.

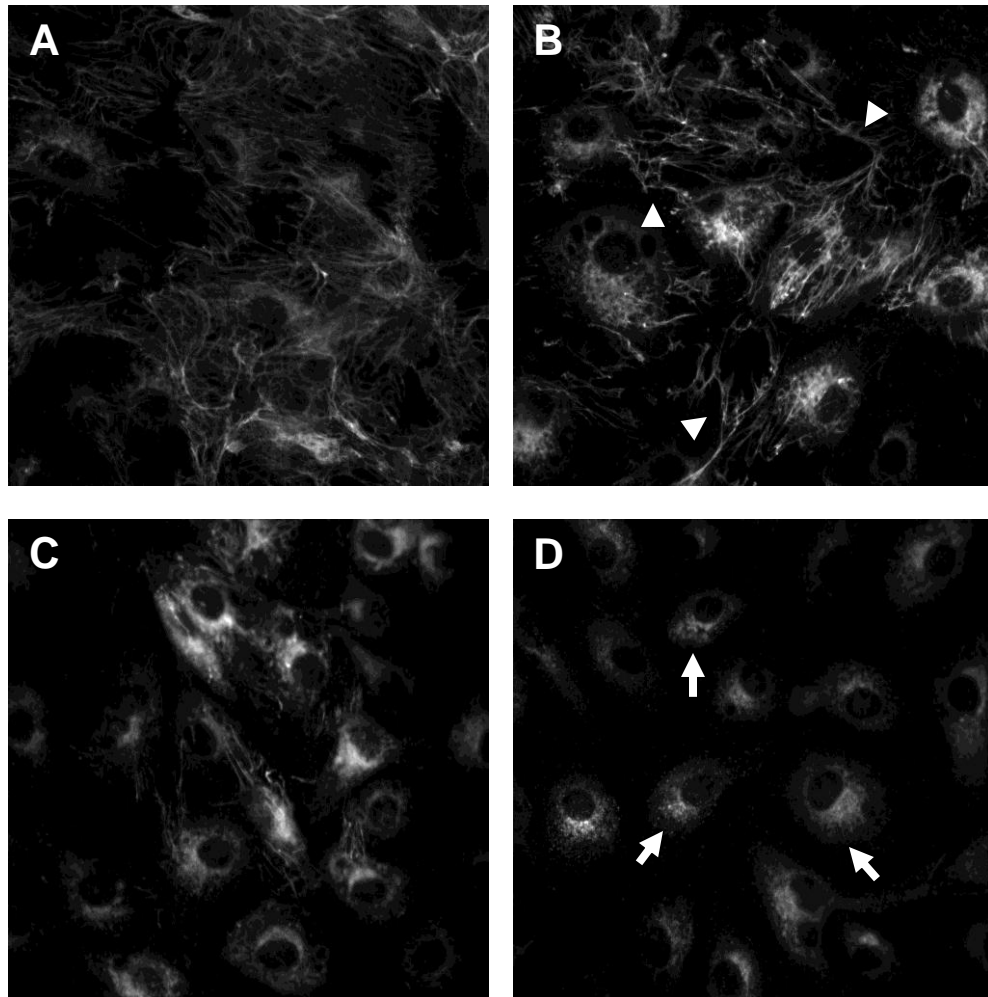


Figure 2 Dose response to assembly blocking peptide. Fibronectin staining in BAEC treated with (A) 0, (B) 0.1, (C) 0.25, or (D) 0.5 $\mu\text{g/mL}$ assembly blocking peptide. Fibrous structures are extracellular fibronectin fibrils (arrowheads, B), while punctate, perinuclear structures are intracellular fibronectin not yet secreted by the cell (arrows, D).

2.1.7 Preparing confluent BAEC interacting with assembled fibronectin

Glass surfaces were coated with 15 $\mu\text{g/mL}$ bovine plasma fibronectin in PBS for 1 hour at room temperature, rinsed 3 times for 5-10 minutes each time with PBS, and finally rinsed with complete growth media. BAEC were then plated at 50,000 cells/cm² and allowed to grow for 60 hours. For experiments that required serum starvation, BAEC were starved in media containing 0.5% NCS for 12 hours before application of shear stress.

2.1.8 Function Blocking Antibodies

For migration studies that required blocking various integrin subunits, BAEC were treated with function blocking antibodies. Samples were incubated with 20 $\mu\text{g/mL}$ of the blocking antibodies listed in Table 1 for 1 hour at 37°C, then immediately assembled into the flow chamber and subjected to shear stress and image acquisition.

Table 1. Integrin blocking antibodies

Antibody	Source
Mouse anti-human $\alpha_v\beta_3$, clone LM609	Millipore
Mouse anti-human α_5 , clone JBS5	Santa Cruz Biotechnology
Mouse anti-human α_2 , clone P1E6	Santa Cruz Biotechnology

2.2 Shear Stress Application

2.2.1 Flow Loop and Shear Stress

A recirculating flow loop was constructed to generate shear stress across the surface of BAEC. A diagram of the loop design is show below. (Figure 3) The lower

reservoir contained 100 mL of either complete growth media or media containing 0.5% NCS, and was connected to a humidified supply of 5% CO₂ to maintain a pH of 7.4. Both the lower and upper reservoirs were heated, using a water bath and heated syringe holder respectively, to maintain a temperature of 37°C. The flow loop was assembled under sterile conditions and media circulated through the loop with a clean, sterile glass slide in the flow chamber to ensure that there were no air bubbles in the flow loop or chamber before introduction of the cell sample. For application of laminar unidirectional shear stress, the appropriate flow rate to generate 15 dyn/cm² wall shear stress in a parallel plate flow chamber was calculated from the equation

$$\tau_w = \frac{6\mu Q}{wh^2}$$

where μ is the fluid viscosity, Q is volumetric flow rate, w is the chamber width and h is the chamber height.

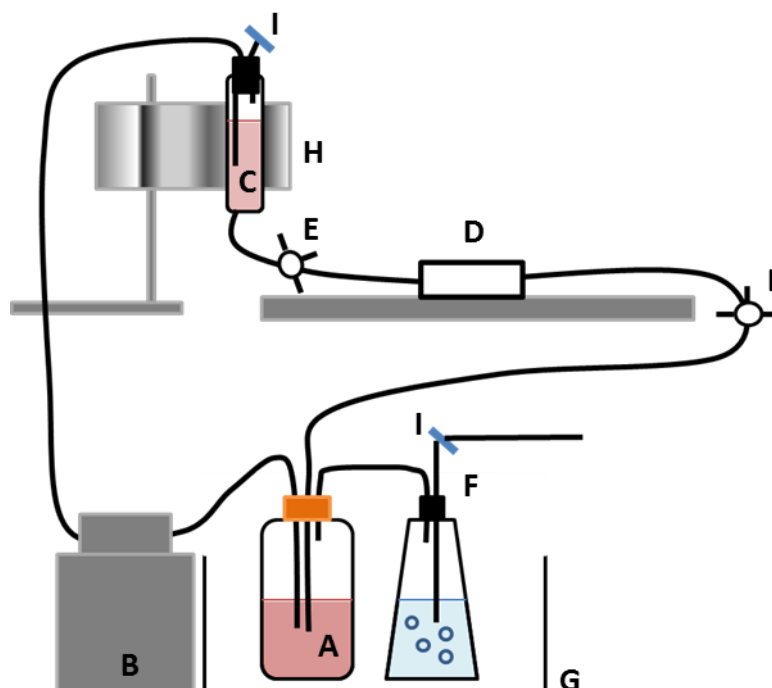


Figure 3. Gravity-driven recirculating flow loop. Media in the lower reservoir (A), is drawn through tubing connected to a peristaltic pump (B) to maintain a constant fluid level in the upper reservoir (C). Media flows from the upper reservoir through the flow chamber (D) and back to the lower reservoir. Fluid flow through the chamber is controlled by stopcocks (E). Temperature and pH are maintained by a humidified supply of CO₂ (F) and a water bath (G) and heat block (H) to maintain the lower and upper reservoirs at 37°C. The CO₂ line and upper reservoir outlet to the atmosphere contain sterile gas filters (I) to maintain the sterility of the system.

2.2.2 Fluorescence Imaging Studies

For experiments that required fluorescence imaging, cells were exposed to shear stress in a Biopetechs (Butler, PA) FCS2 parallel plate flow chamber connected to the gravity-driven recirculating flow loop described above. To incorporate cells into this chamber, BAEC were cultured as described in Section 2.1 on 40 mm round German glass coverslips (BellCo, Vineland NJ) that had been soaked in 1% Sparkleen overnight, rinsed for 15 minutes with tap water, rinsed for 15 minutes with distilled water, and then autoclaved. Given a fluid viscosity of 1.2 cP, chamber height of .025 cm and chamber

width of 1.4 cm, the flow rate used to generate 15 dyn/cm^2 shear stress was 11 mL/min. To maintain a constant temperature of 37°C , the chamber was connected to a feedback temperature controller.

2.2.3 Cell Migration Studies

For experiments on cell migration, cells were exposed to shear stress in a custom-built parallel plate flow chamber connected to the gravity-driven flow loop described above. For this chamber, BAEC were cultured as described in Section 2.1 on 38 x 75 mm glass slides (Corning, Tewksbury MA) which had been prepared in the same manner as the round coverslips described above. Before culturing BAEC, a gasket cut from press-to-seal silicone (Invitrogen, Carlsbad CA) was applied and pressed firmly to create a 6 mm sealed border along all edges of the slide. This gasket remained intact throughout the entire culture and experiment period. Given a fluid viscosity of 1.2 cP, chamber height of .025 cm, and chamber width of 1.4 cm, the flow rate used to generate 15 dyn/cm^2 shear stress was 88 mL/min.

2.3 Data Collection

2.3.1 Microscopy

Imaging of both live and fixed samples was performed on a Deltavision restoration microscopy system. This system is made up of an Olympus IX70 microscope, cooled CCD camera, mercury lamp for fluorescence imaging and halogen lamp transillumination for brightfield or phase contrast imaging. For fluorescence imaging, the filter sets implemented included red ($\lambda_{\text{ex}}=555 \text{ nm}$, $\lambda_{\text{em}}=617 \text{ nm}$), green ($\lambda_{\text{ex}}=490 \text{ nm}$,

$\lambda_{em}=528$ nm), and blue ($\lambda_{ex}=360$ nm, $\lambda_{em}=457$ nm) emission. For fixed samples, fluorescence imaging was performed with either a 60X/1.4NA oil immersion objective or a 40X/0.75NA air objective. Samples were imaged by taking serial image planes through the sample 0.2 μ m apart at 10 different fields of view.

Live cell fluorescence studies were performed to concurrently image GFP-vinculin-labeled focal adhesions and rhodamine-labeled fibronectin. Cells expressing a moderate level of GFP were chosen for imaging. Serial image planes through the sample were taken 0.2 μ m apart every 90 seconds using a 60X/1.4NA oil immersion objective. After imaging the sample under no-flow conditions for 15 minutes, shear stress was initiated and imaging continued for another 15 minutes.

Migration and monolayer alignment studies were performed by imaging live samples in a single plane at using a 10X/0.3NA phase objective. Samples were imaged every 5 minutes starting 15 minutes before the onset of shear stress and continuing for up to 18 hours of shear stress exposure.

2.3.2 Immunofluorescence

Immunofluorescence was performed to visualize the distribution and organization of fibronectin, cytoskeleton, and other adhesive structures. The antibodies used are listed in Table 2. Generally, BAEC samples were fixed in ice-cold 4% paraformaldehyde for 20 minutes, then rinsed 3 times with PBS for 5 minutes each time. Samples were permeabilized with 0.2% Triton X-100 in PBS for 2 minutes, then again rinsed 3 times with PBS for 5 minutes each time. Samples were blocked with 1% BSA in PBS for 1 hour, followed by incubation with the primary antibody diluted in 0.1% BSA in PBS for 1 hour at room temperature. Samples were rinsed 3 times with PBS for 10 minutes each

time, blocked with 2% normal goat serum (NGS) in PBS for 30 minutes (for secondaries raised in goat), and incubated with the secondary antibody diluted in 2% NGS in PBS for 1 hour in the dark at room temperature. Samples were rinsed 3 times with PBS for 10 minutes each time, and mounted on a slide with SlowFade Gold mounting media (Invitrogen, Carlsbad CA). To visualize actin, samples were fixed, permeabilized, and incubated with 0.5 $\mu\text{g/mL}$ tetramethylrhodamine B isothiocyanate-phalloidin (TRITC-phalloidin, Sigma-Aldrich, St. Louis MO) for 30 minutes. Samples were rinsed 3 times for 5 minutes each time, then mounted. When immunostaining for $\alpha_v\beta_3$ with the LM609 antibody, a 3 hour primary incubation time was used.

Table 2. Antibodies used for immunofluorescence

antibody	source	dilution
Anti-human fibronectin, clone FN-15	Sigma-Aldrich	1:200
TRITC-phalloidin (anti-F-actin)	Sigma-Aldrich	0.5 $\mu\text{g/mL}$
Mouse anti-human $\alpha_v\beta_3$, clone LM609	Millipore	1:100
Mouse anti-human $\alpha_5\beta_1$, clone HA5	Millipore	1:500
Rabbit anti-human α_v , polyclonal	Millipore	1:200
AMCA-labeled goat anti-rabbit IgG	Jackson ImmunoResearch	1:100
DyLight 488-labeled goat anti-mouse IgG	Jackson ImmunoResearch	1:300
Cy3-labeled goat anti-mouse IgG	Jackson ImmunoResearch	1:300
Cy2-labeled goat anti-mouse IgG	Jackson ImmunoResearch	1:300

2.3.3 Integrin Crosslinking

To crosslink and isolate ligand bound integrins, a method adapted from Keselowsky and Garcia [69] was used. Cell samples plated on rhodamine-fibronectin were exposed to shear stress, then immediately treated with ice cold 1 mM 3,3'-Dithiobis[sulfosuccinimidylpropionate] (DTSSP, Pierce, Rockford IL) in PBS to cross

link bound integrins. This reaction was quenched with the addition of 50 mM Tris in PBS for 10 minutes at room temperature. Non cross-linked cell material was removed by incubation with 0.1% sodium dodecyl sulfate (SDS, Bio-Rad, Hercules CA) and 2 mM phenylmethylsulfonyl fluoride (PMSF, Pierce, Rockford IL) in PBS for 10 minutes at room temperature, then samples were rinsed 3 times with PBS. Following this treatment, immunostaining was performed for both $\alpha_5\beta_1$ and α_v integrins.

2.4 Data Analysis

2.4.1 Image Analysis and Tracking

Monolayer alignment was quantified using a custom Matlab algorithm created by our lab. [14] This algorithm first automatically segmented cells in a monolayer using the bright phase boundary at the edges of cells. The x and y coordinate of each cell centroid in each image was recorded, as well as morphometric measurements of cell shape including area, orientation, and eccentricity. For each time point, the distribution of cell orientations within the monolayer was plotted as a histogram, which was normally distributed. The standard deviation of this histogram (“average deviation”) then represented the degree of alignment of the monolayer. A large average deviation reflected randomly oriented cells, while a small average deviation represented a totally aligned monolayer.

Tracking of single cell migration was performed both manually and using an adaptive snake algorithm plugin for ImageJ. In manual tracking, the position of the center of the cell as identified by the nucleus was tracked over 6 hours of imaging and cell movement. In using the active snake algorithm, the position of the center of the cell

was defined by the centroid calculated from the outline of the cell identified by the algorithm. In both cases, cell positions were exported to Excel for calculating cell speed and direction under shear stress.

Focal adhesion and fibronectin fibril tracking were performed manually in SoftWorx. Registration points and structural features were identified and marked in the first and last images of a 15 minute time period either immediately before or immediately after the onset of shear stress. Features were also tracked in the first minute after the onset of shear stress. Position data were exported to Matlab for analysis.

F-actin content was quantified from deconvolved image stacks of F-actin staining. The three most in-focus images in the stack were summed. Then the resulting image was thresholded using the Li thresholding function, which is an iterative minimum cross entropy method. [70] The percentage of the image above the threshold was averaged across 10 images for each time point, normalized to time zero, and reported as “relative F-actin content.”

Correlation between displacements of focal adhesions and fibronectin fibrils was evaluated by choosing a focal adhesion and its nearest measurement of fibronectin fibril displacement within a neighborhood of 10 μm . If no measurement of fibronectin fibril displacement existed within 10 μm of the focal adhesion, that focal adhesion was not included. Focal adhesion and fibronectin fibril displacement angles and magnitudes were then plotted against each other for both the no-flow condition and after the onset of shear stress.

2.4.2 Statistics

Since the distribution of focal adhesion displacement data was not normal, a non-parametric Mann-Whitney U test was performed to test the null hypothesis that the data came from the same distribution. The null hypothesis was rejected at a significance level of $p < 0.01$. For all other data, a t test was performed at a significance level of $p < 0.05$. For correlation analysis, a t test was performed on the Pearson's correlation coefficient using the statistic:

$$t = \frac{r\sqrt{N-2}}{\sqrt{1-r^2}}$$

where r is the Pearson's correlation coefficient and N is the number of samples. The correlation was considered significant for $p < 0.05$, indicating that the null hypothesis that the correlation coefficient was zero could be rejected with 95% confidence.

Chapter 3: Results

3.1 Sparse Cells

3.1.1 Migration

Mechanotaxis, or shear stress-induced downstream migration, is a well-established fundamental indicator of single endothelial cell mechanosensitivity. Therefore, we hypothesized that if fibronectin assembly regulates mechanotransduction, we would observe assembly-dependent differences in cell motility under shear stress. We tracked the movement of individual BAEC on unassembled or assembled fibronectin over the 6 hours after the onset of shear stress, calculated average cell speed, and plotted the path of migration of each cell. While there was no significant difference at any time point ($p > 0.05$, t test) in the average speed of sparse cells migrating on assembled fibronectin compared to sparse cells migrating on unassembled fibronectin (Figure 4), fibronectin assembly did regulate direction of migration. (Figure 5) Downstream mechanotaxis has been previously observed in single endothelial cells exposed to shear stress, [22] and we also observe downstream migration under shear stress in sparse cells on unassembled fibronectin. However, in sparse BAEC on assembled fibronectin, downstream mechanotaxis did not occur and cells migrate in random directions under shear stress, suggesting that fibronectin assembly inhibits shear stress-induced directional motility. This difference in downstream migration was quantified by measuring

cumulative migration in the x direction, which is the direction of flow. (Figure 6) We found that beginning 1 hour after the onset of shear stress, cells on unassembled fibronectin migrated significantly farther in the x direction than cells on assembled fibronectin ($p < 0.05$, t test). Shear stress is reported to also transiently induce single cell spreading. [71] When we measured cell area and normalized to the area at the onset of shear stress, we saw that on average shear stress induced spreading on a similar time scale and magnitude to previous reports in cells on unassembled fibronectin. This spreading response was initially non-directional, but quickly established a downstream lamellipodia to guide mechanotaxis. Spreading was still induced in cells on assembled fibronectin, but the magnitude was significantly smaller at 15 minutes after the onset of shear stress ($p < 0.05$, t test). (Figure 7)

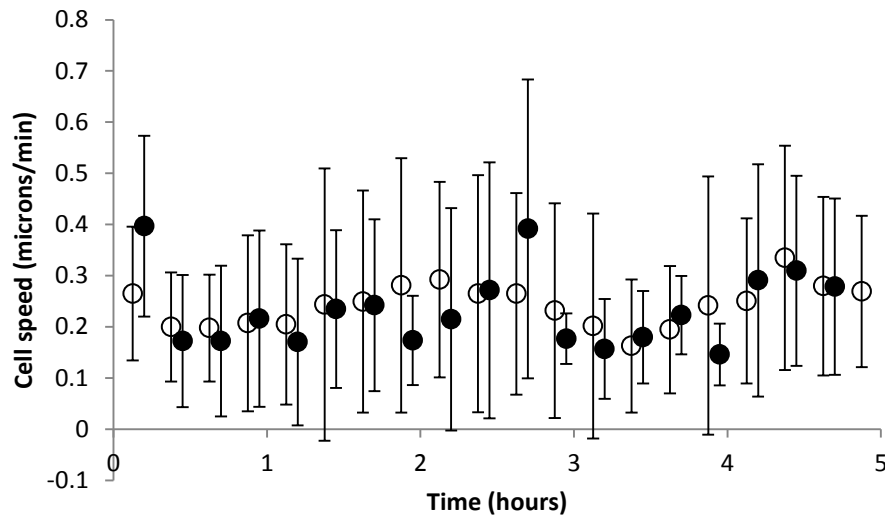


Figure 4. Migration speed of sparse BAEC interacting with assembled (closed circles) or unassembled (open circles) fibronectin under shear stress. Migration speed is not significantly different between the two fibronectin assembly conditions for any time point. ($p > 0.05$, t test)

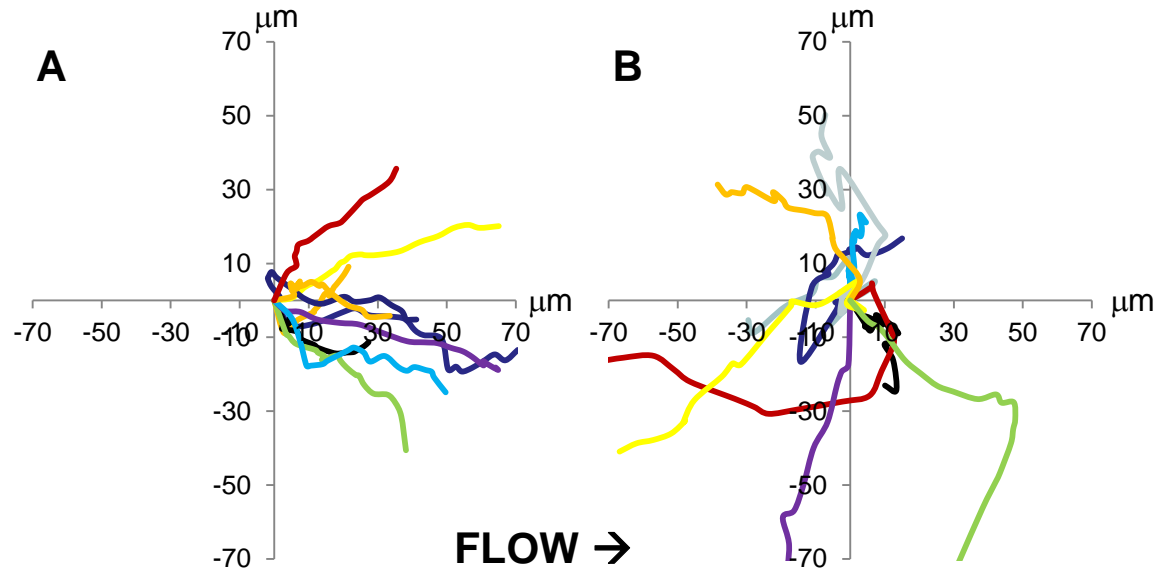


Figure 5. Migration paths of individual BAEC tracked for 6 hours after the onset of shear stress. BAEC interacting with unassembled fibronectin (A), display downstream mechanotaxis (flow is from left to right), while BAEC interacting with assembled fibronectin (B) migrate in random directions under flow.

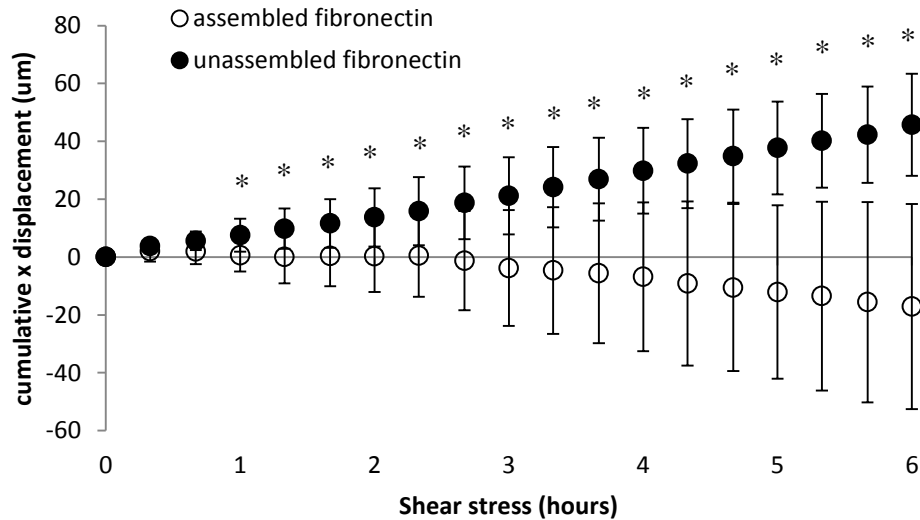


Figure 6. Migration in the direction of flow, as measured by cumulative x displacement, is significantly higher (* $p < 0.05$, t test) in cells interacting with unassembled fibronectin than in cells interacting with assembled fibronectin starting 1 hour after the onset of shear stress.

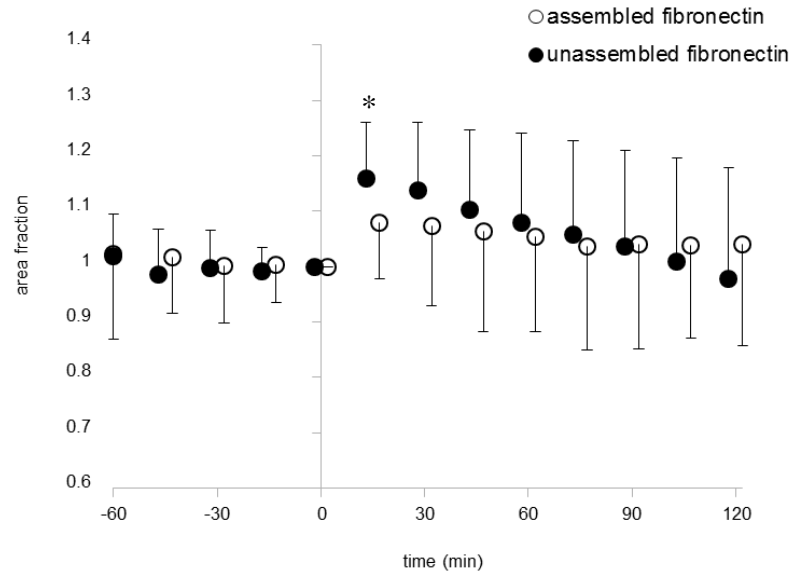


Figure 7. Area of sparse BAEC exposed to shear stress interacting with unassembled (closed circles) or assembled (open circles) fibronectin. Cell area at each time point was normalized to cell area at the onset of shear stress ($t=0$). At 15 minutes after the onset of shear stress, the transient increase in area caused by the onset of shear stress is significantly larger in BAEC interacting with unassembled fibronectin than in BAEC interacting with assembled fibronectin. (* $p<0.05$, t test)

3.1.2 F-actin Remodeling

In order to determine whether fibronectin assembly regulated shear stress-induced actin remodeling in sparse cells in a manner that could explain differences in directional motility and spreading, sparse cells on unassembled or assembled fibronectin were exposed to 0, or 15 minutes of shear stress and stained for F-actin. This staining revealed qualitative but visually apparent assembly-dependent difference in actin organization under no shear stress. In cells on unassembled fibronectin, stress fibers were prominent and cells were well-spread. In comparison, cells on assembled fibronectin had fewer stress fibers, were less spread, and displayed a more polarized, spindle-like morphology. (Figure 8) On both on unassembled and assembled fibronectin, stress fiber content and organization did not visibly change 15 minutes after the onset of shear stress compared to no-flow conditions. In cells on unassembled fibronectin, significantly increased ruffling

($p < 0.05$, t test), or edge-associated actin polymerization, was observed under shear stress consistent with previous reports of shear stress-induced actin remodeling. [13, 71] However, in cells on assembled fibronectin, the shear stress-induced formation of actin ruffles was not significant. ($p = 0.35$, t test) (Figure 9)

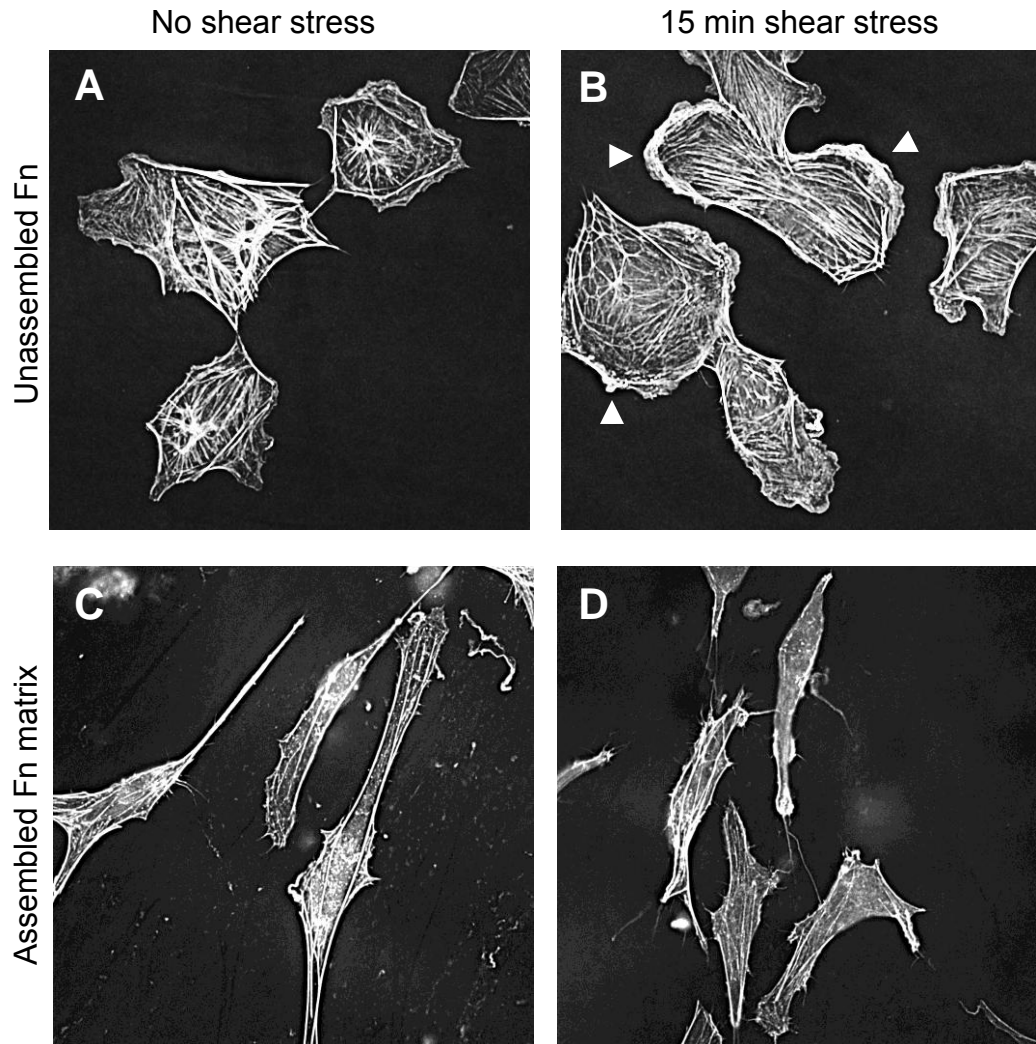


Figure 8. F-actin staining in sparse BAEC interacting with assembled or unassembled fibronectin. BAEC interacting with unassembled fibronectin under no-flow conditions (A) are well spread and display an organized stress fiber network. When shear stress is applied, these cells form peripheral actin ruffles (arrowheads, B). BAEC interacting with assembled fibronectin under no-flow conditions (C) are less spread and have fewer stress fibers, and when shear stress is applied (D), do not form an increased number of visually obvious actin ruffles.

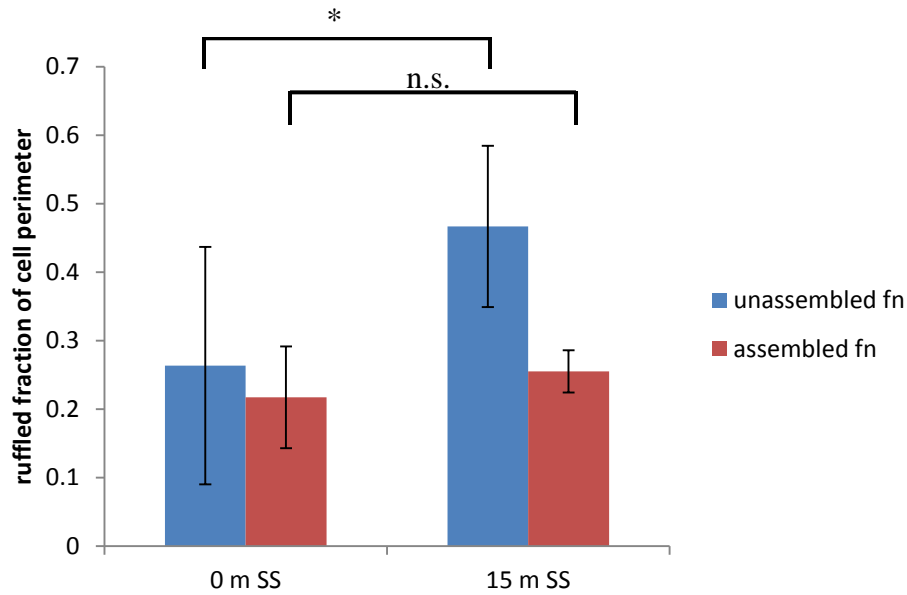


Figure 9. Ruffling at edges of sparse BAEC interacting with assembled or unassembled fibronectin. Ruffling was quantified from images of F-actin staining as the fraction of the cell perimeter that displayed a ruffled morphology. BAEC interacting with unassembled fibronectin display a significantly increased fraction of edge ruffling when exposed to shear stress, (* $p < 0.05$, t test) while BAEC interacting with assembled fibronectin do not. (n.s.=not significant, $p = 0.35$, t test)

3.1.3 Focal Adhesion Displacement

Adhesion to the fibronectin substrate is an important regulator of both motility and mechanotransduction. We hypothesized that fibronectin assembly regulated the mechanical interaction of single cells with the ECM, so we used GFP-vinculin as a marker of focal adhesions to track the movement of individual focal adhesions within a cell. This focal adhesion displacement represents a combination of mechanical movement and biochemical turnover of the adhesion and is indicative of the force balance across the adhesion interface. As previously reported [13], focal adhesion displacement in sparse cells interacting with unassembled fibronectin is reduced at the onset of shear stress. Here, median focal adhesion displacement rate decreased significantly ($p < 0.01$, Mann Whitney U test) from $0.037 \mu\text{m}/\text{min}$ under no-flow

conditions to $0.017 \mu\text{m}/\text{min}$ after the onset of shear stress. (Figure 10) However, in sparse cells interacting with assembled fibronectin, focal adhesion displacement rate did not change significantly with the onset of shear stress. ($p=0.16$, Mann Whitney U test) In this case, under no-flow conditions the median focal adhesion displacement rate was $0.073 \mu\text{m}/\text{min}$, which was significantly higher than the no-flow adhesion displacement rate in cells on unassembled fibronectin. ($p<0.01$, Mann Whitney U test) After the onset of shear stress, displacement rate was $0.058 \mu\text{m}/\text{min}$. (Figure 10) On both unassembled and assembled fibronectin, the direction of focal adhesion displacement under no-flow conditions appeared to be randomly distributed and peripheral adhesions moved centripetally. We also observed that the direction of focal adhesion displacement was transiently shifted downstream in subconfluent cells on assembled fibronectin in the first minute after the onset of shear stress and then returned to a distribution similar to that in the no-flow condition. (Figure 11) This is similar to previous observations in confluent monolayers interacting with assembled fibronectin, [13] and suggests that transient downstream displacement is mainly due to the deformability of the substrate with which the cells are interacting.

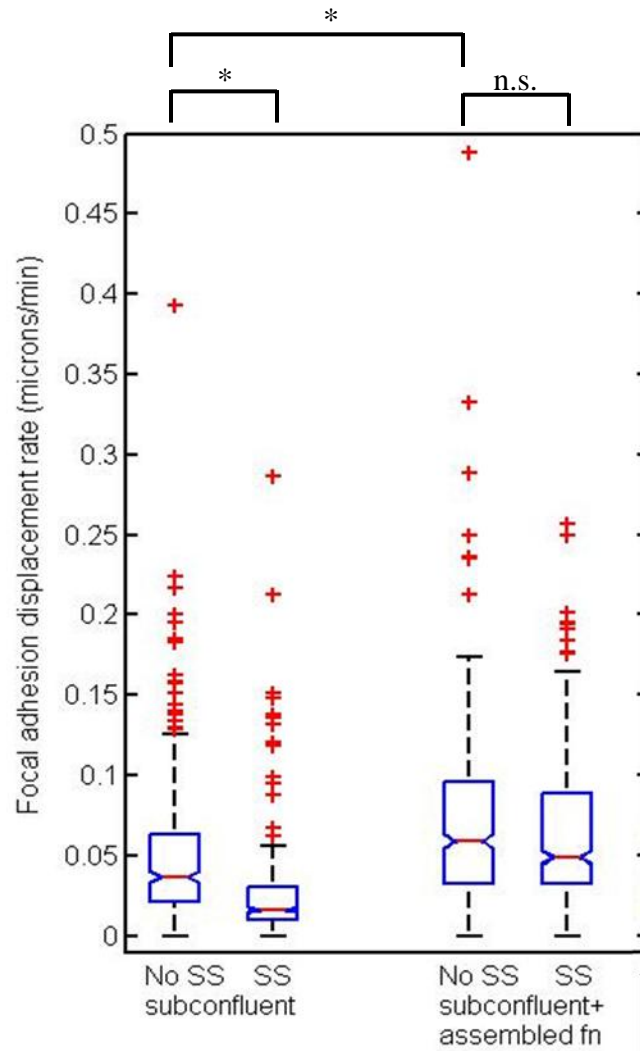


Figure 10. Focal adhesion displacement rate is assembly dependent. Box plots of the distribution of individual focal adhesion displacement rates for sparse BAEC on unassembled fibronectin (left pair of box plots) and assembled fibronectin (right pair of box plots). The red line represents the population median, the blue box represents the interquartile range, and the red crosses represent outliers. In each pair of box plots, the left box plot is displacement rates over 15 minutes before the onset of shear stress (No SS), and the right box plot is displacement rates over 15 minutes after the onset of shear stress (SS). Shear stress causes a significant decrease in median focal adhesion displacement in cells on unassembled fibronectin, (* $p < 0.01$, Mann Whitney U test) but not cells on assembled fibronectin (n.s.=not significant, $p = 0.16$, Mann Whitney U test). Focal adhesion displacement rate under no shear stress conditions was significantly higher in cells on assembled fibronectin than cells on unassembled fibronectin. (* $p < 0.01$, Mann Whitney U test)

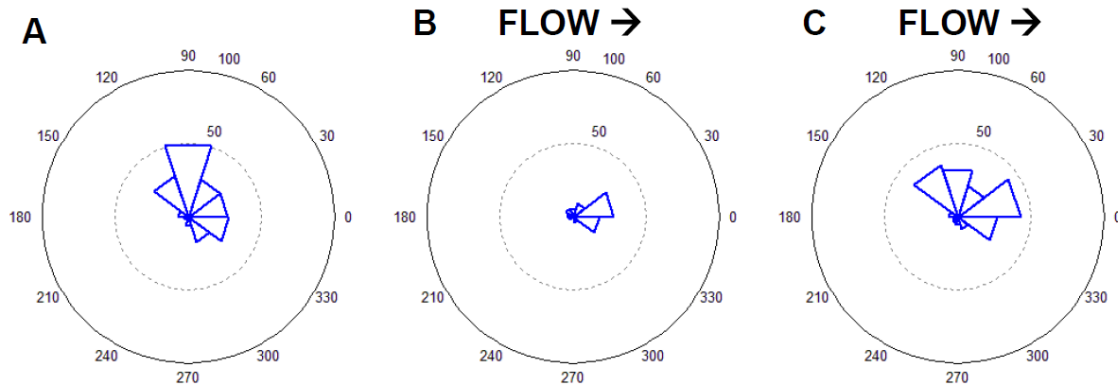


Figure 11. Angular distribution of focal adhesion displacement in sparse BAEC interacting with assembled fibronectin. Under no-flow conditions (A), focal adhesions appeared to move randomly. After 1 minute of flow (B), focal adhesions displacement is directed downstream, but displacement returns to a distribution similar to the no-flow condition after 15 minutes of shear stress (C).

3.1.4 Fibronectin Fibril Displacement

Because we expect focal adhesions to be physically linked to the ECM, we compared the magnitude and direction of focal adhesion displacements with the displacements of nearby fibronectin fibrils. Previous studies had shown that in confluent monolayers the patterns of fibronectin fibril displacement were qualitatively similar to the patterns of focal adhesion displacement. [13] We hypothesized that this effect was due to direct interaction of focal adhesions with the fibronectin fibrils, and that a similar effect would be seen in single cells interacting with assembled fibronectin. We quantified the displacement of individual fibronectin fibrils underneath cells to evaluate how forces were transmitted through the cell to the underlying ECM. Similar to focal adhesions, fibronectin fibril displacement rate did not change significantly with the onset of shear stress ($p=0.08$, Mann Whitney U test); however, the direction of fibril displacement was transiently downstream in the first minute after the onset of shear stress as was observed for focal adhesion displacement. (Figure 12) We then quantified this similarity by

correlating the displacement magnitudes and angles of focal adhesions and their nearest fibronectin fibril, within 10 μm . In sparse cells interacting with assembled fibronectin, both under no shear conditions and after 15 minutes of shear stress, the magnitude and direction of focal adhesion and fibronectin fibril displacement are highly correlated. (Figure 13) The Pearson's correlation coefficient for angle of displacement was 0.90 under no shear stress and 0.85 after the onset of shear stress, and in both cases was statistically significant when tested. ($p < 0.05$, t test) For displacement magnitude, the Pearson's correlation coefficient was 0.45 under no shear stress and 0.84 after the onset of shear stress. Again, in both cases the correlation was statistically significant. ($p < 0.05$, t test)

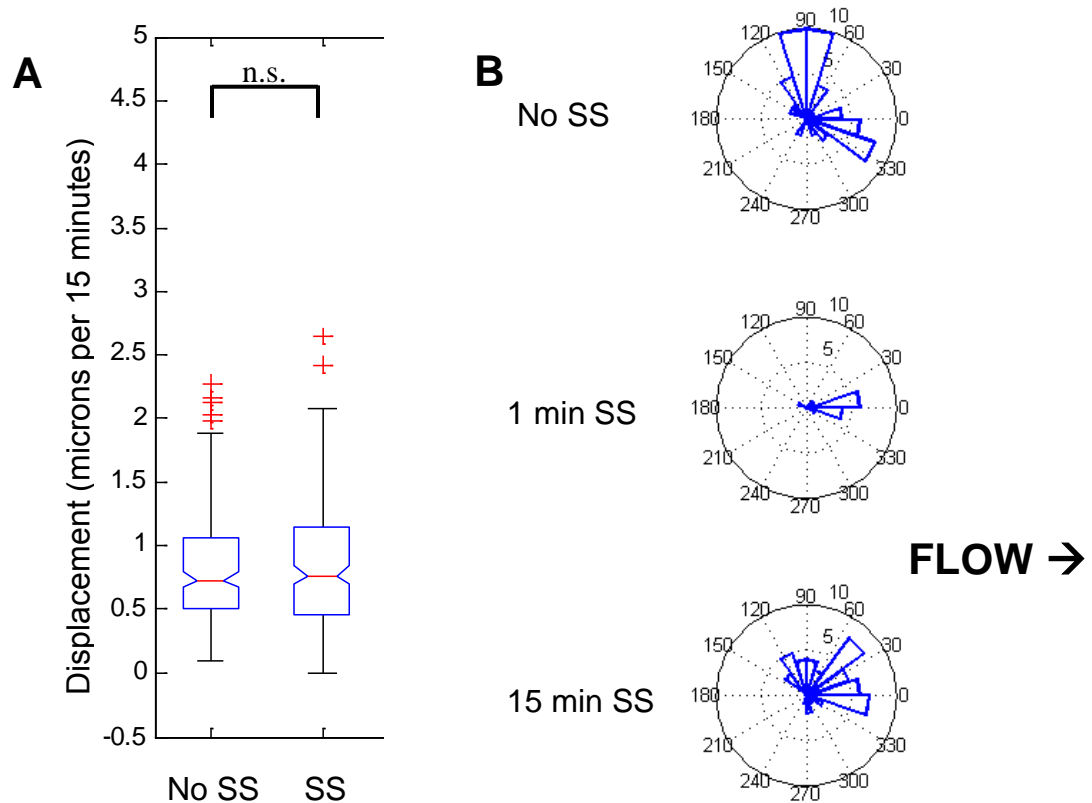


Figure 12. Rate and direction of displacement of fibronectin fibrils beneath sparse BAEC on assembled fibronectin. (A) box plots of fibronectin fibril displacement in 15 minutes before the onset of shear stress (No SS) and 15 minutes after the onset of shear stress (SS). (n.s.= not significant, $p=0.08$, Mann-Whitney U test) (B) angular distribution of fibronectin fibril displacement under no-flow conditions, after 1 minute of shear stress, and after 15 minutes of shear stress.

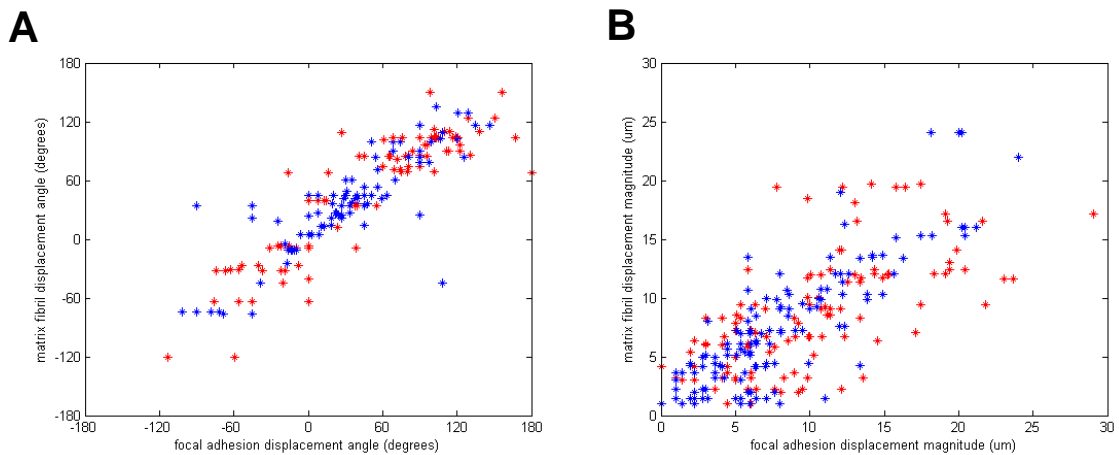


Figure 13. Correlation between displacement of focal adhesions and nearby fibronectin fibrils in sparse BAEC interacting with assembled fibronectin. Both angle (A) and magnitude (B) of focal adhesion displacement significantly correlate with fibronectin fibril displacement both under no flow conditions (red) and after 15 minutes of shear stress (blue) ($p<0.05$, t test).

3.1.5 Integrin Distribution

Since shear stress-induced structural remodeling requires integrin-dependent signaling, we hypothesized that fibronectin assembly regulates shear stress-induced structural remodeling by controlling relative levels of $\alpha_5\beta_1$ and $\alpha_v\beta_3$ binding. To test this hypothesis, we fixed and immunostained samples of sparse BAEC for $\alpha_5\beta_1$ and $\alpha_v\beta_3$ integrins. Sparse BAEC interacting either with assembled or unassembled fibronectin were exposed to either 0 or 15 minutes of shear stress. Cells on unassembled fibronectin displayed $\alpha_v\beta_3$ staining in structures strongly reminiscent of focal adhesions and focal contacts, mainly around the periphery of cells. These cells also showed some $\alpha_5\beta_1$ staining, limited to the center of the cell and the uropod in either very long fibrillar structures or small punctate dots. (Figure 14) This pattern is consistent with previous reports of the segregation of $\alpha_v\beta_3$ and $\alpha_5\beta_1$ into focal adhesions and fibrillar adhesions respectively. [72] When exposed to 15 minutes of shear stress, the overall distribution of integrin staining was unchanged. Cells on assembled fibronectin displayed a different pattern of integrin staining. Instead of being organized into focal adhesion-like spots, $\alpha_v\beta_3$ staining was diffuse over the entire basal surface of the cell. Staining of $\alpha_5\beta_1$ was still organized into fibrillar adhesions, but these adhesions were much more numerous and distributed throughout the cell rather than being limited to the center and back of the cell as was observed in cells interacting with unassembled fibronectin. (Figure 15)

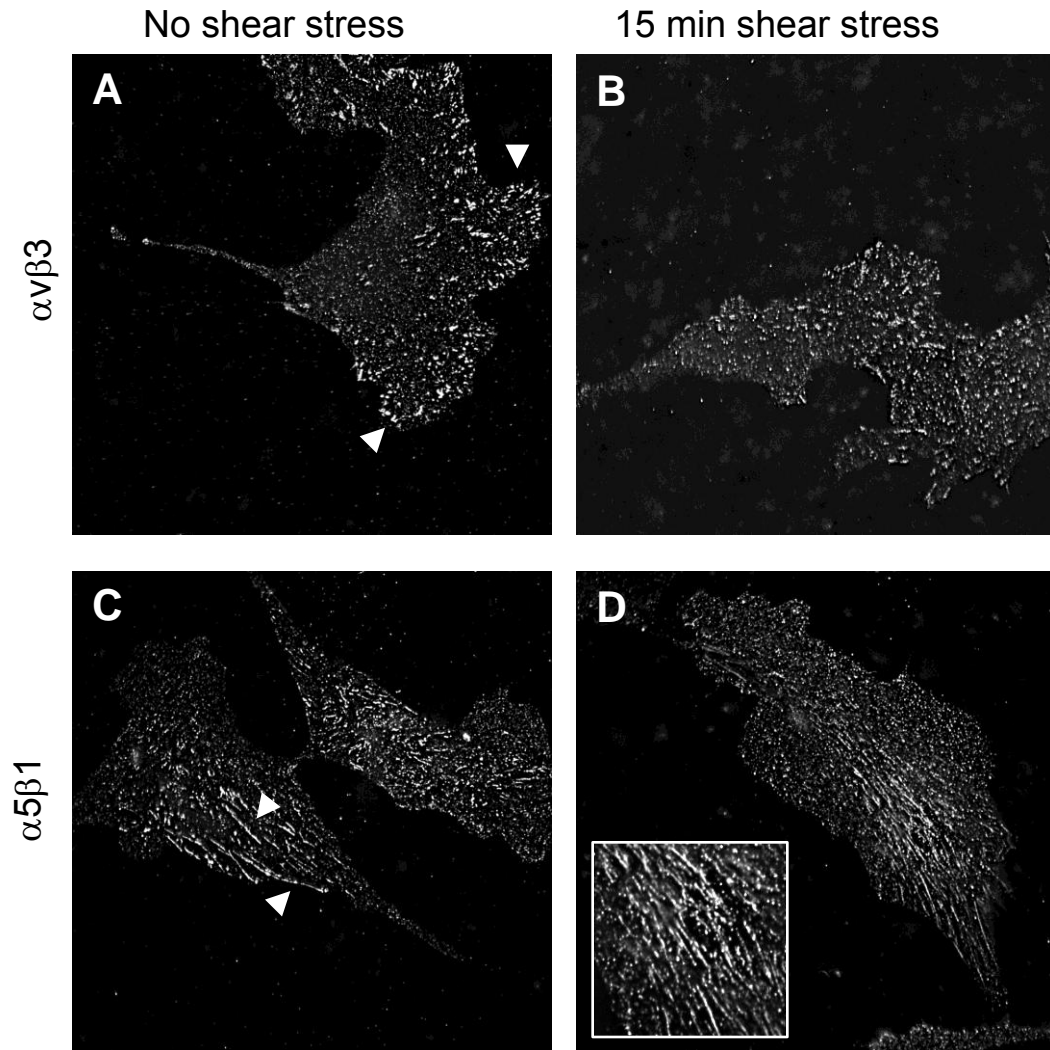


Figure 14. $\alpha_v\beta_3$ and $\alpha_5\beta_1$ immunostaining in sparse BAEC interacting with unassembled fibronectin under no shear stress and after 15 minutes of shear stress. $\alpha_v\beta_3$ was distributed (A and B) in adhesion-like spots towards the leading edge of the cell (arrowheads, A), while $\alpha_5\beta_1$ (C and D) was distributed into structures reminiscent of fibrillar adhesions towards the back of the cell (arrowheads, C and inset, D).

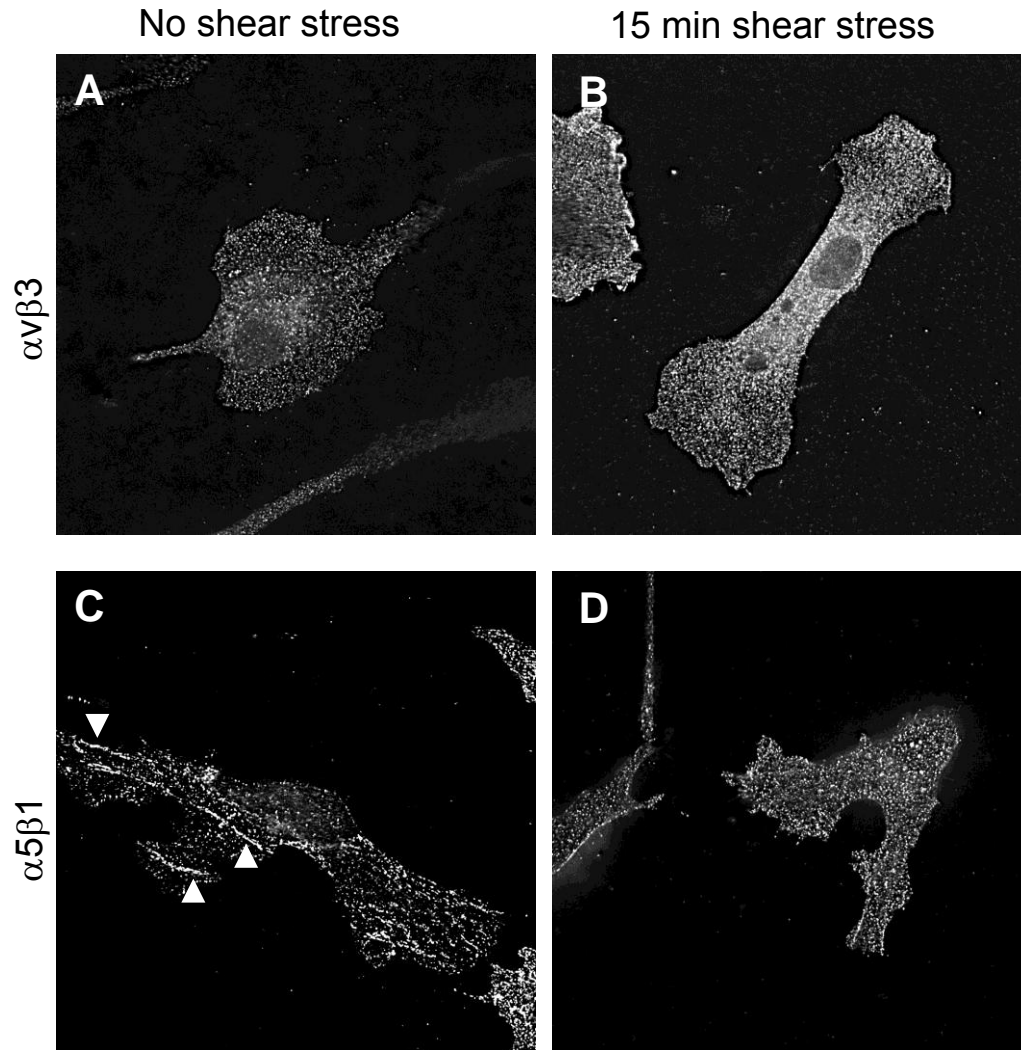


Figure 15. $\alpha_v\beta_3$ and $\alpha_5\beta_1$ immunostaining in sparse BAEC interacting with assembled fibronectin. Under no shear stress (A) and after 15 minutes of shear stress (B), $\alpha_v\beta_3$ staining is distributed across the basal surface and punctate. $\alpha_5\beta_1$ staining (C and D) is also punctate, but organized into larger fibrillar adhesion-like structures (arrowheads, C).

To evaluate the effect of fibronectin assembly on the relative levels of bound $\alpha_v\beta_3$ and $\alpha_5\beta_1$, we crosslinked bound integrins and solubilized the non-crosslinked cell material. These samples were then immunostained for both $\alpha_5\beta_1$ and α_v . The pattern of integrin staining was qualitatively similar to that seen in previously immunostained samples not treated by the crosslinking protocol. The crosslinking protocol only retains and immunostains integrins that are bound to the substrate, so we expected that any

fluorescence observed in previously immunostained samples that was due to unbound integrins either on the cell surface or inside the cell would be gone in the crosslinked samples. As expected, in both cells on unassembled and assembled fibronectin the crosslinked samples showed that integrins organized into focal adhesion-like patches were left behind while diffuse integrin staining on the basal surface and in cytoplasmic vesicles was not visible. On unassembled fibronectin, α_v is distributed in the same pattern as previously seen using the $\alpha_v\beta_3$ antibody, but $\alpha_5\beta_1$ staining is limited to small puncta towards the center of the cell, rather than appearing to form fibrillar structures. In samples exposed to 15 minutes of shear stress, edge regions likely associated with shear stress-induced ruffling and protrusion displayed exclusively $\alpha_v\beta_3$ -based focal adhesions. (Figure 16) On assembled fibronectin, α_v staining is almost completely absent, and $\alpha_5\beta_1$ -based adhesions are prominent throughout the entire cell. After the onset of shear stress, there was no visible formation of $\alpha_v\beta_3$ -based adhesions at edges as was seen in cells on unassembled fibronectin. (Figure 17) Interestingly, $\alpha_v\beta_3$ -based adhesion spots were visible in some cells in samples containing assembled fibronectin. (Figure 18) However, these spots were only visible in cases where there was a hole or space in the assembled fibronectin and cells were able to then interact with fibronectin-coated glass. The amount and organization of $\alpha_5\beta_1$ -based adhesion spots in cells on unassembled fibronectin varied. While most of the fibronectin on the glass surface is unassembled, there can be some regions of limited assembly especially if there are small groups of cells. (Figure 19) In these regions where fibronectin assembly had been initiated, $\alpha_5\beta_1$ staining was more prominent and well-organized into larger fibrillar adhesions reminiscent of those seen in cells on assembled fibronectin.

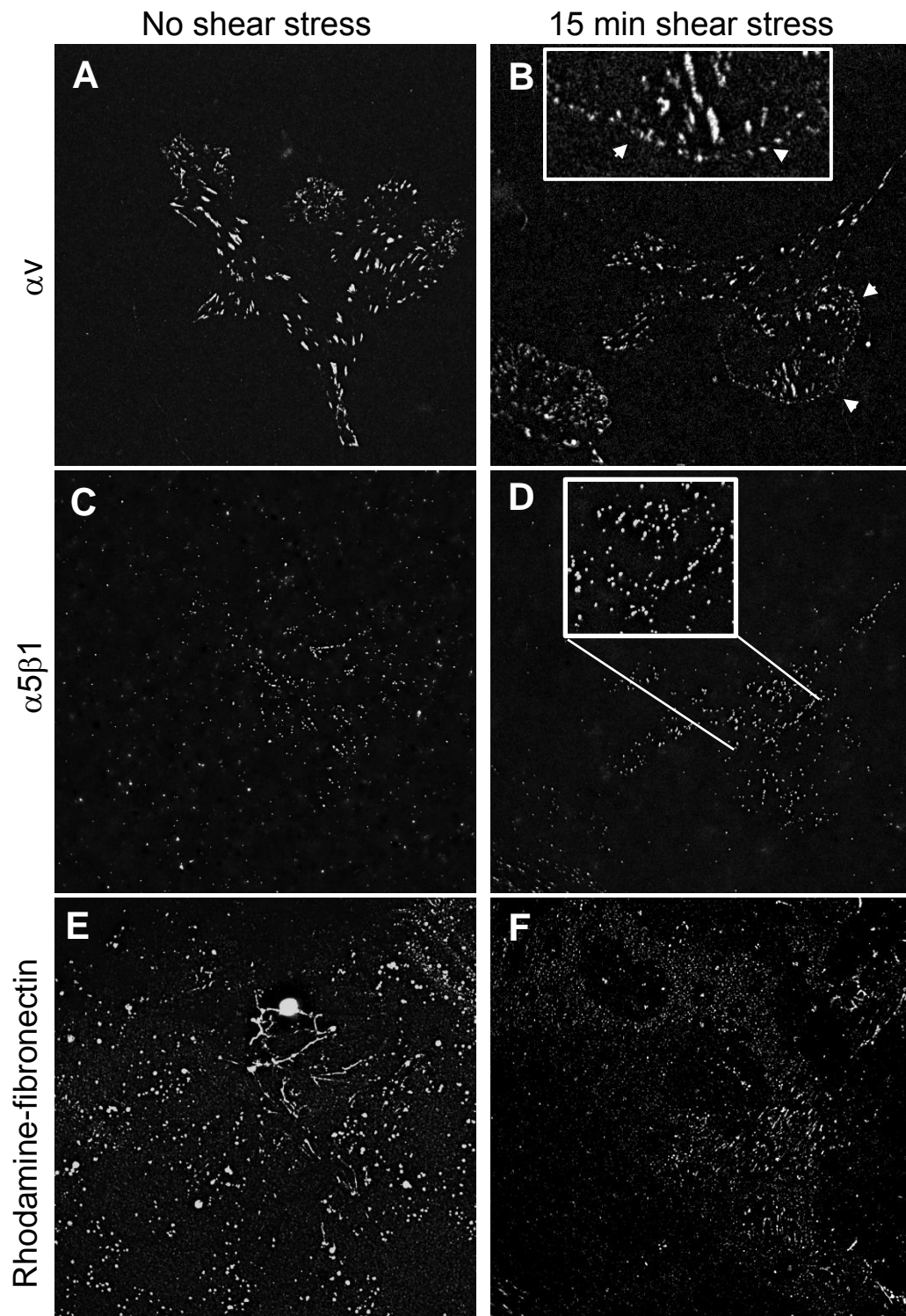


Figure 16. Crosslinked α_v , $\alpha_5\beta_1$, and rhodamine-fibronectin staining in sparse BAEC on unassembled fibronectin. α_v (A) was distributed into focal adhesions, and was recruited to adhesion spots after 15 minutes of shear stress (arrowheads and inset, B). $\alpha_5\beta_1$ distribution (C and D) was limited to small, punctate spots (inset, D). Rhodamine-fibronectin (E and F) demonstrates minimal fibronectin assembly.

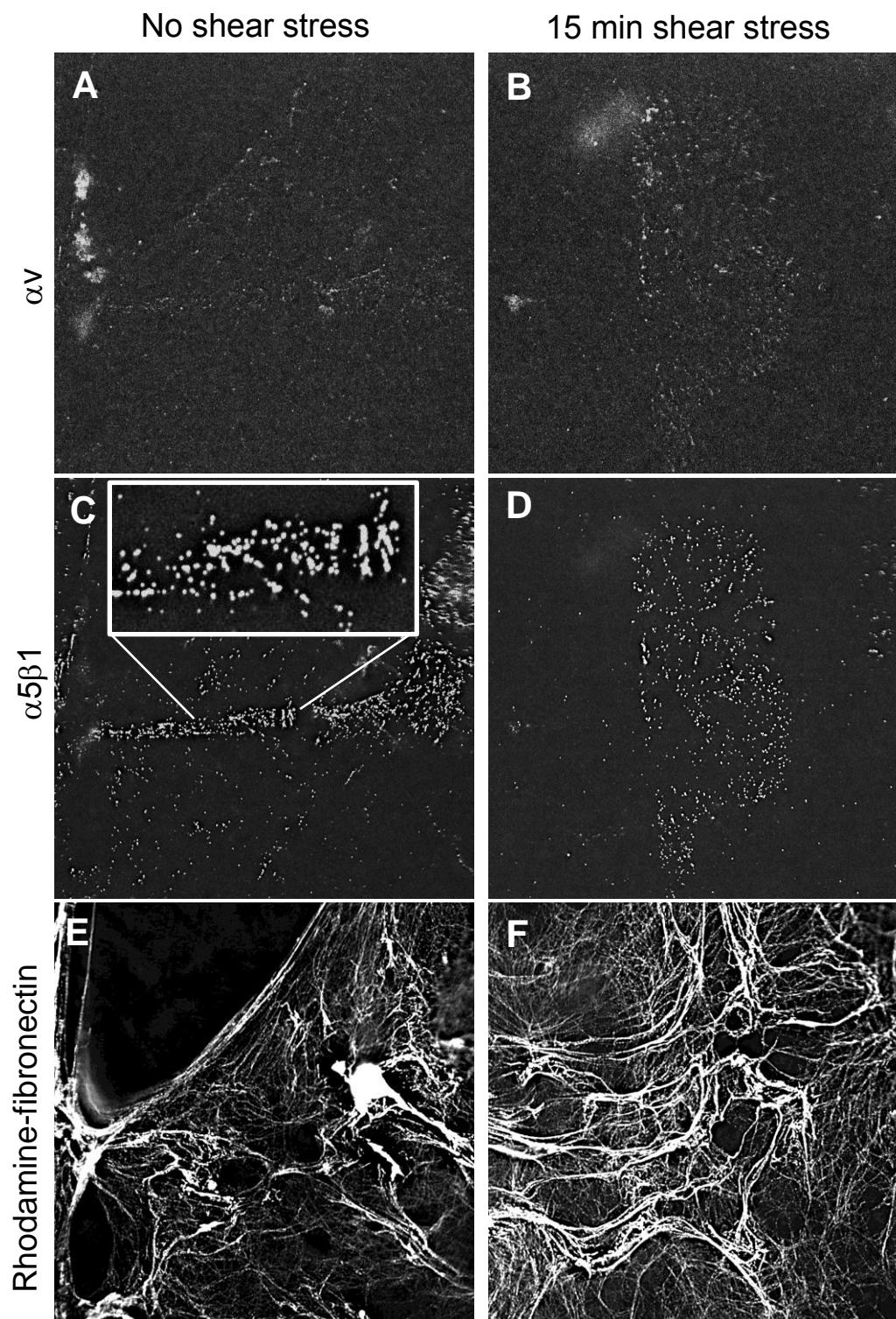


Figure 17. Crosslinked α_v , $\alpha_5\beta_1$, and rhodamine-fibronectin staining in sparse BAEC on assembled fibronectin. Both under no shear stress and after 15 minutes of shear stress α_v staining is almost non-existent (A and B). $\alpha_5\beta_1$ is distributed in punctate spots throughout the cell, reminiscent of small adhesions (C and D, inset C). Rhodamine-fibronectin shows the organization of assembled fibronectin beneath the cell (E and F).

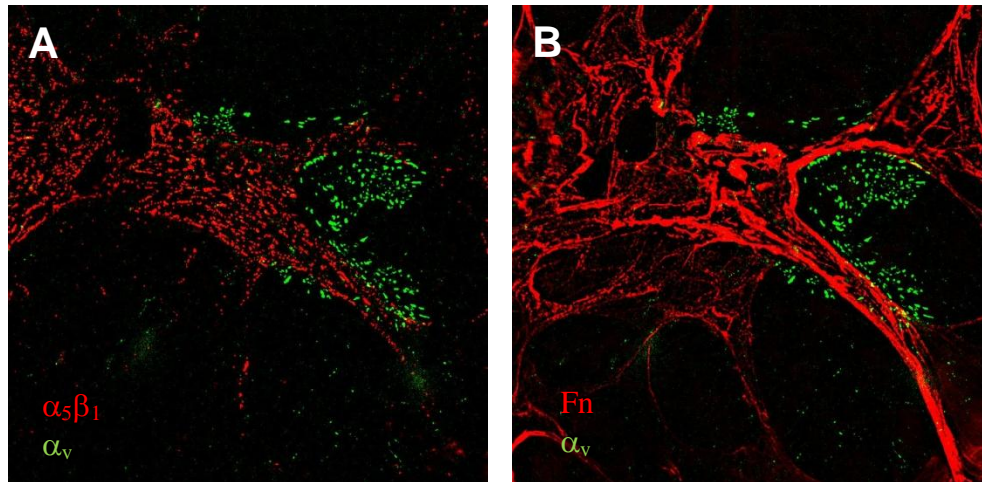


Figure 18. Example of crosslinked α_v staining on assembled fibronectin. (A) This cell displays a combination of $\alpha_5\beta_1$ (red) and α_v (green) staining. However, α_v -based adhesion spots are spatially segregated from $\alpha_5\beta_1$ -based adhesions. (B) α_v (green) is also spatially segregated from assembled fibronectin (red) and only visible in regions of the cell not interacting with assembled fibronectin (dark, non-fibrillar areas).

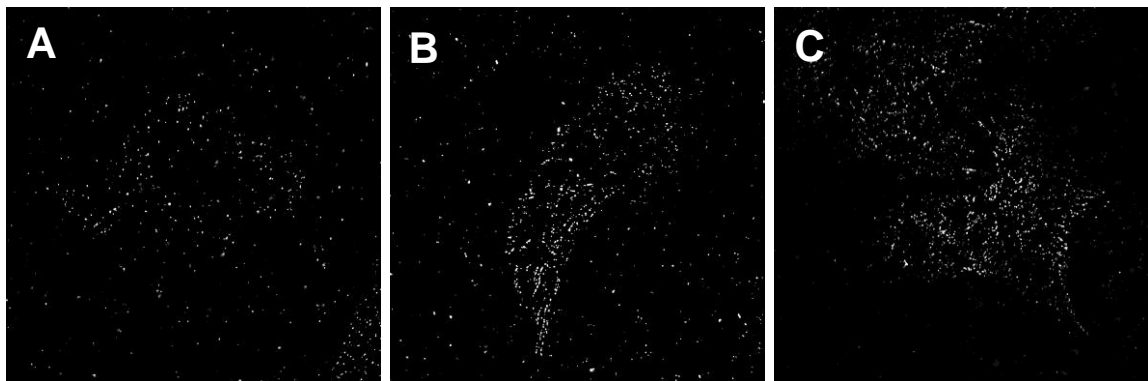


Figure 19. Example of variation in crosslinked $\alpha_5\beta_1$ staining on unassembled fibronectin. Depending on to what degree fibronectin assembly has been initiated, $\alpha_5\beta_1$ staining can vary from a very random, punctate distribution (A), to a more adhesion-associated distribution (B and C).

3.1.6 Integrin Blocking and Migration

Since directed actin ruffling and protrusion are essential to guiding mechanotaxis and $\alpha_v\beta_3$ integrin staining was associated with protrusions, we hypothesized that $\alpha_v\beta_3$ ligation played an important role in downstream mechanotaxis. To test the specific roles of $\alpha_v\beta_3$ and $\alpha_5\beta_1$ integrins in shear stress-induced mechanotaxis, sparse cells on

unassembled fibronectin were incubated with blocking antibodies, then assembled into the flow chamber and exposed to shear stress. Tracking cell movement under shear stress showed that pretreatment with LM609 to block $\alpha_v\beta_3$ appeared to inhibit shear stress-induced downstream mechanotaxis. (Figure 20) When cumulative migration in the x direction was quantified, the difference between the LM609 and untreated cells was significant only during the first hour of shear stress ($p < 0.05$, t test). (Figure 21) Measurements of cell area showed that LM609 also significantly inhibited transient shear stress induced spreading during the first 40 minutes after the onset of shear stress ($p < 0.05$, t test). (Figure 22) When cells were alternatively treated with anti- α_5 or anti- α_2 antibodies as controls, they were still able to migrate downstream with the direction of flow. (Figure 23) When cells were treated with anti- α_5 , they migrated significantly farther downstream than untreated cells beginning 2 hours after the onset of shear stress. ($p < 0.05$, t test) However, there was no significant difference in cumulative x direction migration under shear stress when cells were treated with anti- α_2 . ($p > 0.05$, t test) (Figure 24)

To summarize, fibronectin assembly caused changes to the pattern of $\alpha_v\beta_3$ and $\alpha_5\beta_1$ binding under no flow conditions. (Table 3) Fibronectin assembly also caused significant differences in shear stress-induced responses including mechanotaxis, actin ruffling, and focal adhesion displacement. (Table 4)

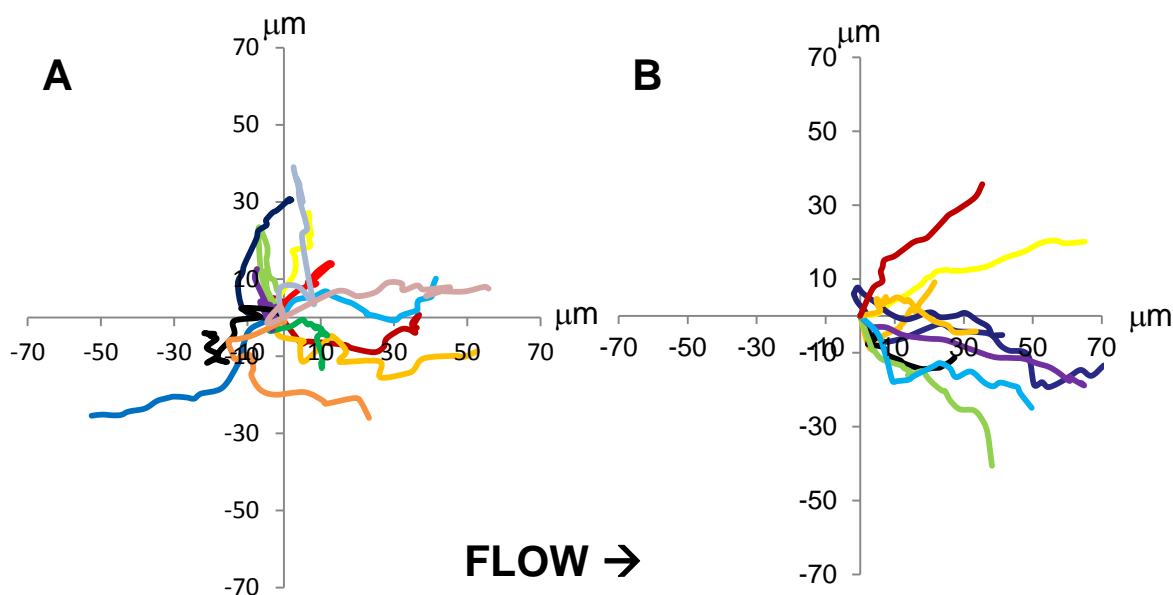


Figure 20. Migration tracks of sparse BAEC in the 6 hours after the onset of shear stress either (A) treated with LM609 or (B) untreated. Untreated cells migrated downstream, while BAEC treated with LM609 migrated more randomly.

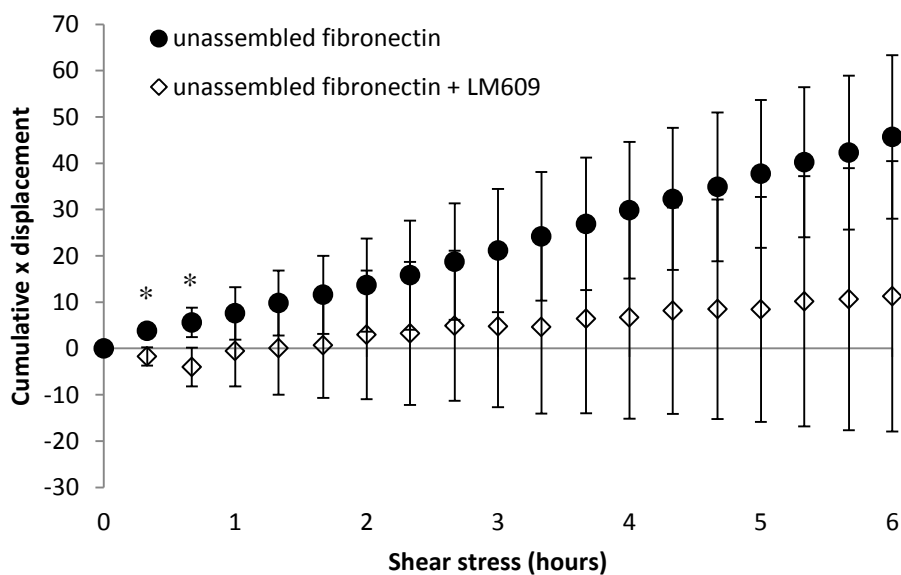


Figure 21. Migration in the direction of flow, as measured by cumulative x displacement, is significantly smaller for LM609 treated cells than untreated cells during the first 40 minutes of shear stress. (* $p < 0.05$, t test)

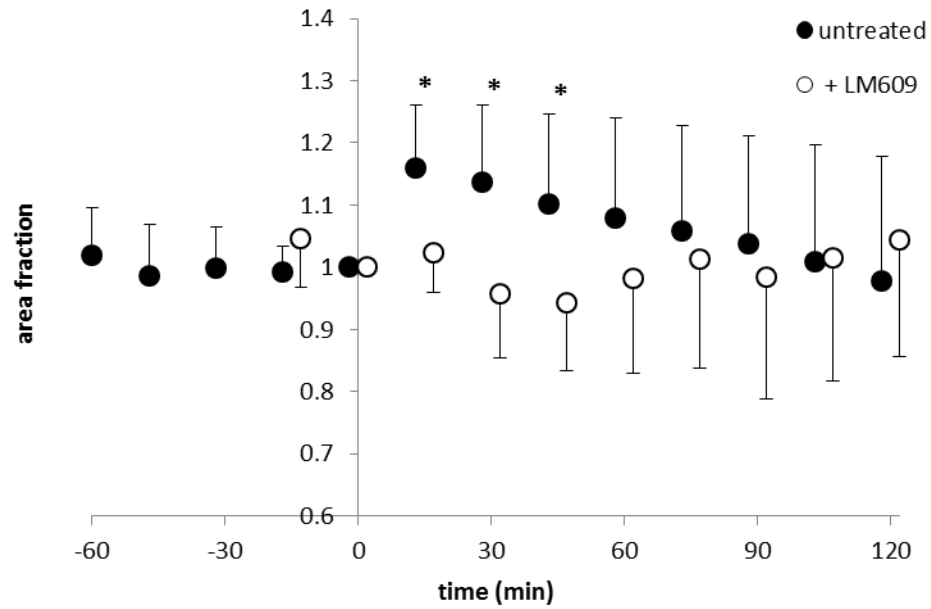


Figure 22. Transient shear stress-induced spreading of sparse BAEC is inhibited by LM609 treatment. The shear stress-induced increase in area is significantly inhibited for the first 45 minutes after the onset of shear stress when BAEC are pretreated with LM609. (* $p < 0.05$, t test)

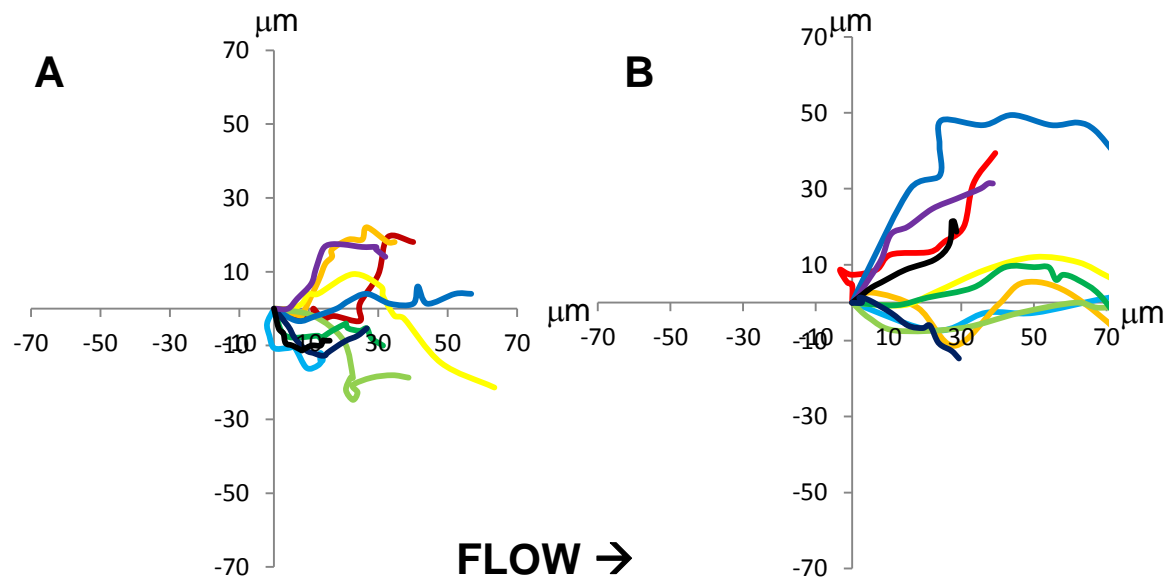


Figure 23. Migration tracks of sparse BAEC in the 6 hours after the onset of shear stress either (A) pretreated with anti- α_2 or (B) pretreated with anti- α_5 . In both cases, cells still display downstream migration.

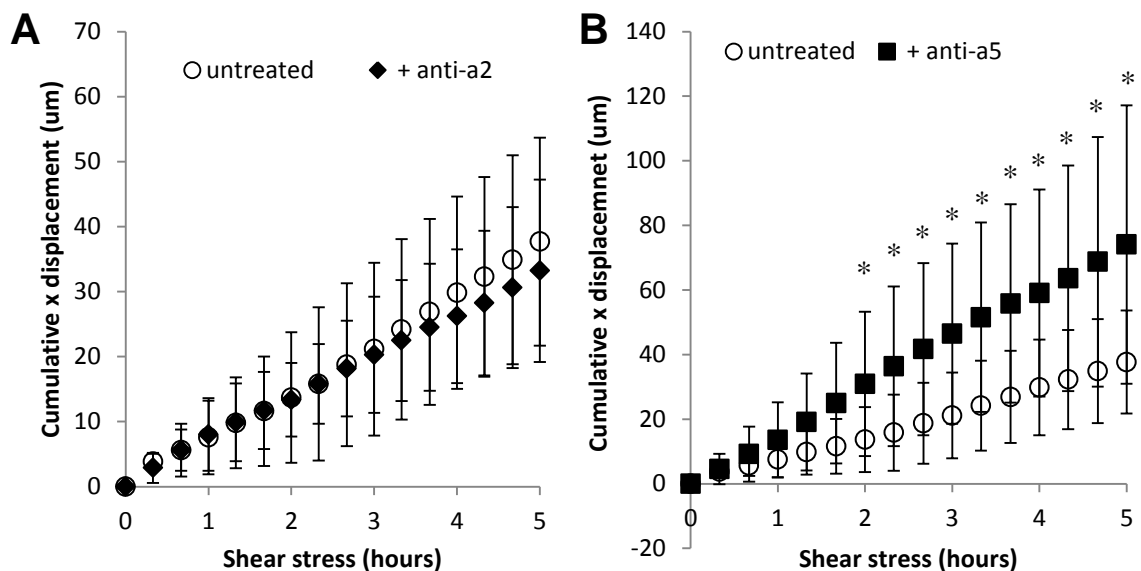


Figure 24. (A) there is no significant difference in cumulative x displacement under shear stress between cells treated with anti- α_2 and untreated cells. ($p > 0.05$, t test) (B) Migration in the direction of flow, as measured by cumulative x displacement, is significantly greater for anti- α_5 treated cells after 2 hours of shear stress than untreated cells. (* $p < 0.05$, t test)

Table 3. Readouts modulated in single cells by fibronectin assembly under no-flow conditions

Readout	Unassembled fibronectin	Assembled fibronectin
Crosslinked $\alpha_v\beta_3$	Yes	No
Crosslinked $\alpha_5\beta_1$	No	Yes

Table 4. Readouts of shear stress responses in single cells significantly affected by fibronectin assembly.

Readout	Unassembled fibronectin	Assembled fibronectin
Mechanotaxis	Yes	No
Actin ruffles	Increased	No change
Focal adhesion displacement	Decreased	No change

3.2 Confluent Monolayers

3.2.1 Migration and Alignment

As downstream mechanotaxis is a fundamental indicator of mechanosensitivity of single endothelial cells under shear stress, the fundamental readout of monolayer mechanosensitivity is cell shape alignment parallel to the direction of flow. Since fibronectin assembly inhibited downstream mechanotaxis, we hypothesized fibronectin assembly might also regulate cell shape adaptation under shear stress. To measure alignment, we tracked shape change of individual cells within the monolayer. Alignment in response to shear stress was quantified by the standard deviation of cell orientation. (Figure 25) Because the histogram is normally distributed, the standard deviation reflects the spread in the histogram. A wider peak, and therefore larger standard deviation, describes a more randomly oriented population, while a narrow peak and smaller standard deviation represents alignment with the mean orientation. In the case of aligning monolayers, this mean orientation is 0 degrees and is the flow direction. At the onset of shear stress, monolayers on both assembled and unassembled fibronectin were unaligned. During 14 hours of shear stress, the monolayers progressively aligned, and average standard deviation decreased. Confluent monolayers interacting with unassembled fibronectin aligned more quickly than those interacting with assembled fibronectin, as shown by a significant difference in average deviation after 5 hours of shear stress ($p < 0.05$, t test). (Figure 26) As evidenced by a smaller standard deviation, the progression of alignment of monolayers interacting with unassembled fibronectin was also much less variable than that of monolayers interacting with assembled fibronectin. There were no significant differences in migration speed of monolayers interacting with

unassembled or assembled fibronectin ($p > 0.05$, t test). (Figure 27) In both conditions, migration speed was low at the initial onset of shear stress, and after 10-12 hours gradually increased.

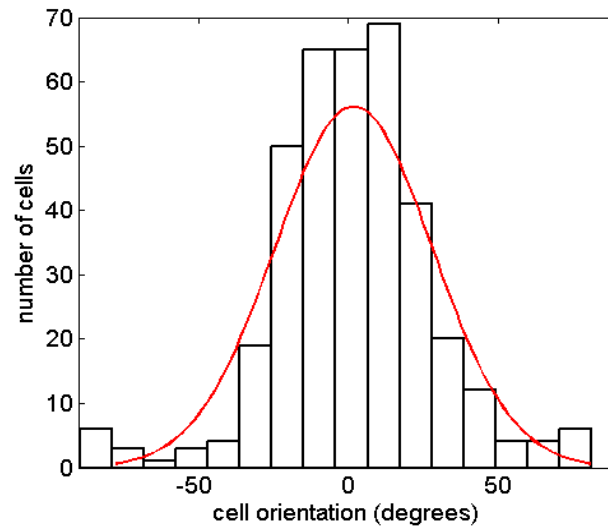


Figure 25. Example histogram of cell orientations within a monolayer. This example shows a fitted normal distribution in red, and when tested these data are normally distributed ($p < 0.05$, Jarque-Bera test)

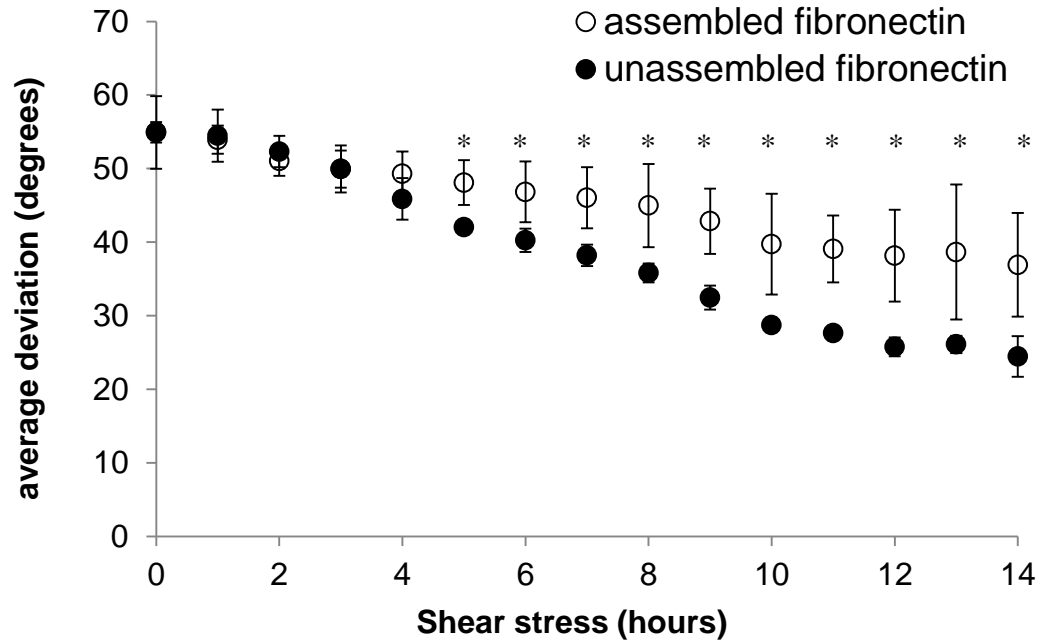


Figure 26. Fibronectin assembly regulates speed of monolayer alignment. Average deviation of monolayer orientation under shear stress decreases more quickly for cells interacting with unassembled fibronectin (closed circles) than for cells interacting with assembled fibronectin (open circles) and is significantly different after 5 hours of shear stress. (* $p < 0.05$, t test)

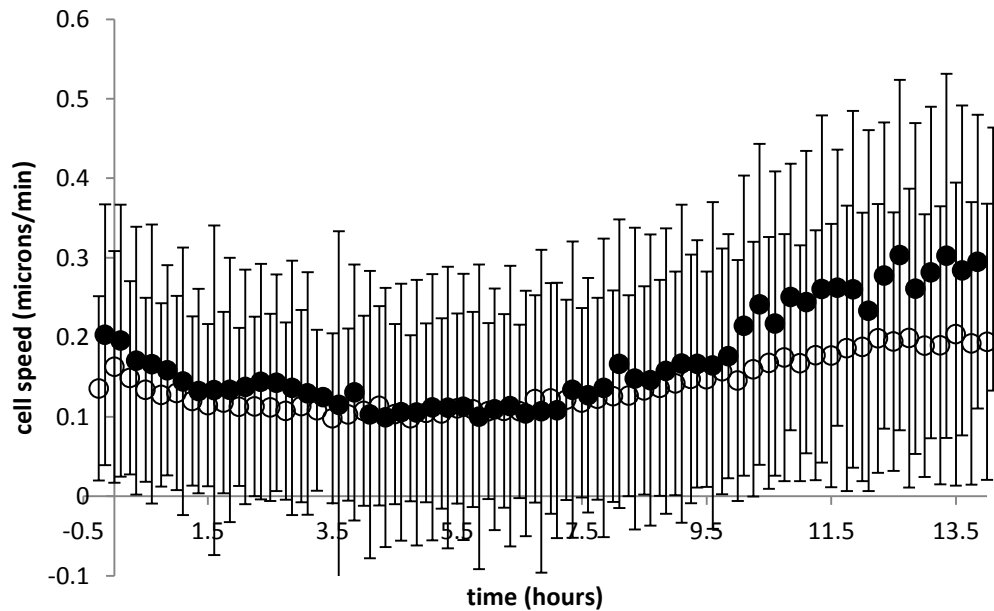


Figure 27. Monolayer migration speed is not significantly affected by fibronectin assembly. The migration speed of cells interacting with unassembled fibronectin (closed circles) is not significantly different than that of cells interacting with assembled fibronectin (open circles) ($p > 0.05$, t test).

3.2.2 F-actin Remodeling

Dynamic cytoskeletal remodeling is activated within minutes of the onset of shear stress and is required for cell shape alignment in monolayers. We observed that fibronectin assembly regulated cytoskeletal remodeling in single cells and that fibronectin assembly regulated speed of monolayer alignment. Therefore, we hypothesized that fibronectin assembly also regulates cytoskeletal remodeling in monolayers. To investigate actin cytoskeletal remodeling, we evaluated stress fiber content of confluent monolayers interacting with assembled or unassembled fibronectin and exposed to 0, 5, or 15 minutes of shear stress. Under no-flow conditions, the stress fiber content of confluent monolayers was similar in both assembly conditions. In confluent monolayers interacting with assembled fibronectin, stress fiber content was visually reduced after 15 minutes of shear stress compared to no-flow conditions. (Figure 28) We quantified these differences by measuring the area of the image covered by stress fibers. We found that after 5 minutes of shear stress, there were no significant changes in stress fiber content ($p=0.13$ for samples on assembled fibronectin, and $p=0.65$ for samples on unassembled fibronectin, t test). After 15 minutes of shear stress, there was a significant decrease in stress fiber content ($p<0.05$, t test) in monolayers interacting with assembled fibronectin, but there was no significant change in stress fiber content in monolayers interacting with unassembled fibronectin ($p=0.10$, t test). (Figure 29) This observation of stress fiber disassembly has been previously reported and has been suggested to be required for alignment. [26] In contrast to the published report, in monolayers interacting with unassembled fibronectin, stress fiber content was not decreased after 5 and 15 minutes of shear stress.

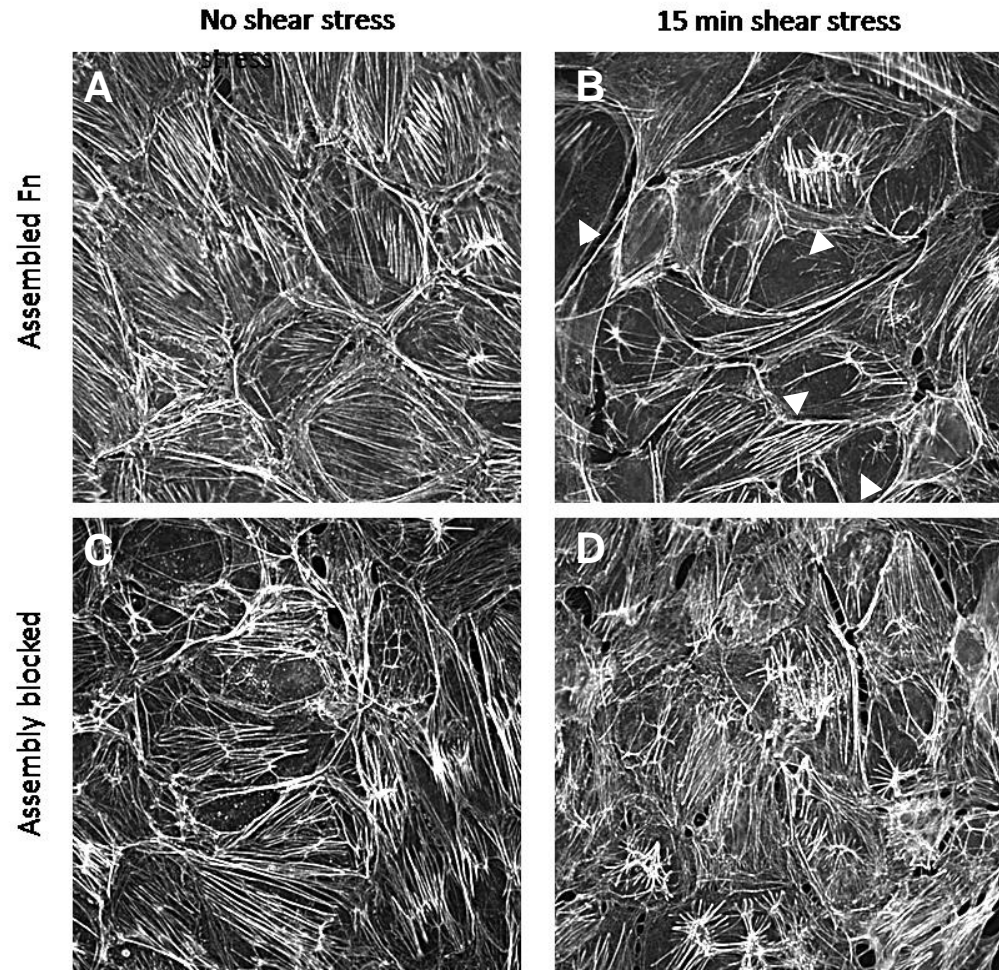


Figure 28. Representative images of F-actin staining in confluent monolayers interacting with assembled or unassembled fibronectin. Compared to the no shear stress condition (A), monolayers interacting with assembled fibronectin after 15 minutes of shear stress show regions devoid of stress fibers (arrowheads, B). In contrast, there is no visual decrease in stress fibers when comparing monolayers interacting with unassembled fibronectin under no shear stress (C) and 15 minutes of shear stress (D).

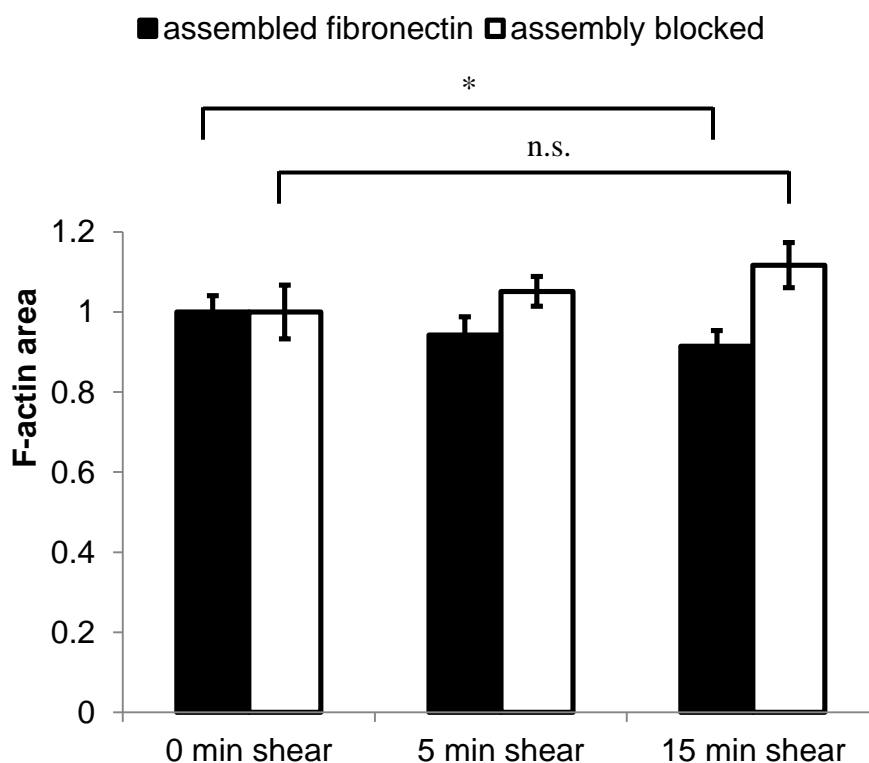


Figure 29. Quantification of F-actin content of monolayers from F-actin staining. Relative area of F-actin coverage is significantly decreased after 15 minutes of shear stress in monolayers interacting with assembled fibronectin (* $p < 0.05$, t test), but not significantly changes in monolayers interacting with unassembled fibronectin. (n.s.= not significant, $p = 0.10$, t test)

3.2.3 Focal Adhesion Displacement

Intracellular forces and applied shear force due to fluid flow are transmitted to focal adhesions through actin stress fibers, and shear stress induces both cytoskeletal remodeling and deformation. [26, 31, 73] Changes to stress fiber organization could alter force transmission to focal adhesions and therefore alter the force balance at focal adhesions. We observed that shear stress-induced stress fiber remodeling is modulated by fibronectin assembly. Therefore, we hypothesized that fibronectin assembly might also modulate shear stress-induced changes in the force balance at focal adhesions. To test this

hypothesis, we measured focal adhesion displacement as a readout of the balance of forces at the adhesive interface.

In confluent monolayers, which normally are interacting with a well-assembled fibrillar fibronectin matrix, treatment with fibronectin assembly-blocking peptide resulted in complete abrogation of fibril formation. When confluent monolayers interacting with assembled fibronectin were exposed to shear stress focal adhesion displacement rate was maintained, which is similar to what has been previously reported. [13] Under no-flow conditions the median focal adhesion displacement rate was $0.062 \mu\text{m}/\text{min}$, and after the onset of shear stress median focal adhesion displacement rate increased significantly to $0.086 \mu\text{m}/\text{min}$ ($p < 0.01$, Mann Whitney U test). (Figure 30) In contrast, when confluent monolayers interacting with unassembled fibronectin were exposed to shear stress, median focal adhesion displacement rate was significantly reduced, similar to the effect observed in sparse cells interacting with unassembled fibronectin ($p < 0.01$, Mann Whitney U test). In this case, under no-flow conditions the median focal adhesion displacement rate was $0.043 \mu\text{m}/\text{min}$, and after the onset of shear stress was $0.026 \mu\text{m}/\text{min}$. As observed in sparse cells interacting with assembled fibronectin, focal adhesion displacement was transiently directed downstream in the first minute after the onset of shear stress. (Figure 31)

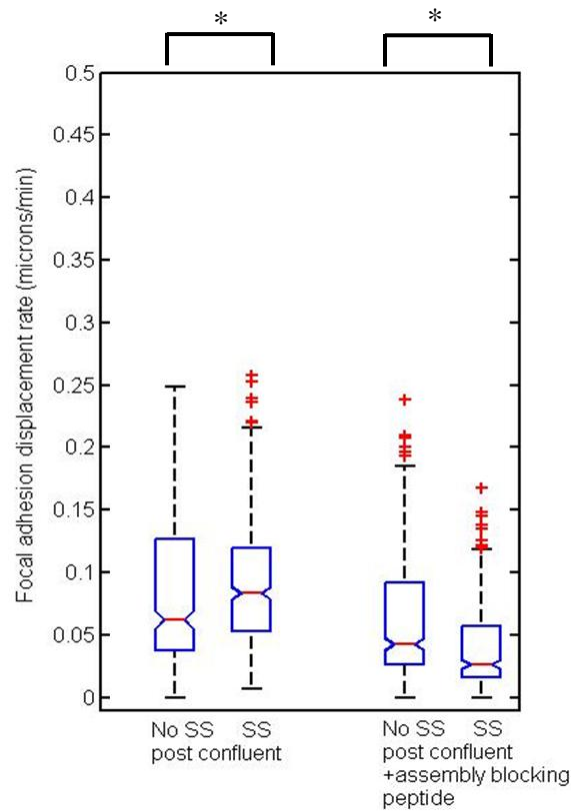


Figure 30. Focal adhesion displacement rate is increased at the onset of shear stress in confluent monolayers interacting with assembled fibronectin, but decreased in confluent monolayers interacting with unassembled fibronectin. . Box plots of the distribution of individual focal adhesion displacement rates for monolayers on assembled fibronectin (left pair of box plots) and unassembled fibronectin (right pair of box plots). In each pair of box plots, the left box plot is displacement rates over 15 minutes before the onset of shear stress (No SS), and the right box plot is displacement rates over 15 minutes after the onset of shear stress (SS). For monolayers on both assembled and unassembled fibronectin, the onset of shear stress caused a statistically significant change in focal adhesion displacement rate. (* $p < 0.01$, Mann-Whitney U test)

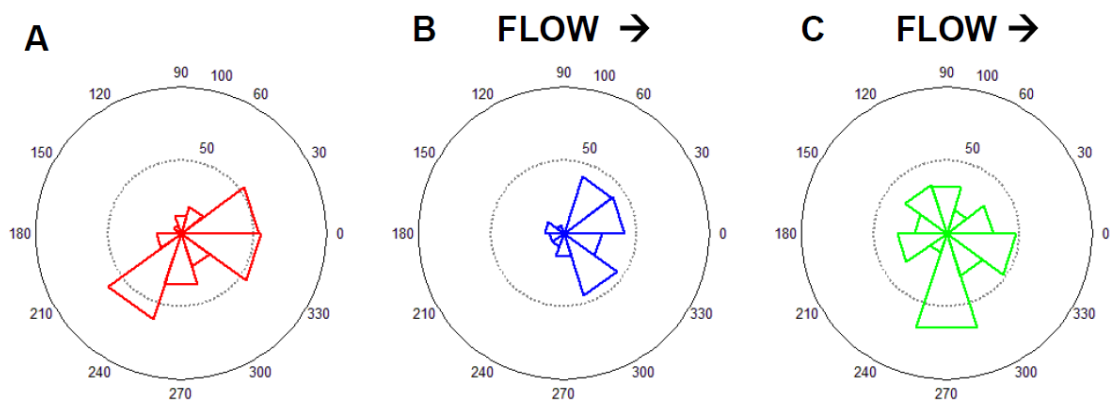


Figure 31. Angular distribution of focal adhesion displacement (A) 15 minutes before the onset of shear stress, (B) one minute after the onset of shear stress and (C) 15 minutes after the onset of shear stress.

3.2.4 Fibronectin Fibril Displacement

We observed that in confluent monolayers interacting with assembled fibronectin the displacement pattern of fibronectin fibrils in the ECM is similar to that of GFP-vinculin labeled focal adhesions, akin to our observations in sparse BAEC interacting with assembled fibronectin. When individual fibronectin fibrils were tracked, we again observed that fibril displacement was downstream in the first minute after the onset of shear stress. (Figure 32) As in single cells on assembled fibronectin, fibronectin fibril displacement direction and magnitude significantly correlated with displacement of local focal adhesions, indicating mechanical connectivity of these structures. (Figure 33) In the case of displacement angle, the Pearson's correlation coefficient was 0.77 under no shear stress conditions and 0.73 after the onset of shear stress. These correlations were both statistically significant ($p < 0.05$, t test) as measured by a t test of the correlation coefficient. For displacement magnitude, the Pearson's correlation coefficient was 0.93 under no shear stress conditions and 0.90 after the onset of shear stress. Again, this correlation was statistically significant in both cases ($p < 0.05$, t test).

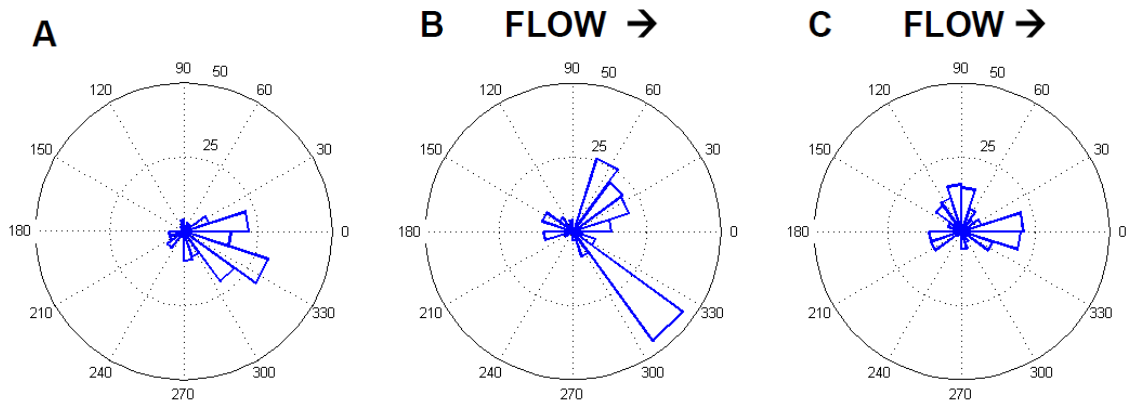


Figure 32. Angular distribution of fibronectin fibril displacement beneath confluent monolayers (A) 15 minutes before the onset of shear stress, (B) one minute after the onset of shear stress and (C) 15 minutes after the onset of shear stress.

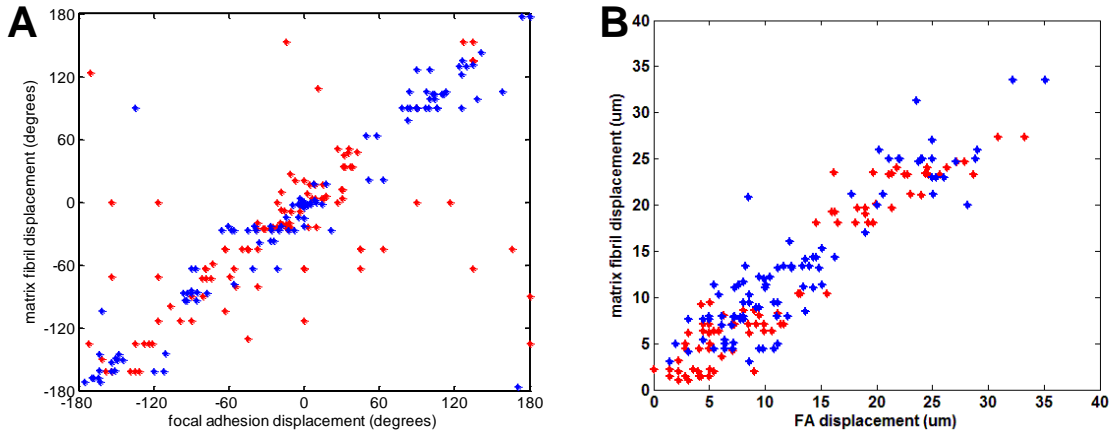


Figure 33. Correlation of displacement direction (A) and magnitude (B) between focal adhesions and nearby fibronectin fibrils both under no-flow conditions (red) and after 15 minutes of shear stress (blue). All correlations shown are statistically significant ($p < 0.05$, t test).

3.2.5 Integrin Distribution

Since fibronectin assembly regulates relative levels of $\alpha_5\beta_1$ and $\alpha_v\beta_3$ binding in single endothelial cells, we hypothesized that the same effect would be observed in confluent monolayers. When we immunostained confluent monolayers interacting with unassembled or assembled fibronectin and exposed to 0 or 15 minutes of shear stress, we saw that the distribution of integrins was dependent on fibronectin assembly. In monolayers on unassembled fibronectin, $\alpha_v\beta_3$ staining was organized into focal adhesion-like structures while $\alpha_5\beta_1$ was punctate but evenly distributed over the basal surface of the monolayer. (Figure 34) In monolayers on assembled fibronectin, the relative distribution of these two integrins was reversed. $\alpha_v\beta_3$ was distributed evenly across the basal surface, while $\alpha_5\beta_1$ was organized into structures that looked like fibrillar adhesions. (Figure 35)

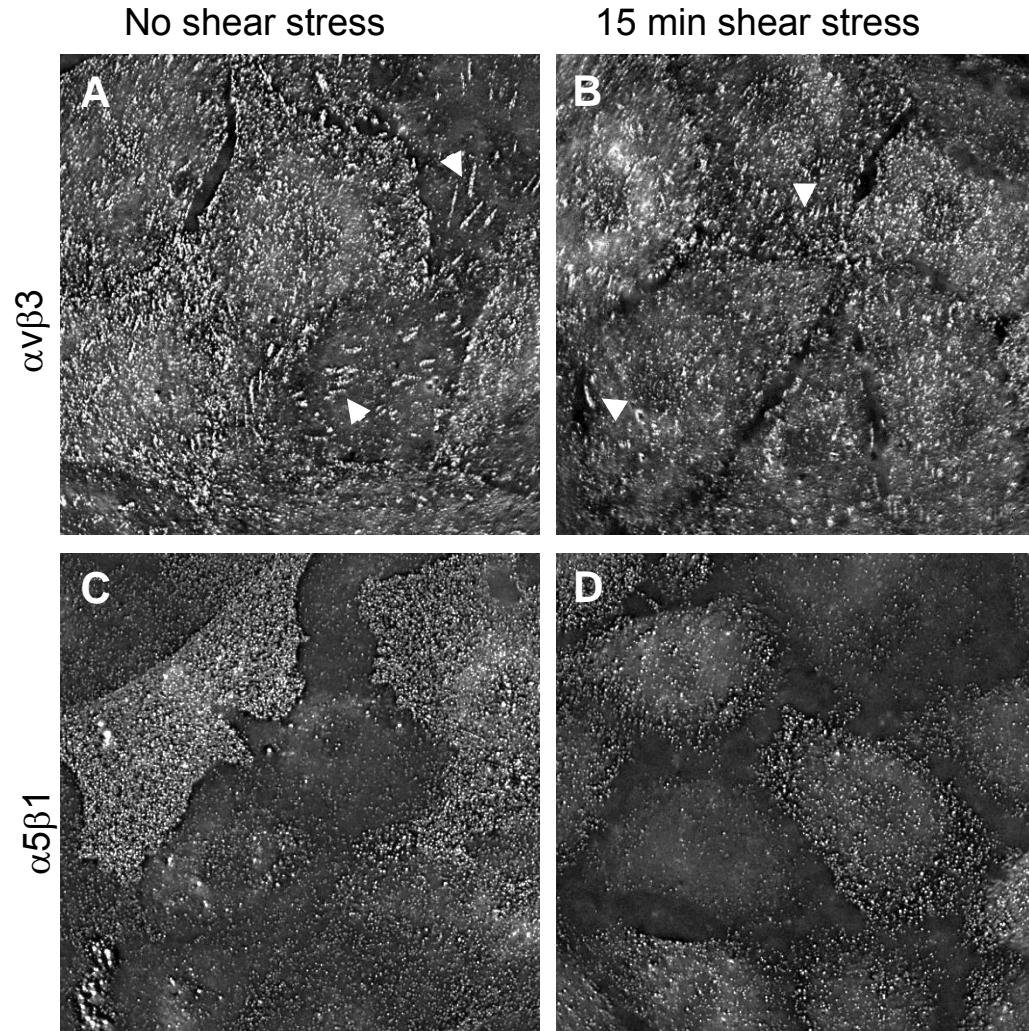


Figure 34. Integrin $\alpha_v\beta_3$ and $\alpha_5\beta_1$ immunostaining in confluent monolayers on assembled fibronectin. Both under no shear stress (A) and after 15 minutes of shear stress (B), $\alpha_v\beta_3$ is visible in focal adhesion-like spots on the basal cell surface (arrowheads). In contrast, both under no shear stress (C) and after 15 minutes of shear stress (D), $\alpha_5\beta_1$ staining is punctate and relatively evenly distributed.

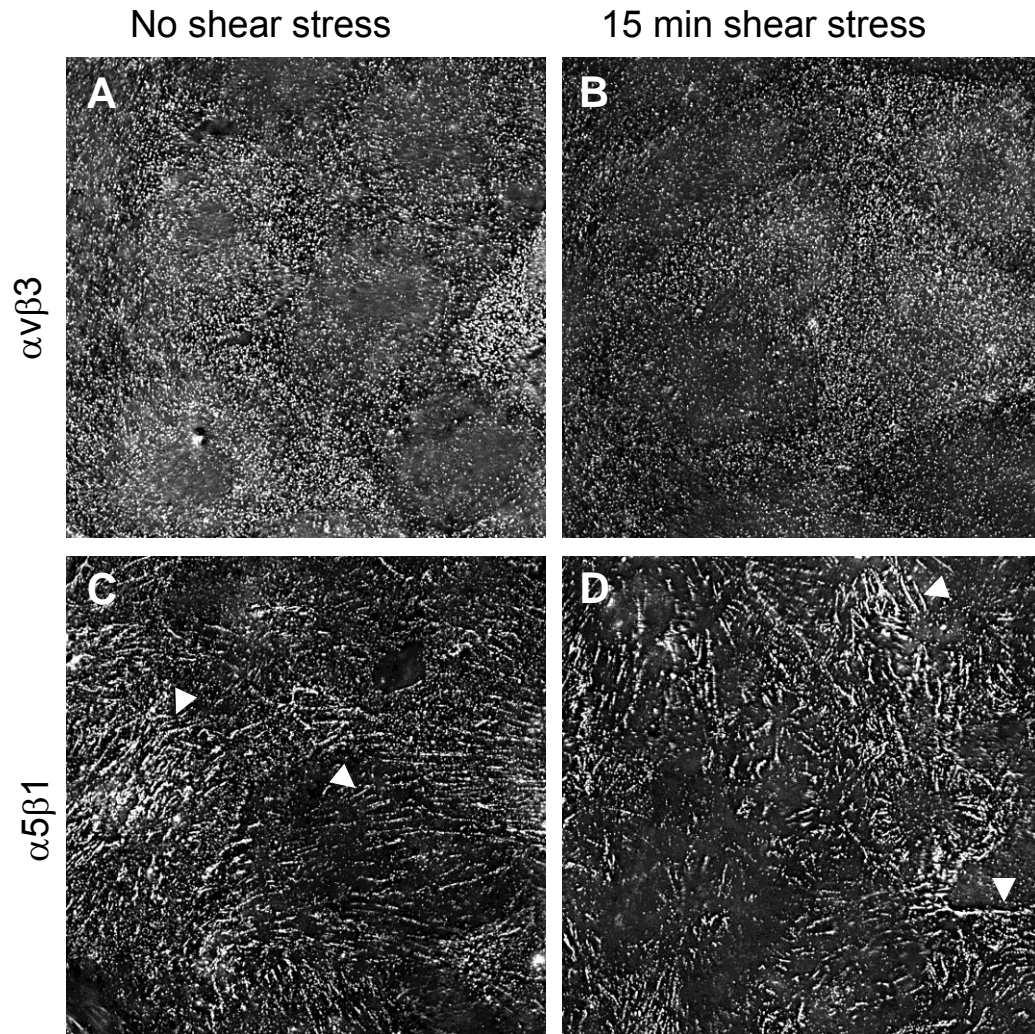


Figure 35. Integrin $\alpha_v\beta_3$ and $\alpha_5\beta_1$ immunostaining in confluent monolayers on assembled fibronectin. Both under no shear stress (A) and after 15 minutes of shear stress (B), $\alpha_v\beta_3$ staining is punctate and relatively evenly distributed. In contrast, both under no shear stress (C) and after 15 minutes of shear stress (D), $\alpha_5\beta_1$ is visible in large fibrillar adhesion-like structures on the basal surface (arrowheads).

To evaluate whether this immunostaining was representative of differences in integrin binding, we crosslinked ligand-bound integrins and used detergent to remove the non-crosslinked components of the cell. These samples were then dually immunostained for α_v and $\alpha_5\beta_1$. We found that integrins which were clustered into focal adhesions were bound to the substrate, but those displaying uniform surface staining were not. The

distribution of integrins in these images corroborated the previous integrin immunostaining results in that confluent monolayers interacting with unassembled fibronectin displayed mainly α_v -based focal adhesion structures, (Figure 36) while confluent monolayers interacting with assembled fibronectin showed mainly $\alpha_5\beta_1$ -based adhesive structures. (Figure 37) In confluent monolayers interacting with unassembled fibronectin there was no difference in $\alpha_5\beta_1$ staining intensity of samples exposed to 15 minutes of shear stress compared to those not exposed to shear stress ($p=0.54$, t test). However, there was a significant increase in α_v staining intensity after the onset of shear stress ($p<0.05$, t test). (Figure 38)

In summary, fibronectin assembly caused changes to the pattern of $\alpha_v\beta_3$ and $\alpha_5\beta_1$ binding in confluent monolayers under no-flow conditions. (Table 5) There were also significant differences between confluent monolayers interacting with assembled or unassembled fibronectin in measurements of shear stress induced alignment, actin stress fiber remodeling, and focal adhesion displacement. (Table 6)

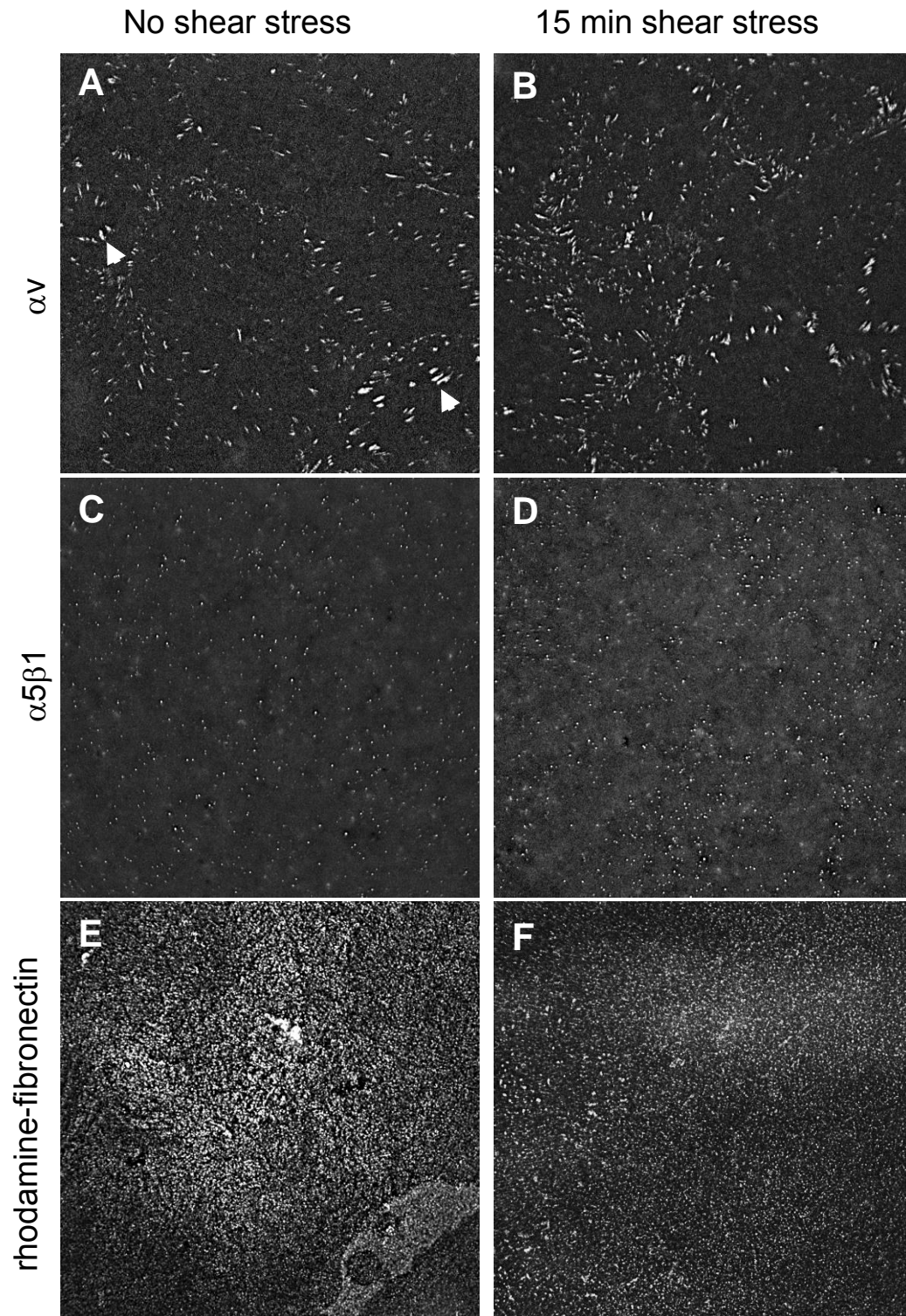


Figure 36. Immunostaining of crosslinked α_v , $\alpha_5\beta_1$ and rhodamine-fibronectin in confluent monolayers interacting with unassembled fibronectin. α_v (A and B) was distributed into focal adhesions (arrowheads). $\alpha_5\beta_1$ (C and D) staining was minimal. Rhodamine-fibronectin (E and F) demonstrates minimal fibronectin assembly.

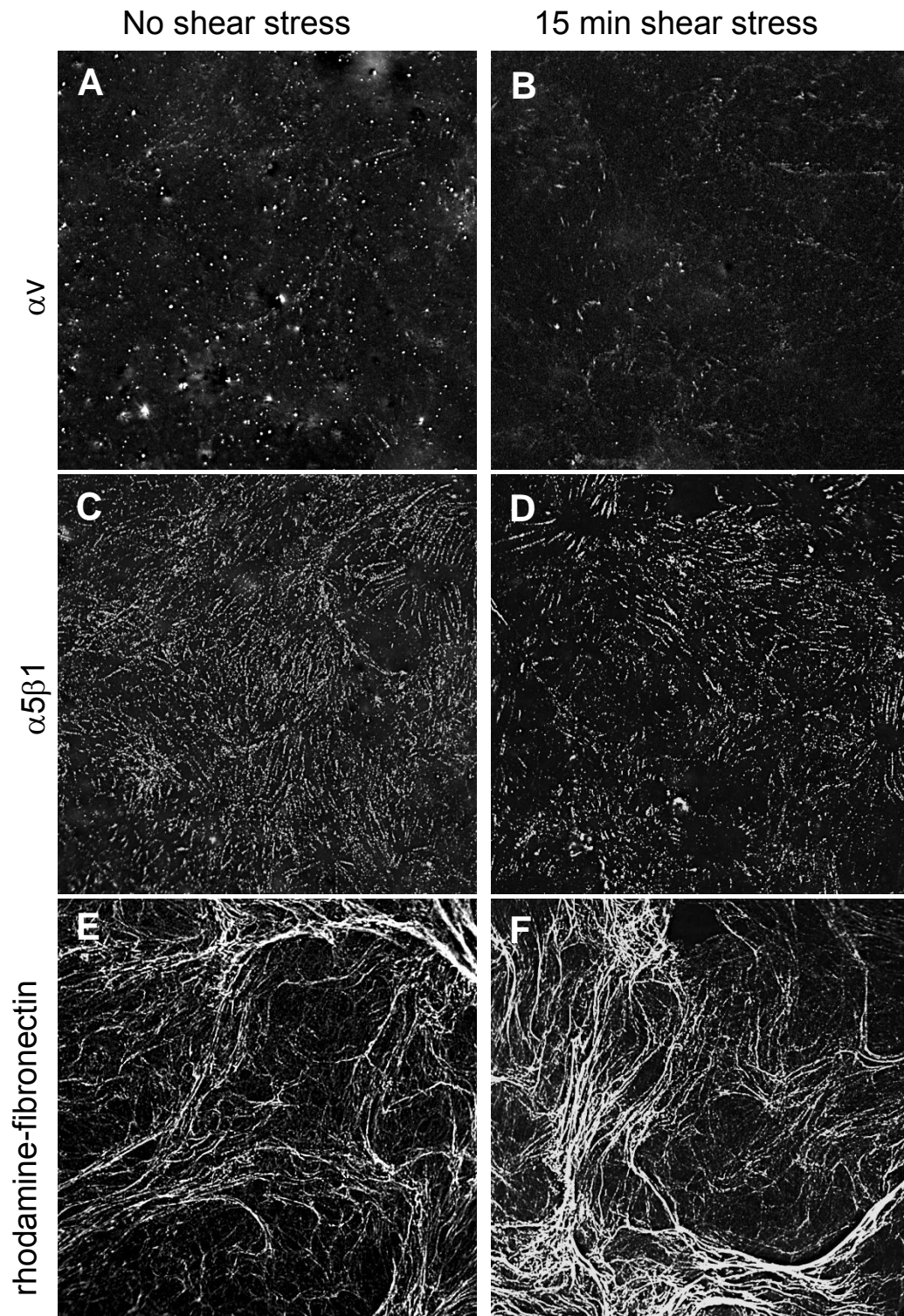


Figure 37. Immunostaining of crosslinked α_v , $\alpha_5\beta_1$ and rhodamine-fibronectin in confluent monolayers interacting with assembled fibronectin. A few α_v -based adhesion spots were visible. (A and B) $\alpha_5\beta_1$ (C and D) staining was distributed into fibrillar adhesion structures. Rhodamine-fibronectin (E and F) demonstrates fibronectin assembly beneath the monolayer.

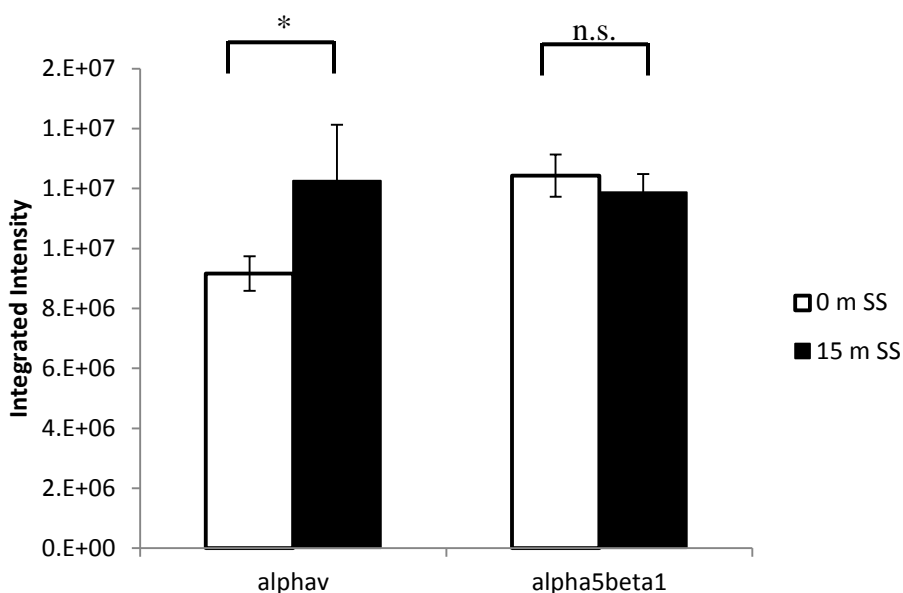


Figure 38. Relative levels of crosslinked integrin staining in monolayers interacting with unassembled fibronectin quantified by total image intensity after background subtraction. After 15 minutes of shear stress, there is a significant increase in α_v intensity (* $p < 0.0$, t test), but no significant change in $\alpha_5\beta_1$ intensity (n.s.=not significant, $p = 0.54$, t test).

Table 5. Readouts modulated in confluent monolayers by fibronectin assembly under no-flow conditions

Readout	Unassembled fibronectin	Assembled fibronectin
$\alpha_v\beta_3$ binding	Yes	No
$\alpha_5\beta_1$ binding	No	Yes

Table 6. Readouts of shear stress responses in confluent monolayers significantly affected by fibronectin assembly.

Readout	Unassembled fibronectin	Assembled fibronectin
Cell alignment	Faster	Slower
Actin stress fiber remodeling	No change	Disassembly
Focal adhesion displacement	Decreased	Increased

Chapter 4: Discussion

This work demonstrates for the first time that fibronectin assembly regulates shear stress-induced structural remodeling and specificity of integrin binding in endothelial cells. Observations in single cells and monolayers revealed that while fibronectin assembly regulates integrin specificity similarly in both cell density conditions, the resulting cytoskeletal and cell shape remodeling induced by the onset of shear stress is different depending on cell density. In single cells fibronectin assembly regulates lamellipodial protrusion and downstream mechanotaxis, while in monolayers fibronectin assembly regulates initial stress fiber remodeling and speed of alignment. Fibronectin assembly likely alters both the presentation of ligands and the material properties of the substrate cells are interacting with, and both these variables have the potential to regulate mechanosensitive signaling. Changes in stiffness could still contribute to our observations, and future studies addressing the contribution of substrate stiffness to shear stress-induced endothelial structural remodeling will be useful. However, it is unlikely that that is the sole factor at work. The dramatic switch in relative binding of $\alpha_v\beta_3$ and $\alpha_5\beta_1$ integrins suggests that this is not simply a graded response to substrate stiffness.

In vivo, fibronectin is found in the vasculature as a major component of the provisional matrix that is the basis of the ECM in wounds and during development. In these regions fibronectin is most likely assembled into fibrils. However, in early wound healing or angiogenesis, it is possible that fibronectin expressed locally by fibroblasts is resident in the ECM, but not yet incorporated into a fibrillar structure. Fibronectin deposition in atherosclerotic lesions has been observed *in vivo*, and *in vitro* studies of fibronectin deposition and assembly suggest that the fibronectin in these regions is

assembled. If fibronectin exists mainly as assembled fibrils *in vivo*, our data would then suggest that single cell downstream mechanotaxis might not occur *in vivo*, and may be an artifact of the system of fibronectin coated glass that is widely used to study mechanoresponses *in vitro*. However, this system still provides insight into the signaling pathways involved in shear stress-induced mechanotransduction and helps us to begin to understand how endothelial responses to shear stress might be altered when interacting with the surface of an implanted device, especially since plasma fibronectin would become adsorbed to the surface of an implant exposed to blood flow.

While there have been previous reports that altering the molecular structure of fibronectin or the availability of binding sites can regulate the relative binding of $\alpha_v\beta_3$ and $\alpha_5\beta_1$ integrins, this is the first report directly comparing unassembled fibronectin to assembled fibronectin matrix. Because $\alpha_5\beta_1$ integrins are so closely linked to fibronectin assembly it is not surprising that $\alpha_5\beta_1$ binding is promoted by interacting with assembled fibronectin. However, it is unexpected that assembled fibronectin seems to also inhibit $\alpha_v\beta_3$ binding. Both $\alpha_5\beta_1$ and $\alpha_v\beta_3$ integrins bind to the RGD site in the 10th type III repeat in fibronectin but $\alpha_5\beta_1$ additionally binds the synergy site in the 9th type III repeat, suggesting that fibronectin assembly could regulate integrin binding by regulating accessibility of the synergy site. Indeed, CHO cells interacting with assembled fibronectin lacking the synergy site use $\alpha_v\beta_3$ integrins to migrate but use $\alpha_5\beta_1$ integrins to migrate on wild type assembled fibronectin. [64] However, there have not been any studies of how fibronectin assembly might promote synergy site availability, or whether this actually occurs. Since there is no antibody available to gauge accessibility of the synergy site, it might be possible to use purified and tagged integrins or integrin

fragments as a synergy site binding partner to evaluate whether synergy site availability is regulated by fibronectin organization.

In both single cells and confluent monolayers, patterns of focal adhesion displacement were regulated by fibronectin assembly. In cells interacting with unassembled fibronectin shear stress caused arrest of focal adhesion displacement, which did not occur in cells interacting with assembled fibronectin. Because displacement reflects a force balance that is a combination of biochemical turnover and mechanical movement, adhesion arrest could be due to either reduced forces applied to the adhesion or increased adhesive force. Since applying shear stress should increase force on adhesions, reducing applied force would have to be due to reduced cell contractility or reduced cytoskeletal linkage to adhesions. However, we don't see any decrease in stress fiber content. Increased integrin binding could increase adhesive force, effectively resisting forces applied through the cytoskeleton and causing focal adhesion arrest. Consistent with this model, we are able to measure a small increase in $\alpha_v\beta_3$ adhesion as measured by increased immunofluorescence staining intensity in monolayers interacting with unassembled fibronectin. It is important to note that increased adhesive force can also be due to increased recruitment of talin or vinculin. [74] Cytoskeletal deformation and pulling on adhesions can cause stretching of talin and increased vinculin recruitment. [75] Since talin and integrins are so closely linked, this mechanism could also promote increased recruitment of integrins. Interestingly, it has been noted that arrest of focal adhesions was associated with the local formation of new protrusions. [76] This suggests a model in which physical force on adhesions causes increased recruitment of focal

adhesion proteins followed by Rac activation, which would then in turn recruit $\alpha_v\beta_3$ integrins to the leading edge of the cell to stabilize the new protrusion.

In contrast, focal adhesion displacement in cells interacting with assembled fibronectin was unchanged by the onset of shear stress in single cells, but increased at the onset of shear stress in monolayers. Because assembled fibronectin forms a distensible matrix, the potential passive deformation of this structure by fluid flow must be considered. Shearing of assembled fibronectin isolated from monolayers but without sparse cells replated on it reveals that the onset of shear stress induces a small, non-uniform, transient movement of fibronectin fibrils. (Figure 39) This passive deformation may contribute to the transient downstream displacement of focal adhesions and fibronectin fibrils observed in the first minute after the onset of shear stress in both single cells and monolayers. However, it remains to be determined whether this type of passive deformation plays a role in modulating mechanotransduction.

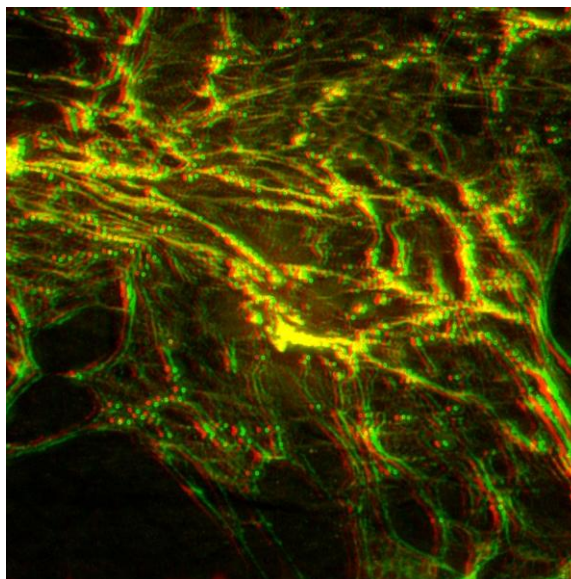


Figure 39. Overlay of isolated rhodamine-fibronectin exposed to 15 minute of shear stress. Image from immediately before the onset of shear stress (red) is overlaid with image after 15 minutes of shear stress (green).

Fibronectin itself is sensitive to mechanical forces in that applying force changes the conformation of the protein and the organization of assembled fibronectin matrix. This means that shear stress can cause changes in fibronectin ECM both at the level of fibrillar organization and at the level of conformation of individual fibronectin proteins. As cells align with the direction of flow, so do fibronectin fibrils as they are guided by the orientation of applied force. [66] We have not observed alignment of fibrils within our 18 hour alignment studies. However, it likely occurs subsequent to monolayer alignment and could take up to 24-48 hours. Once fibrils are aligned, the ECM likely acts as a much more anisotropic material, with aligned fibers working with unidirectional shear stress to guide cell polarity and shape. Our data regarding single cell mechanotaxis suggests that fibril guidance in a random fibril network may compete with signals from unidirectional shear stress that guide cell migration. However, it would be informative to know whether fibrils aligned parallel to the direction of flow act synergistically with shear stress, as suggested by previous studies using grooved topographies. [43, 44] We have shown that focal adhesion and nearby fibronectin fibril displacements are highly correlated. This suggests that forces applied to focal adhesions, whether due to fluid flow or cell contractility, are transferred to the matrix beneath. Not only does this guide alignment of fibrils, but could regulate fibril biochemistry. Studies of fibril and ECM stretching have shown that extension of fibrils alters their mechanical properties and the availability of cryptic binding sites. As a single fibril is stretched, its elastic modulus varies from kilopascals to megapascals as a function of extension. [53] Stretching of fibrils also causes fibril unfolding and exposure of cryptic binding sites. [53] When assembled fibronectin matrices are crosslinked to stiffen them, more new fibronectin is

assembled into the matrix and these new fibrils are more stretched. This suggests that either stretching or crosslinking of existing ECM would stiffen it, drive the assembly of new, stiffened fibrils, and potentially expose new binding sites for other ECM components or for cells. In the context of shear stress, long term unidirectional flow stimulates the formation of actin stress fibers, suggesting increased cell contractility. This increased force generation might then promote not only fibronectin fibril alignment, but increased assembly and changes in fibril biochemistry.

4.1 Modulation of shear stress responses in single cells by fibronectin assembly

In single endothelial cells, fibronectin assembly alters remodeling of both the actin cytoskeleton and focal adhesions to ultimately control shear stress-induced mechanotaxis. The observations that $\alpha_v\beta_3$ integrin binding is reduced on assembled fibronectin and that blocking $\alpha_v\beta_3$ ligation at least temporarily inhibits mechanotaxis suggest that $\alpha_v\beta_3$ is a pivotal player in guiding shear stress-induced downstream migration. Binding and activation of $\alpha_v\beta_3$ at the leading edge has already been implicated in directed cell migration. [77] Furthermore, engagement of $\alpha_v\beta_3$ results in more persistent directed migration because $\alpha_v\beta_3$ is recycled along a short loop endocytic pathway and $\alpha_5\beta_1$ recycling occurs in a long loop endocytic pathway. Interestingly, this mechanism regulates migration not only through promoting recruitment of $\alpha_v\beta_3$ to the leading edge, but also by suppressing $\alpha_5\beta_1$ recycling back to the cell membrane. [78] Recruitment of $\alpha_v\beta_3$ to the leading edge in cells undergoing chemotaxis has been shown to be Rac-dependent. [77] This suggests that in our system another upstream

mechanosensor activates Rac, which recruits activated $\alpha_v\beta_3$ to stabilize newly formed protrusions, and local accumulation of $\alpha_v\beta_3$ suppresses transport of $\alpha_5\beta_1$ to the leading edge. Understanding whether Rac activity is directly regulated by fibronectin assembly or whether fibronectin assembly regulates this mechanism by controlling $\alpha_v\beta_3$ binding would help clarify how fibronectin assembly is regulating this pathway.

Although we provide evidence via integrin immunostaining and integrin blocking that differential integrin binding is likely important in the mechanism by which fibronectin assembly regulates mechanotaxis, the potential contribution of ECM material properties cannot be ignored. The modulus of assembled fibronectin is reported to be 400 Pa, [65] which is 7 orders of magnitude lower than glass, and the decreased spreading and decreased stress fiber content in cells on assembled fibronectin is consistent with interacting with a surface much less stiff than glass. Increased substrate modulus is known to promote integrin binding and clustering, which could influence integrin-dependent signaling under shear stress. It has been shown specifically for $\alpha_5\beta_1$ integrins that increased substrate stiffness promotes both increased integrin binding and increased FAK activity. [79] This idea has been investigated extensively in the context of cancer where ECM crosslinking causes stiffening that drives increased formation of focal adhesions, increased contractility, and increased activation of downstream signaling molecules including FAK and p130Cas. Activation of these pathways promotes migration and proliferation. [80, 81] Increased shear stress-induced integrin recruitment and clustering on unassembled fibronectin would be consistent with our observations of focal adhesion arrest and stabilization of protrusions that facilitate spreading and mechanotaxis. On assembled fibronectin, reduced shear stress-induced integrin

recruitment would also be consistent with the lack of focal adhesion arrest and reduced spreading. This could be tested by cross-linking assembled fibronectin to stiffen the matrix structure without altering the fibronectin organization, which we hypothesize would promote shear stress-induced integrin recruitment. Alternatively, rather than integrin binding being directly regulated, substrate stiffness might regulate signaling downstream of integrins. In the context of shear stress, p130Cas is activated at the downstream edge of the cell and activates Rac through the RacGEF DOCK180 to promote downstream protrusion and migration. [20] On substrates of varying stiffness, p130Cas is activated downstream of $\alpha_v\beta_3$ at the leading edge of the cell in a stiffness-dependent manner. [82] This results in reduced spreading as substrate stiffness decreases, and would certainly affect the ability of the cell to migrate. While we observed no effect of fibronectin assembly on migration speed, this mechanism could contribute to reduced downstream protrusion in cells on assembled fibronectin. This could be tested by using fibronectin-coated gels of varying stiffness and evaluating shear stress responses, including spreading and migration, as a function of gel stiffness.

4.2 Modulation of shear stress responses in monolayers by fibronectin assembly

In confluent monolayers, fibronectin assembly regulates both short-term cytoskeletal remodeling and long term shape adaptation to shear stress. Since these behaviors are known to be ultimately dependent on integrin-mediated signaling, it is likely that the observed assembly-dependent differences in cytoskeletal remodeling and alignment are linked to the differences in relative $\alpha_5\beta_1$ and $\alpha_v\beta_3$ binding observed in monolayers on assembled and unassembled fibronectin.

Transient shear stress-induced stress fiber disassembly, as observed in monolayers interacting with assembled fibronectin, is dependent on activation of p190RhoGAP and inactivation of Rho. Activation of this pathway is required for shear stress-induced alignment, since cells expressing dominant-negative p190RhoGAP do not align. [36] Interestingly, monolayers interacting with unassembled fibronectin do not display this disassembly response, yet are able to align with the direction of shear stress more quickly than monolayers interacting with assembled fibronectin. It is unlikely that stress fiber disassembly is simply occurring more rapidly in these cells, since even monolayers exposed to only 5 minutes of shear stress show the same trend in increased stress fiber content. This suggests two things. First, that either p190RhoGAP is regulated differently in monolayers on unassembled fibronectin than in monolayers on assembled fibronectin, or there is a competing mechanism controlling stress fiber remodeling. Second, that transient stress fiber disassembly may not be required for alignment to occur, which would contradict the current dogma that transient stress fiber disassembly at the onset of shear stress is required for alignment.

Under shear stress, phosphorylation and activation of p190RhoGAP is dependent on β_1 integrins and Src. Activation of p190RhoGAP in this pathway is consistent with our observations of actin organization and integrin binding. In monolayers on assembled fibronectin, $\alpha_5\beta_1$ integrin binding dominates over $\alpha_v\beta_3$ and shear stress induces stress fiber disassembly. In contrast, $\alpha_5\beta_1$ binding is almost non-existent in monolayers interacting with unassembled fibronectin and shear stress does not induce stress fiber disassembly in this case, suggesting that perhaps p190RhoGAP is not activated by shear stress in monolayers interacting with unassembled fibronectin. However, it is also

possible that p190RhoGAP is activated in the unassembled case, and is counterbalanced by activation of a RhoGEF. One likely candidate is the RhoGEF LARG. This GEF is also activated downstream of initial adhesion of fibronectin binding integrins, [83] and is involved in reinforcement of adhesion in magnetic bead pulling assays. [84] Interestingly, in the context of initial cell adhesion and spreading on fibronectin-coated glass, LARG is responsible for increased Rho activity subsequent to transient p190RhoGAP-dependent Rho downregulation. This is the same pattern of dynamic Rho activity that has been reported by others to be induced at the onset of shear stress. Whether activation of this RhoGEF is specific to $\alpha_5\beta_1$ or $\alpha_v\beta_3$ integrins is unclear. Activation of LARG in magnetic bead pulling assays was inhibited by addition of an anti- β_1 blocking antibody. However, activation of LARG was also shown to be dependent on Fyn, which can also be activated by $\alpha_v\beta_3$ integrins. In the context of our studies, a mechanism involving $\alpha_v\beta_3$, Fyn, and LARG would be consistent with the role of $\alpha_v\beta_3$ in adhesion reinforcement and the observation that $\alpha_v\beta_3$ -based adhesion area increases and focal adhesion displacement decreases after the onset of shear stress in monolayers on unassembled fibronectin. However, the role of LARG in the context of shear stress and this hypothetical mechanism both remain to be investigated.

While it has been suggested that the initial cytoskeletal remodeling stimulated within minutes after the onset of shear stress is required for shear stress-induced alignment, the mechanism linking short-term and long-term structural remodeling is still unknown. The studies suggesting the importance of short-term remodeling have used complete blocks of relevant signaling pathways, which could inhibit cytoskeletal remodeling on multiple time scales without those different remodeling events being

dependent on each other. Indeed, recent data from our lab suggests that in monolayers subjected to unidirectional substrate stretch, early remodeling events such as actin ruffling are not required for stress fibers to align. [85] Because $\alpha_v\beta_3$ binding is increased in monolayers on unassembled fibronectin, and these monolayers align more quickly, this suggests a model in which $\alpha_v\beta_3$ -dependent signaling promotes alignment. Furthermore, since $\alpha_v\beta_3$ binding plays a role in guiding single cell mechanotaxis, this integrin may also provide a polarity cue in the context of monolayer alignment. While none of our observations in monolayers suggested a polarized distribution of $\alpha_v\beta_3$ that might direct alignment, it has been noted that in aligned monolayers, $\alpha_v\beta_3$ expression becomes localized to the upstream side of the cell. [86]

Chapter 5: Conclusions

5.1 Achievements of this study

These studies demonstrate for the first time evidence that fibronectin assembly inhibits mechanosensing under shear stress. This effect is likely mediated through assembly-dependent regulation of relative levels of $\alpha_5\beta_1$ and $\alpha_v\beta_3$ binding. Fibronectin assembly was observed to promote $\alpha_5\beta_1$ engagement over $\alpha_v\beta_3$. In both single cells and confluent monolayers fibronectin assembly modulated cytoskeletal remodeling and adhesive interactions with the ECM, but this manifested differently in terms of cell shape change and migration. In single cells fibronectin assembly inhibited downstream mechanotaxis, while in confluent monolayers fibronectin assembly inhibited monolayer alignment. Single cell mechanotaxis was also inhibited by blocking $\alpha_v\beta_3$ binding to fibronectin. This result combined with the observed assembly-dependent differences in integrin binding, suggests that $\alpha_v\beta_3$ is essential for directing downstream mechanotaxis.

Together, these data suggest a model in which fibronectin assembly promotes engagement of $\alpha_5\beta_1$ over $\alpha_v\beta_3$. When cells are exposed to shear stress, this results in differential structural remodeling due to differences in integrin-dependent signaling. Based on our observations of cytoskeletal remodeling, shape change and motility, we hypothesize that $\alpha_v\beta_3$ engagement is associated with Rac activity, protrusion, mechanotaxis and alignment and that $\alpha_5\beta_1$ engagement is associated with transient Rho inactivation and stress fiber remodeling. (Figure 40)

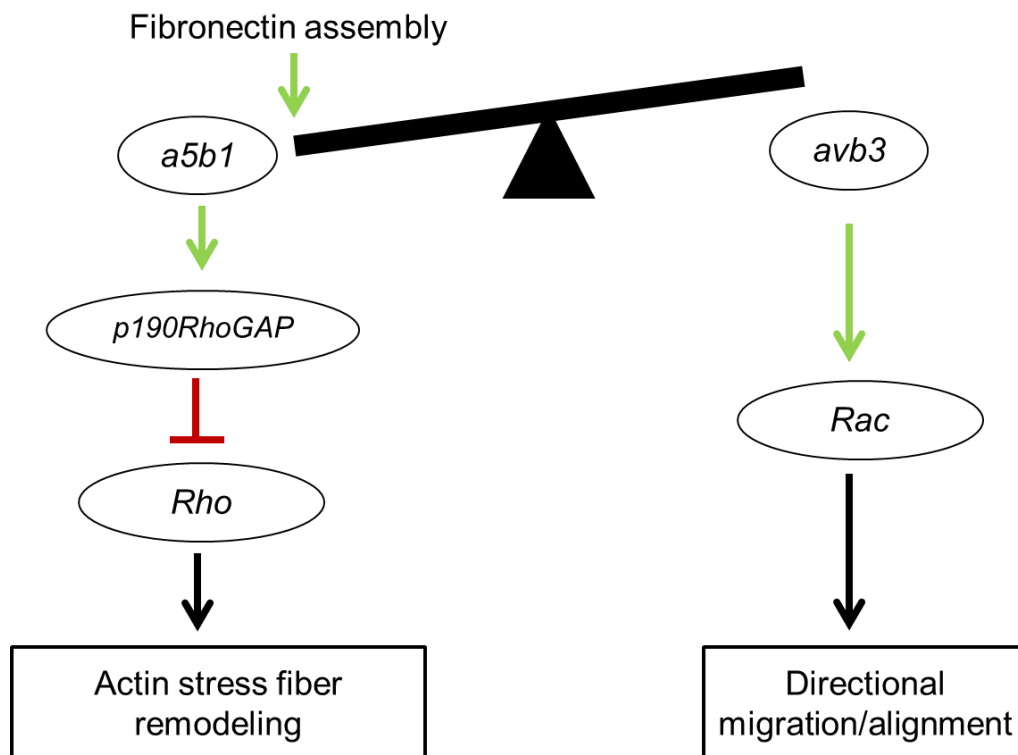


Figure 40. Hypothesized model of how fibronectin assembly regulates shear stress-induced structural remodeling.

5.2 Future work

While this study is the first suggesting that fibronectin assembly modulates endothelial responses to shear stress, systematic studies using more controlled surfaces would be provide more specific information about what design parameters are most important for controlling endothelial behavior under shear stress. Using cell-derived ECM is more similar to what cells interact with *in vivo* than an artificially generated substrate; however, material parameters including substrate stiffness, topology, and ligand density are confounded in this system. Furthermore, using materials with properties similar to those used in stents and other implantable devices would supply information that would be translatable to device design.

In order to separate the variables of substrate stiffness and fibrillar structure, endothelial cells should be plated on two different types of surfaces. First, fibronectin-coated acrylamide gels of varying stiffness have been widely used to study how cells respond to changes in substrate stiffness. These gels are typically less than 100 μm thick, and could easily be implemented in combination with a flow chamber to specifically investigate the effect of substrate stiffness on shear stress-induced structural remodeling. These gels also have the advantage of being uniform, which allows for better characterization of the mechanical environment and allows the implementation of traction force microscopy to measure the forces exerted on the substrate. Both sparse and confluent endothelial cells would be plated on fibronectin-coated gels of stiffnesses ranging from hundreds of pascals, similar to the stiffness of native assembled fibronectin, up to 10 kilopascals. These stiffnesses are still significantly lower than the stiffness of glass; however, altering substrate stiffness in this range has already been shown to regulate other endothelial behaviors including spreading, monolayer formation, and migration. [87, 88, 89] Furthermore, this is a range of stiffnesses that could conceivably exist *in vivo*, representing a range from normal fibronectin matrix to a highly crosslinked matrix. Both glass and acrylamide gel substrates could also be used to interrogate the effect of ligand density on shear stress-induced structural remodeling. Studies combinatorially varying substrate stiffness and ligand density could be conducted to evaluate the combined effect of these variables.

In order to evaluate the effect of fibrillar structure or topography, both artificial polymer substrates and cell-assembled fibronectin matrices should be used in order to separate the effect of fibrillar topography from any potential biochemical differences

between fibronectin fibrils and adsorbed fibronectin. Fibrillar polymer substrates have been produced through the use of electrospinning, which can create random or aligned polymer fibrils on the order of microns to tens of nanometers. By adsorbing fibronectin on these fibrils the same way as we previously did on glass, we can create a substrate with fibrillar structure, but without fibronectin polymerized into fibrils. While we have already characterized shear stress-induced structural remodeling in cells on fibrillar fibronectin isolated from monolayers, we can again investigate the interaction of substrate stiffness and fibrillar structure by crosslinking assembled fibronectin. This will tell us whether cells respond differently to changes in substrate stiffness on a flat substrate versus a fibrillar substrate. All of these factors can be integrated into a model for designing stent or vascular implant surfaces to optimize endothelial motility, proliferation, and monolayer formation.

While systematic interrogation of substrate properties will help elucidate empirically how ECM organization regulates structural remodeling and endothelial behaviors under shear stress, understanding the biochemical pathways involved will be equally important in understanding and intervening in this system. Previous work in both shear stress-induced structural remodeling and substrate regulation of cell behavior and structure have clearly established several pathways that likely contribute to assembly-dependent regulation of shear stress-dependent structural remodeling.

The GTPases Rho and Rac are central regulators of cytoskeletal organization, shape remodeling, and motility. Establishing whether the dynamic patterns of Rho and Rac activity induced by shear stress are regulated by fibronectin assembly will be essential. While global, biochemical information about Rho and Rac activity will be

informative, using a FRET probe or some other method that can provide spatial information about GTPase activity would provide even more insight into how these pathways are regulated. The two most likely upstream regulators of Rho activity are p190RhoGAP, which has already been shown to play a role in regulating Rho activity under shear stress, and the RhoGEF LARG, which is implicated in integrin-mediated Rho activation both in spreading and in response to mechanical forces. In terms of investigating Rac regulation, p130Cas is clearly an important regulator of polarized Rac activity and DOCK180/ELMO is one likely RacGEF already shown to be downstream of p130Cas, so understanding whether this pathway is modulated by fibronectin assembly might be important in potentially explaining differences in Rac activation. However, since we have evidence that fibronectin assembly directly regulates relative levels of $\alpha_v\beta_3$ and $\alpha_5\beta_1$ binding, regulation of Rho and Rac under shear stress might occur directly through modulation of integrin binding. While we have some preliminary evidence that $\alpha_v\beta_3$ is linked to Rac activity, ruffling and protrusion, further investigation of this pathway is needed. Aside from antibody blocking, using siRNA against $\alpha_v\beta_3$ would more completely block $\alpha_v\beta_3$ -dependent signaling.

Ultimately, these studies show that extracellular matrix organization, not just biochemistry, alters patterns of integrin binding and regulates cell responses to shear stress. This provides insight relevant to understanding the role of fibronectin in atherosclerosis, and suggests variables to incorporate into stent and engineered vessel design to better control endothelial behavior under shear stress.

REFERENCES

- 1 Nakashima Y, Raines EW, Plump AS, Breslow JL, Ross R. *Upregulation of VCAM-1 and ICAM-1 at atherosclerosis-prone sites on the endothelium in the ApoE-deficient mouse*. Arterioscler Thromb Vasc Biol. 1998 May;18(5):842-51.
- 2 Iiyama K, Hajra L, Iiyama M, Li H, DiChiara M, Medoff BD, Cybulsky MI. *Patterns of vascular cell adhesion molecule-1 and intercellular adhesion molecule-1 expression in rabbit and mouse atherosclerotic lesions and at sites predisposed to lesion formation*. Circ Res. 1999 Jul 23;85(2):199-207.
- 3 Levesque MJ, Liepsch D, Moravec S, Nerem RM. Correlation of endothelial cell shape and wall shear stress in a stenosed dog aorta. Arteriosclerosis. 1986 Mar-Apr;6(2):220-9.
- 4 Hajra L, Evans AI, Chen M, Hyduk SJ, Collins T, Cybulsky MI. *The NF-kappa B signal transduction pathway in aortic endothelial cells is primed for activation in regions predisposed to atherosclerotic lesion formation*. Proc Natl Acad Sci U S A. 2000 Aug 1;97(16):9052-7.
- 5 Lloyd-Jones D, Adams RJ, Brown TM, Carnethon M, Dai S, De Simone G, Ferguson TB, Ford E, Furie K, Gillespie C, Go A, Greenlund K, Haase N, Hailpern S, Ho PM, Howard V, Kissela B, Kittner S, Lackland D, Lisabeth L, Marelli A, McDermott MM, Meigs J, Mozaffarian D, Mussolino M, Nichol G, Roger VL, Rosamond W, Sacco R, Sorlie P, Roger VL, Thom T, Wasserthiel-Smoller S, Wong ND, Wylie-Rosett J; American Heart Association Statistics Committee and Stroke Statistics Subcommittee. *Heart disease and stroke statistics--2010 update: a report from the American Heart Association*. Circulation. 2010 Feb 23;121(7):e46-e215.
- 6 Moore J Jr, Berry JL. *Fluid and solid mechanical implications of vascular stenting*. Ann Biomed Eng. 2002 Apr;30(4):498-508.
- 7 Joner M, Finn AV, Farb A, Mont EK, Kolodgie FD, Ladich E, Kutys R, Skorija K, Gold HK, Virmani R. *Pathology of drug-eluting stents in humans: delayed healing and late thrombotic risk*. J Am Coll Cardiol. 2006 Jul 4;48(1):193-202.
- 8 Vartanian KB, Berny MA, McCarty OJ, Hanson SR, Hinds MT. *Cytoskeletal structure regulates endothelial cell immunogenicity independent of fluid shear stress*. Am J Physiol Cell Physiol. 2010 Feb;298(2):C333-41.
- 9 Walpole PL, Gotlieb AI, Cybulsky MI, Langille BL. *Expression of ICAM-1 and VCAM-1 and monocyte adherence in arteries exposed to altered shear stress*. Arterioscler Thromb Vasc Biol. 1995 Jan;15(1):2-10.
- 10 Barron V, Brougham C, Coghlan K, McLucas E, O'Mahoney D, Stenson-Cox C, McHugh PE. *The effect of physiological cyclic stretch on the cell morphology, cell orientation and protein expression of endothelial cells*. J Mater Sci Mater Med. 2007 Oct;18(10):1973-81.
- 11 Osborn EA, Rabodzey A, Dewey CF Jr, Hartwig JH. *Endothelial actin cytoskeleton remodeling during mechanostimulation with fluid shear stress*. Am J Physiol Cell Physiol. 2006 Feb;290(2):C444-52.
- 12 Noria S, Cowan DB, Gotlieb AI, Langille BL. *Transient and steady-state effects of shear stress on endothelial cell adherens junctions*. Circ Res. 1999 Sep 17;85(6):504-14.

- 13 Mott RE, Helmke BP. *Mapping the dynamics of shear stress-induced structural changes in endothelial cells*. Am J Physiol Cell Physiol. 2007 Nov;293(5):C1616-26.
- 14 Lin X, Helmke BP. *Micropatterned structural control suppresses mechanotaxis of endothelial cells*. Biophys J. 2008 Sep 15;95(6):3066-78.
- 15 Galbraith CG, Skalak R, Chien S. *Shear stress induces spatial reorganization of the endothelial cell cytoskeleton*. Cell Motil Cytoskeleton. 1998;40(4):317-30.
- 16 Kadohama T, Akasaka N, Nishimura K, Hoshino Y, Sasajima T, Sumpio BE. *p38 Mitogen-activated protein kinase activation in endothelial cell is implicated in cell alignment and elongation induced by fluid shear stress*. Endothelium. 2006 Jan-Feb;13(1):43-50.
- 17 Hsiai TK, Cho SK, Honda HM, Hama S, Navab M, Demer LL, Ho CM. *Endothelial cell dynamics under pulsating flows: significance of high versus low shear stress slew rates ($d(\tau)/dt$)*. Ann Biomed Eng. 2002 May;30(5):646-56.
- 18 Riveline D, Zamir E, Balaban NQ, Schwarz US, Ishizaki T, Narumiya S, Kam Z, Geiger B, Bershadsky AD. *Focal contacts as mechanosensors: externally applied local mechanical force induces growth of focal contacts by an mDial-dependent and ROCK-independent mechanism*. J Cell Biol. 2001 Jun 11;153(6):1175-86.
- 19 von Wichert G, Haimovich B, Feng GS, Sheetz MP. *Force-dependent integrin-cytoskeleton linkage formation requires downregulation of focal complex dynamics by Shp2*. EMBO J. 2003 Oct 1;22(19):5023-35.
- 20 Zaidel-Bar R, Kam Z, Geiger B. *Polarized downregulation of the paxillin-p130Cas-Rac1 pathway induced by shear flow*. J Cell Sci. 2005 Sep 1;118(Pt 17):3997-4007.
- 21 Davies PF, Robotewskyj A, Griem ML. *Quantitative studies of endothelial cell adhesion. Directional remodeling of focal adhesion sites in response to flow forces*. J Clin Invest. 1994 May;93(5):2031-8.
- 22 Li S, Butler P, Wang Y, Hu Y, Han DC, Usami S, Guan JL, Chien S. *The role of the dynamics of focal adhesion kinase in the mechanotaxis of endothelial cells*. Proc Natl Acad Sci U S A. 2002 Mar 19;99(6):3546-51.
- 23 Na S, Collin O, Chowdhury F, Tay B, Ouyang M, Wang Y, Wang N. *Rapid signal transduction in living cells is a unique feature of mechanotransduction*. Proc Natl Acad Sci U S A. 2008 May 6;105(18):6626-31.
- 24 Ridley AJ, Paterson HF, Johnston CL, Diekmann D, Hall A. *The small GTP-binding protein rac regulates growth factor-induced membrane ruffling*. Cell. 1992 Aug 7;70(3):401-10.
- 25 Ridley AJ, Hall A. *The small GTP-binding protein rho regulates the assembly of focal adhesions and actin stress fibers in response to growth factors*. Cell. 1992 Aug 7;70(3):389-99.
- 26 Tzima E, del Pozo MA, Shattil SJ, Chien S, Schwartz MA. *Activation of integrins in endothelial cells by fluid shear stress mediates Rho-dependent cytoskeletal alignment*. EMBO J. 2001 Sep 3;20(17):4639-47.
- 27 Tzima E, Del Pozo MA, Kiosses WB, Mohamed SA, Li S, Chien S, Schwartz MA. *Activation of Rac1 by shear stress in endothelial cells mediates both cytoskeletal reorganization and effects on gene expression*. EMBO J. 2002 Dec 16;21(24):6791-800.
- 28 Tzima E. *Role of small GTPases in endothelial cytoskeletal dynamics and the shear stress response*. Circ Res. 2006 Feb 3;98(2):176-85.

- 29 Malek AM, Izumo S. *Mechanism of endothelial cell shape change and cytoskeletal remodeling in response to fluid shear stress*. J Cell Sci. 1996 Apr;109 (Pt 4):713-26.
- 30 Noria S, Xu F, McCue S, Jones M, Gotlieb AI, Langille BL. *Assembly and reorientation of stress fibers drives morphological changes to endothelial cells exposed to shear stress*. Am J Pathol. 2004 Apr;164(4):1211-23.
- 31 Wojciak-Stothard B, Ridley AJ. *Shear stress-induced endothelial cell polarization is mediated by Rho and Rac but not Cdc42 or PI 3-kinases*. J Cell Biol. 2003 Apr 28;161(2):429-39.
- 32 Ren XD, Kiosses WB, Schwartz MA. *Regulation of the small GTP-binding protein Rho by cell adhesion and the cytoskeleton*. EMBO J. 1999 Feb 1;18(3):578-85.
- 33 Tzima E, Irani-Tehrani M, Kiosses WB, Dejana E, Schultz DA, Engelhardt B, Cao G, DeLisser H, Schwartz MA. *A mechanosensory complex that mediates the endothelial cell response to fluid shear stress*. Nature. 2005 Sep 15;437(7057):426-31.
- 34 Tzima E, Kiosses WB, del Pozo MA, Schwartz MA. *Localized cdc42 activation, detected using a novel assay, mediates microtubule organizing center positioning in endothelial cells in response to fluid shear stress*. J Biol Chem. 2003 Aug 15;278(33):31020-3.
- 35 Hu YL, Li S, Miao H, Tsou TC, del Pozo MA, Chien S. *Roles of microtubule dynamics and small GTPase Rac in endothelial cell migration and lamellipodium formation under flow*. J Vasc Res. 2002 Nov-Dec;39(6):465-76.
- 36 Yang B, Radcliff C, Hughes D, Kelemen S, Rizzo V. *p190 RhoGTPase-activating protein links the β 1 integrin/caveolin-1 mechanosignaling complex to RhoA and actin remodeling*. Arterioscler Thromb Vasc Biol. 2011 Feb;31(2):376-83.
- 37 Arthur WT, Burridge K. *RhoA inactivation by p190RhoGAP regulates cell spreading and migration by promoting membrane protrusion and polarity*. Mol Biol Cell. 2001 Sep;12(9):2711-20.
- 38 Goldfinger LE, Tzima E, Stockton R, Kiosses WB, Kinbara K, Tkachenko E, Gutierrez E, Groisman A, Nguyen P, Chien S, Ginsberg MH. *Localized α 4 integrin phosphorylation directs shear stress-induced endothelial cell alignment*. Circ Res. 2008 Jul 18;103(2):177-85. Epub 2008 Jun 26.
- 39 Orr AW, Sanders JM, Bevard M, Coleman E, Sarembock IJ, Schwartz MA. *The subendothelial extracellular matrix modulates NF- κ B activation by flow: a potential role in atherosclerosis*. J Cell Biol. 2005 Apr 11;169(1):191-202.
- 40 Hahn C, Wang C, Orr AW, Coon BG, Schwartz MA. *JNK2 promotes endothelial cell alignment under flow*. PLoS One. 2011;6(8):e24338. Epub 2011 Aug 31.
- 41 Orr AW, Ginsberg MH, Shattil SJ, Deckmyn H, Schwartz MA. *Matrix-specific suppression of integrin activation in shear stress signaling*. Mol Biol Cell. 2006 Nov;17(11):4686-97.
- 42 Wu CC, Li YS, Haga JH, Kaunas R, Chiu JJ, Su FC, Usami S, Chien S. *Directional shear flow and Rho activation prevent the endothelial cell apoptosis induced by micropatterned anisotropic geometry*. Proc Natl Acad Sci U S A. 2007 Jan 23;104(4):1254-9.
- 43 Uttayarat P, Chen M, Li M, Allen FD, Composto RJ, Lelkes PI. *Microtopography and flow modulate the direction of endothelial cell migration*. Am J Physiol Heart Circ Physiol. 2008 Feb;294(2):H1027-35.

- 44 Morgan JT, Wood JA, Shah NM, Hughbanks ML, Russell P, Barakat AI, Murphy CJ. *Integration of basal topographic cues and apical shear stress in vascular endothelial cells*. Biomaterials. 2012 Jun;33(16):4126-35.
- 45 Rozario T, Dzamba B, Weber GF, Davidson LA, DeSimone DW. *The physical state of fibronectin matrix differentially regulates morphogenetic movements in vivo*. Dev Biol. 2009 Mar 15;327(2):386-98.
- 46 Larsen M, Wei C, Yamada KM. *Cell and fibronectin dynamics during branching morphogenesis*. J Cell Sci. 2006 Aug 15;119(Pt 16):3376-84.
- 47 Sevilla CA, Dalecki D, Hocking DC. *Extracellular matrix fibronectin stimulates the self-assembly of microtissues on native collagen gels*. Tissue Eng Part A. 2010 Dec;16(12):3805-19.
- 48 Shi F, Harman J, Fujiwara K, Sottile J. *Collagen I matrix turnover is regulated by fibronectin polymerization*. Am J Physiol Cell Physiol. 2010 May;298(5):C1265-75.
- 49 Sabatier L, Chen D, Fagotto-Kaufmann C, Hubmacher D, McKee MD, Annis DS, Mosher DF, Reinhardt DP. *Fibrillin assembly requires fibronectin*. Mol Biol Cell. 2009 Feb;20(3):846-58.
- 50 Chiang HY, Korshunov VA, Serour A, Shi F, Sottile J. *Fibronectin is an important regulator of flow-induced vascular remodeling*. Arterioscler Thromb Vasc Biol. 2009 Jul;29(7):1074-9.
- 51 Hahn C, Orr AW, Sanders JM, Jhaveri KA, Schwartz MA. *The subendothelial extracellular matrix modulates JNK activation by flow*. Circ Res. 2009 Apr 24;104(8):995-1003. Epub 2009 Mar 12.
- 52 Feaver RE, Gelfand BD, Wang C, Schwartz MA, Blackman BR. *Atheroprone hemodynamics regulate fibronectin deposition to create positive feedback that sustains endothelial inflammation*. Circ Res. 2010 Jun 11;106(11):1703-11.
- 53 Baneyx G, Baugh L, Vogel V. *Fibronectin extension and unfolding within cell matrix fibrils controlled by cytoskeletal tension*. Proc Natl Acad Sci U S A. 2002 Apr 16;99(8):5139-43.
- 54 Klotzsch E, Smith ML, Kubow KE, Muntwyler S, Little WC, Beyeler F, Gourdon D, Nelson BJ, Vogel V. *Fibronectin forms the most extensible biological fibers displaying switchable force-exposed cryptic binding sites*. Proc Natl Acad Sci U S A. 2009 Oct 27;106(43):18267-72.
- 55 Sottile J, Hocking DC. *Fibronectin polymerization regulates the composition and stability of extracellular matrix fibrils and cell-matrix adhesions*. Mol Biol Cell. 2002 Oct;13(10):3546-59.
- 56 McDonald JA, Quade BJ, Broekelmann TJ, LaChance R, Forsman K, Hasegawa E, Akiyama S. *Fibronectin's cell-adhesive domain and an amino-terminal matrix assembly domain participate in its assembly into fibroblast pericellular matrix*. J Biol Chem. 1987 Mar 5;262(7):2957-67.
- 57 Zhong C, Chrzanowska-Wodnicka M, Brown J, Shaub A, Belkin AM, Burridge K. *Rho-mediated contractility exposes a cryptic site in fibronectin and induces fibronectin matrix assembly*. J Cell Biol. 1998 Apr 20;141(2):539-51.
- 58 Bourdoulous S, Orend G, MacKenna DA, Pasqualini R, Ruoslahti E. *Fibronectin matrix regulates activation of RHO and CDC42 GTPases and cell cycle progression*. J Cell Biol. 1998 Oct 5;143(1):267-76.

- 59 Danen EH, Sonneveld P, Brakebusch C, Fassler R, Sonnenberg A. *The fibronectin-binding integrins $\alpha 5 \beta 1$ and $\alpha v \beta 3$ differentially modulate RhoA-GTP loading, organization of cell matrix adhesions, and fibronectin fibrillogenesis*. J Cell Biol. 2002 Dec 23;159(6):1071-86.
- 60 Sechler JL, Corbett SA, Schwarzbauer JE. *Modulatory roles for integrin activation and the synergy site of fibronectin during matrix assembly*. Mol Biol Cell. 1997 Dec;8(12):2563-73.
- 61 Meckmongkol TT, Harmon R, McKeown-Longo P, Van De Water L. *The fibronectin synergy site modulates TGF-beta-dependent fibroblast contraction*. Biochem Biophys Res Commun. 2007 Sep 7;360(4):709-14.
- 62 Takahashi S, Leiss M, Moser M, Ohashi T, Kitao T, Heckmann D, Pfeifer A, Kessler H, Takagi J, Erickson HP, Fässler R. *The RGD motif in fibronectin is essential for development but dispensable for fibril assembly*. J Cell Biol. 2007 Jul 2;178(1):167-78.
- 63 Cseh B, Fernandez-Sauze S, Grall D, Schaub S, Doma E, Van Obberghen-Schilling E. *Autocrine fibronectin directs matrix assembly and crosstalk between cell-matrix and cell-cell adhesion in vascular endothelial cells*. J Cell Sci. 2010 Nov 15;123(Pt 22):3989-99.
- 64 Mao Y, Schwarzbauer JE. *Accessibility to the fibronectin synergy site in a 3D matrix regulates engagement of $\alpha 5 \beta 1$ versus $\alpha v \beta 3$ integrin receptors*. Cell Commun Adhes. 2006 Sep-Dec;13(5-6):267-77.
- 65 Engler AJ, Chan M, Boettiger D, Schwarzbauer JE. *A novel mode of cell detachment from fibrillar fibronectin matrix under shear*. J Cell Sci. 2009 May 15;122(Pt 10):1647-53.
- 66 Thoumine O, Nerem RM, Girard PR. *Changes in organization and composition of the extracellular matrix underlying cultured endothelial cells exposed to laminar steady shear stress*. Lab Invest. 1995 Oct;73(4):565-76.
- 67 Kubow KE, Klotzsch E, Smith ML, Gourdon D, Little WC, Vogel V. *Crosslinking of cell-derived 3D scaffolds up-regulates the stretching and unfolding of new extracellular matrix assembled by reseeded cells*. Integr Biol (Camb). 2009 Dec;1(11-12):635-48.
- 68 Roca-Cusachs P, Gauthier NC, Del Rio A, Sheetz MP. *Clustering of $\alpha (5) \beta 1$ integrins determines adhesion strength whereas $\alpha (v) \beta 3$ and talin enable mechanotransduction*. Proc Natl Acad Sci U S A. 2009 Sep 22;106(38):16245-50.
- 69 Keselowsky BG, García AJ. *Quantitative methods for analysis of integrin binding and focal adhesion formation on biomaterial surfaces*. Biomaterials. 2005 Feb;26(4):413-8.
- 70 Li CH, Tam PKS. *An Iterative Algorithm for Minimum Cross Entropy Thresholding*. Pattern Recognition Letters 1998 18(8): 771-776
- 71 Choi CK, Helmke BP. *Short-Term Shear Stress Induces Rapid Actin Dynamics in Living Endothelial Cells*. Mol Cell Biomech. 2008 Jan 1;5(4):247-258.
- 72 Katz BZ, Zamir E, Bershadsky A, Kam Z, Yamada KM, Geiger B. *Physical state of the extracellular matrix regulates the structure and molecular composition of cell-matrix adhesions*. Mol Biol Cell. 2000 Mar;11(3):1047-60.
- 73 Helmke BP, Rosen AB, Davies PF. *Mapping mechanical strain of an endogenous cytoskeletal network in living endothelial cells*. Biophys J. 2003 Apr;84(4):2691-9.

- 74 Dumbauld DW, Shin H, Gallant ND, Michael KE, Radhakrishna H, García AJ. *Contractility modulates cell adhesion strengthening through focal adhesion kinase and assembly of vinculin-containing focal adhesions*. J Cell Physiol. 2010 Jun;223(3):746-56.
- 75 del Rio A, Perez-Jimenez R, Liu R, Roca-Cusachs P, Fernandez JM, Sheetz MP. *Stretching single talin rod molecules activates vinculin binding*. Science. 2009 Jan 30;323(5914):638-41.
- 76 Mott RE. *The Endothelial Mechanoresponse: Dynamic Mechanochemical Mechanisms at the Cell-Matrix Interface*. Ph.D. Dissertation, University of Virginia, 2008.
- 77 Kiosses WB, Shattil SJ, Pampori N, Schwartz MA. *Rac recruits high-affinity integrin α v β 3 to lamellipodia in endothelial cell migration*. Nat Cell Biol. 2001 Mar;3(3):316-20.
- 78 White DP, Caswell PT, Norman JC. *α v β 3 and α 5 β 1 integrin recycling pathways dictate downstream Rho kinase signaling to regulate persistent cell migration*. J Cell Biol. 2007 May 7;177(3):515-25.
- 79 Friedland JC, Lee MH, Boettiger D. *Mechanically activated integrin switch controls α 5 β 1 function*. Science. 2009 Jan 30;323(5914):642-4.
- 80 Levental KR, Yu H, Kass L, Lakins JN, Egeblad M, Erler JT, Fong SF, Csiszar K, Giaccia A, Weninger W, Yamauchi M, Gasser DL, Weaver VM. *Matrix crosslinking forces tumor progression by enhancing integrin signaling*. Cell. 2009 Nov 25;139(5):891-906.
- 81 Paszek MJ, Zahir N, Johnson KR, Lakins JN, Rozenberg GI, Gefen A, Reinhart-King CA, Margulies SS, Dembo M, Boettiger D, Hammer DA, Weaver VM. *Tensional homeostasis and the malignant phenotype*. Cancer Cell. 2005 Sep;8(3):241-54.
- 82 Kostic A, Sheetz MP. *Fibronectin rigidity response through Fyn and p130Cas recruitment to the leading edge*. Mol Biol Cell. 2006 Jun;17(6):2684-95. Epub 2006 Apr 5.
- 83 Dubash AD, Wennerberg K, García-Mata R, Menold MM, Arthur WT, Burridge K. *A novel role for Lsc/p115 RhoGEF and LARG in regulating RhoA activity downstream of adhesion to fibronectin*. J Cell Sci. 2007 Nov 15;120(Pt 22):3989-98.
- 84 Guilluy C, Swaminathan V, Garcia-Mata R, O'Brien ET, Superfine R, Burridge K. *The Rho GEFs LARG and GEF-H1 regulate the mechanical response to force on integrins*. Nat Cell Biol. 2011 Jun;13(6):722-7.
- 85 Huang L. *Endothelial Edge Dynamics and Cytoskeletal Reorganization in Response to Hemodynamic Forces*. Ph.D. Dissertation, University of Virginia, 2011.
- 86 Girard PR, Nerem RM. *Shear stress modulates endothelial cell morphology and F-actin organization through the regulation of focal adhesion-associated proteins*. J Cell Physiol. 1995 Apr;163(1):179-93.
- 87 Krishnan R, Klumpers DD, Park CY, Rajendran K, Treppe X, van Bezu J, van Hinsbergh VW, Carman CV, Brain JD, Fredberg JJ, Butler JP, van Nieuw Amerongen GP. *Substrate stiffening promotes endothelial monolayer disruption through enhanced physical forces*. Am J Physiol Cell Physiol. 2011 Jan;300(1):C146-54.

- 88 Byfield FJ, Reen RK, Shentu TP, Levitan I, Gooch KJ. *Endothelial actin and cell stiffness is modulated by substrate stiffness in 2D and 3D*. J Biomech. 2009 May 29;42(8):1114-9.
- 89 Saunders RL, Hammer DA. *Assembly of Human Umbilical Vein Endothelial Cells on Compliant Hydrogels*. Cell Mol Bioeng. 2010 Mar;3(1):60-67. *